Determination of Patient Specific S-values Correlated with Noninvasive Patient Attributes

By

Jason Mace

July, 2025

Director of Dissertation: Dr. Jae Won Jung

Major Department: Physics

ABSTRACT

Introduction: Nuclear medicine procedures are the second largest source of medical ionizing radiation, behind only computed tomography. The current population has been exposed to medical imaging more than previous generations, therefore knowledge of absorbed dose (ionizing) is not only an important component of patient care, but may have epidemiological implications as well. Unlike other modalities, in nuclear medicine a clinician can often decrease the patient's administered activity at the expense of extending the acquisition time, administration therefore is not a binary decision . It should be noted radionuclide dosimetry can be accurately calculated if sufficient data is available. However, in most cases crucial information such as uptake, biokinetics and anatomical details cannot or will not be known a priori. Furthermore, the dosimetric process is often arduous, requiring intensive resources with respect to personnel and technology. Convenient models based on MIRD formalism have been developed to overcome the aforementioned challenges. Unfortunately, the models are not patient specific which causes inaccuracies, one such shortcoming centers around spatial variances. In the MIRD schema S-values denote the mean absorbed dose to a target volume (organ) per unit activity in a source region (organ). The S-values are based on phantom models for specific radionuclides, in the MIRD schema they are separable from the kinetic aspects of nuclear medicine. To improve patient specific nuclear medicine dosimetry S-values will be determined for patients directly. The analysis will be conducted for radionuclides of interest and select organs. The range of organ S-values will be examined to determine the need of personalization and its possible benefit. The

results will be benchmarked against modern phantom models (dosimetric software), with the goal of personalizing phantom results through the utilization of basic patient attributes.

Methods: To evaluate the variances between the S-values of patients and phantoms, one needs diagnostic images. The gold standard modality of anatomical imaging is computed tomography. Fifty-six patient computed tomography exams were made available by the National Institutes of Health (NIH), along with information regarding the patient's sex, age, height and weight. The patient images were de-identified prior, the clinical images contained the structures of the Chest, Abdomen and Pelvis of persons. The diagnostic images (CT) were segmented by TotalSegmentator which is a deep learning model, resulting in various structures. These structures were used to in part to create a source distribution and a lattice model for Monte Carlo implementation. The source energies and yields regarding emission was obtained from ICRP 107. Radiation transport is one of the areas that has greatly benefited from Monte Carlo methods. The Monte Carlo simulations conducted in this work utilize MCNP 6.2 which is a general-purpose, continuous-energy, generalized-geometry, time-dependent, Monte Carlo radiation transport code. The S-values were calculated for a number of target organs (spleen, kidneys, pancreas, stomach, liver and lungs) resulting from activity in the patient's kidneys for (Tc-99m, F-18, Lu-177 and I-131). The results were compared and benchmarked versus NCINM a modern dosimetry program based in part on phantom models.

Results: The variation of S-values for adult target organs were found to significant. The variation between the minimum and maximum S-values for patients ranged from a two-fold to a five-fold factor and therefore supports the need for personalization. Benchmarking the S-values with NCINM revealed in most cases the phantoms were contained within the patient's distribution if not centered, which adds to the simulation's credibility. The patient specific values were normalized to their appropriate NCINM phantom models. Significant correlation was found between the patient's BMI and their normalized S-values irrespective of radionuclide. The correlation is believed to be due to internal shielding. Based on a linear fit the NCINM model was extended or personalized. This extension greatly reduced the variation between actual S-values

and the NCINM dosimetry model. The interquartile range of the distribution of most organ S-values were decreased by 50 percent.

DETERMINATION OF PATIENT SPECIFIC S-VALUES CORRELATED WITH NONINVASIVE PATIENT ATTRIBUTES

A Dissertation

Presented to the Faculty of the Department of Physics

East Carolina University

In Partial Fulfillment of the Requirements for the Degree

Doctor of Philosophy in Biomedical Physics

By

Jason C. Mace

July 2025

Director of Dissertation: Jae Won Jung, Ph.D.

Thesis Committee Members:

Choonsik Lee, Ph.D.

Michael Dingfelder, Ph.D.

Jefferson Shinpaugh, Ph.D.

Zi-Wei Lin, Ph.D.

Acknowledgements

I'm indebted to many individuals that have aided in my professional and educational endeavors. First I must mention the scientific contributions and resources that directly contributed to this research project. I would like to acknowledge Dr. Elizabeth Jones (female cohort) and Dr. Roberto Maass-Moreno (male cohort) for making patient images available. I would also like to credit my research collaborator Dr. Morato Rafet (NCI), who aided this project with pre- and post-processing of segmented images. Additionally, I have greatly benefited from working with Dr. Choonsik Lee who has been instrumental in experimental design, the technical implementation of Monte Carlo methods and as a committee member. Dr. Jung, my advisor has been indispensable in all aspects of my research and degree process. I have enjoyed and benefited from his guidance. I'm humbled and grateful to my committee members Dr. Shinpaugh, Dr. Dingfelder, and Dr. Lin for their encouragement, guidance and commitment. I would like to thank the many additional dedicated faculty members at East Carolina that have aided in my growth as a physicist in general and in particular Dr. Li, Dr. Hu, Dr. Kempf, Dr. Toburen and the late Dr. Dinno.

I would be remiss if I did not acknowledge both the sacrifices and the inspiration of my family. My Father a physicist, opened the world of science to a young child using thought experiments, access to a library of technical books and his encouragement. My late Mother's poor health, inspired me to marry my interests in physics with medicine. While at East Carolina University, I met and married my wife Lesli. She has taken great care of me and supported my educational pursuits. Additionally, I would like to thank my two children Molly and Titus for their understanding and inspiration. I hope to return if possible and pay forward if not these blessings and kindnesses.

TABLE OF CONTENTS

LIST OF TABLES

LIST OF FIGURES

List of Symbols and Abbreviations

CHAPTER 1

INTRODUCTION AND MOTIVATION

Personalized medicine infers the optimization of an individual patient's care. Optimal patient treatment could be characterized as the proper drug or intervention given in the optimal manner in the precise amount at the appropriate time. Traditionally a patient's prescription is not based on their molecular response in the short or long term with regards to the pharmaceutical. A patient's medical response or even drug uptake is usually not known prior to treatment. Due to this fact, a trial and error treatment regimen is the hallmark of modern primary medical care. Increased interest has been given to theranostic agents, these agents can be used in diagnostics and therapeutics. One type of theranostic agent and arguably the first were radionuclides (radio-pharmaceuticals), which if properly utilized can combine nuclear medicine and radiation therapy.[1]

Rigorous optimization is difficult at best until an unbiased quantitative platform is implemented. The scientific process favors quantification because it allows the gradient of progress to be visualized. To personalize patient care, it is instructive to examine the sequential steps in both radionuclide imaging and therapy. Arguably the first step in radionuclide therapy is patient selection (labs, medical history), it is important to note selection is intertwined with diagnostics. Once the patient is selected, instructions (diet, medication) must be considered prior to imaging. Next the imaging modality (Positron Emission Tomography (PET), Single Photon Emission Computed Tomography (SPECT), etc..) parameters (techniques) and administered pharmaceutical require optimization. The final product of the diagnostic realm is guidance to the clinician whom bears the responsibility for patient care. Note each level of the diagnostic pyramid outlined affect subsequent levels therefore optimization must be comprehensive and iterative. Personalized quantification in nuclear medicine is not only needed to implement a thoughtful dosimetry program but can better inform the patient regarding risks in general.

Quantitative methods along with patient compliance with directives may allow patient specific uptake and biological clearing parameters to be known a priori.[2] Current therapies are often not personalized at all or simply scaled by simple patient attributes such as weight, etc.[3] It is important to realize that dosimetry takes time and requires training so these costs must be warranted.

1.1 Importance of Dosimetry in Nuclear Medicine

Why is dose an important metric in nuclear medicine? At the time of this writing nuclear medicine procedures contribute to the second highest exposure of patients behind only computed tomography.[4] Additionally our current population has been exposed to medical imaging more than previous generations, therefore knowledge of dose is not only important for an individual, but is of interest from an epidemiological perspective as well. The increase in Nuclear Medicine procedures is further magnified by the fact that some patient populations are repeatedly imaged by clinicians, which can increase the patient's radiation burden substantially. In recent years new diagnostic exams have been added in previous largely ignored areas of medicine like neurology. Positron emission tomography (PET) is increasingly being utilized for cardiac patients, while PET remains at the forefront of imaging in oncology. Moreover a new Theranostic class of agents are on the rise and their patients are increasing exponentially. The theranostic regiments often contain a diagnostic and therapeutic pair, meaning the patient will undergo diagnostic imaging as a gatekeeper prior to a therapeutic administration.[5] The risk benefit of diagnostic agents of an individual study is often warranted due to the lack of near term toxicity. Unlike other modalities in nuclear medicine a clinician can often decrease the patient's "dose" (reduce the administered activity) at the expense of extending the acquisition time. As nuclear medicine continues to grow and represent a greater radiation burden to the population, dosimetric models must improve to intelligently chart that the field forward.

Personalized radionuclide dosimetry has relied on two different methods each will be introduced. Model-based methods used for risk evaluation are not by definition patient specific but group

individuals into relatively large categories by age and gender. Such methods simplify some tasks with the benefit of accessibility. It is debatable if they adequately account for nonuniformities and variations that exist in practice. It must be remembered, a single absorbed dose volume is meaningful only if it successfully predicts biologic effects. The second method involves patient-specific 3D dosimetry with radiobiologic modeling this improves on the deficiencies of model based approaches but requires significant data and is time intensive. The advantage of 3D internal dosimetry is it uses more accurate anatomy and activity distribution data, and may calculate absorbed dose at the voxel or suborgan level. Advanced methods utilizing Monte Carlo calculations and radiobiologic modeling could improve localization of absorbed dose to produce a more faithful prediction of tumor response and toxicity to normal tissue.[6] Model based programs that utilize phantoms such as Organ Level INternal Dose Assessment (OLINDA) and National Cancer Institute Dosimetry System for Nuclear Medicine (NCINM) have the advantage that they can be employed retrospectively when the data needed for patient based dosimetry programs is incomplete or not practical.[3][7] Because patient based dosimetry techniques are typically intensive and sometimes not possible it is important to extend or improve the accuracy of model based practices (phantoms) to the extent possible. Although patient specific dosimetry has begun, although not widely adopted in the realms of Radiopharmaceutical Therapy (RPT), it is not conducted for diagnostic agents. The post dosimetry for RPT is typically confined to therapy and only accounts for a few organs of interest.[8] In a similar vein to external beam therapy which has been revolutionized with advanced dosimetry, modulation, fractionation and image guidance it is my hypothesis that radionuclide therapy and nuclear medicine dosimetry in general can enjoy similar benefits from a personalized approach.

CHAPTER 2

MEDICAL INTERNAL RADIATION DOSIMETRY

Prior to introducing internal radiation dosimetry, one could argue that one first must introduce the term **Activity**. A simple explanation of activity is it is quantity expressing the time rate of radioactive decay. In terms of radionuclides Activity, (**A**) can be defined as follows,

$$A \equiv A_o e^{-\lambda_p t} \tag{2.1}$$

, where A_o is the initial activity, t denotes time dependence, and λ_p is a decay property of the radioisotope.

$$\lambda_p \equiv ln(2)/T_p \tag{2.2}$$

λ_p can be defined in terms of T_p the physical half-life of the isotope. This becomes slightly more complicated when we realize we are dealing with pharmaceuticals which are being actively eliminated from our bodies. This concept gives rise to the term biological half-life T_b and effective half-life T_e.

$$1/T_e \equiv 1/T_p + 1/T_b \tag{2.3}$$

Note one can then determine the effective λ accordingly.

$$\lambda_e \equiv ln(2)/T_e \tag{2.4}$$

However one dose not typically consider from a dosimetric standpoint the total body effective half-life. The compartmental nature of the body complicates these relatively simplistic equations even if one assumes first order kinetics into a sum of exponential functions![9]
Furthermore it is important to define parameters that remain at the core of dosimetry in general.

Absorbed Dose, D can be defined as follows,

$$D \equiv \frac{d\tilde{E}}{dm} \tag{2.5}$$

, where $d\tilde{E}$ is the mean energy imparted by ionizing radiation to mater and dm is the mass of the matter to which the energy is imparted ($\frac{J}{kg}$). A second item of consideration is the quality of radiation which is deterministic of its radiobiological effectiveness. **Linear Energy Transfer** or LET can be defined as

$$LET \equiv \frac{dE}{dl} \tag{2.6}$$

, where dE is the energy deposited by a charged particle (or a secondary charged particle) over a pathlength dl traversed in matter ($\frac{J}{m}$). The relevance of LET leads to the concept of **Relative biological effectiveness** or RBE. Which can be defined as follows

$$RBE \equiv \frac{D_x}{D_y}, \tag{2.7}$$

where D_x is a reference absorbed dose of radiation of a standard type x (low LET), and D_y is the absorbed dose of radiation of type y that causes the same amount of biological damage. Both doses are quantified by the amount of energy absorbed in the tissue. **Equivalent dose** is derived from the absorbed dose to an organ or tissue, adjusted to account for the aforementioned type of radiation. The adjustment is made by a radiation weighting factor W_R, which ranges from 1 for ionizing photons and electrons to 20 for alpha particles. Therefore equivalent dose can written as:

$$H_T \equiv \sum_R W_R D_{R,T} \tag{2.8}$$

, where W_R is the radiation weighting factor for radiation of quality R and $D_{R,T}$ is the contribution of radiation quality R to the mean absorbed dose to the tissue T ($\frac{J}{kg}$). Different tissues in the body exhibit varying degrees of radiation sensitivity as do members of the population (age, risk factors, etc..). While the term **effective dose** is primarily a radiation

protection quantity it should be introduced. Effective dose can be defined as follows:

$$E \equiv \sum_{T} W_T H_T \tag{2.9}$$

, where W_T represents the tissue-weighting factor for target tissue r_T subject to the condition that due to the complexity and the variety of tissues dosed in nuclear medicine from a single administration, it is typical for effective dose to be the figure of merit. Clinicians often rely on risk factors that are not strictly personalized to make an informed risk versus benefit assessment. It is a scientist obligation to provide the most reliable information possible.

Dosimetry involving radio-pharmaceuticals has been calculated by the Medical Internal Radiation Dose (MIRD) schema, when suitable S-values are available. The MIRD schema denotes tissues as source and/or target regions. The source regions are the tissues where the radio-pharmaceuticals dwell in the body. Target regions are tissues which absorbed dose from radiation emitting from the source tissues. It should be noted that source regions is also simultaneously a target tissues.

Table 2.1: Medical Internal Radiation Dosimetry Terminology

MIRD Basic Terminology			
Parameter	Symbol	Definition	Units
Activity	$A(r_s, t)$	Source Region Activity r_s at time t	MBq
Time-integrated Activity	$\tilde{A}(r_s, \tau)$	Number of radioactive decays in r_s from $t = 0 \rightarrow \tau$	MBq*s
Time-integrated Activity Coefficient formerly residence time	$\tilde{a}(r_s, \tau)$	Number of radioactive decays in r_s from $t = 0 \rightarrow \tau$ per administered activity	s
Administer Activity	A_0	Total Injected Radiopharmaceutical Activity	MBq
Time	t	Time post injection	h
Mass	M_S,M_T	Mass of tissue regions	g
Source region	r_S	Region containing radionuclide emissions	N/A
Target region	r_T	Region where emitted energy is deposited	N/A
Absorbed Dose	$D(r_T, \tau)$	Absorbed dose to target from $t = 0 \rightarrow \tau$	Gy
Absorbed Dose Coefficient	$d(r_T, \tau)$	Absorbed to target from $t = 0 \rightarrow \tau$ per A_0	$\frac{Gy}{MBq}$
Energy	E_i	Energy (or mean energy) of i^{th} emission by administered radionuclide	MeV
Number of radiations per decay	Y_i	Number of i^{th} radiation emitted per decay of administered radionuclide	N/A
Energy per Decay	$\triangle_i$	Energy (or mean energy) of i^{th} radiation emitted per decay of administered radionuclide	MeV
Absorbed Fraction	$\phi(r_T \leftarrow r_S, E_i$	Fraction of energy E_i of the i^{th} radiation emitted in r_s that is absorbed in r_T	N/A
Specific Absorbed Fraction	$\Phi(r_T \leftarrow r_S, E_i)$	Fraction of energy E_i of the i^{th} radiation emitted in r_s that is absorbed in r_T per unit mass of r_T	g^{-1}
S-value	$S(r_T \leftarrow r_S)$	Absorbed dose to r_T per decay in r_S	$\frac{mGy}{MBq*s}$

The computational process with calculating dose according to MIRD schema is as follows:

$$D(r_T, \tau) = \sum_{r_s} \int_0^{\tau} A(r_s, t) \frac{1}{m_{r_T}} \sum E_i Y_i \phi(r_T \leftarrow r_s, E_i)\, dt \tag{2.10}$$

$$D(r_T, \tau) = \sum_{r_s} \int_0^{\tau} A(r_s, t) \sum_i \triangle_i \, \Phi(r_T \leftarrow r_s, E_i)\, dt \tag{2.11}$$

$$D(r_T, \tau) = \sum_{r_s} \int_0^{\tau} A(r_s, t) S(r_T \leftarrow r_s), dt \tag{2.12}$$

The integration time is typically set to infinity, yielding a time invariant version. Note this yields the total absorbed dose to the target region r_T after complete decay of the administered radiopharmaceutical. A brief introduction or explanation of the schema follows in detailed form.

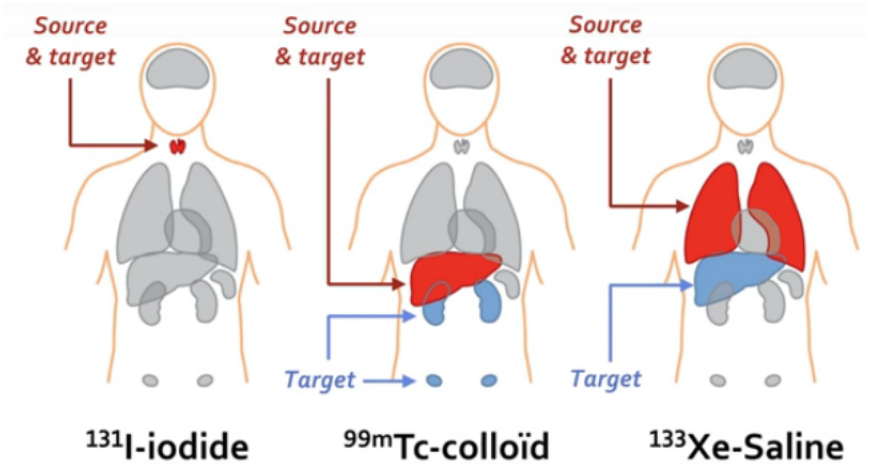

Figure 2.1: A Cartoon example of various source organs and target tissues for several common nuclear medicine procedures. Courtesy of IAEA

The absorbed dose D(r_T) of a target region resulting from radioactive decay in a source region is r_s is given by $\sum \tilde{A}(r_s)S(r_T \leftarrow \mathrm{r}_s)$.[10] Note $\tilde{A}(r_s)$ is the time integrated activity of a radionuclide within a source region. $S(r_T \leftarrow \mathrm{r}_s)$ is defined as the mean absorbed dose to the target region per nuclear decay in the source region, also know as the S-value. This can be expanded to show that $S(r_T \leftarrow \mathrm{r}_s) = \sum_i E_i Y_i \Phi(\mathrm{r}_T \leftarrow \mathrm{r}_s, E_i)$, E_i and Y_i are energies and yields of the i^{th} nuclear transformation of the radionuclide and $\Phi(\mathrm{r}_T \leftarrow \mathrm{r}_s)$ is the **SAF!** (**SAF!**) for radiation particle of energy E_I for a given source-target combination. The SAF can be further expanded to show it is the ratio of the absorbed fraction $\phi(\mathrm{r}_T \leftarrow \mathrm{r}_s, E_i)$, which is the portion of the particle's energy E_i emitted from the source region r_s that is deposited in the the target region r_T with a mass m(r_T). Hence the SAF $= \Phi(\mathrm{r}_T \leftarrow \mathrm{r}_s, E_i) = \dfrac{\phi(r_T \leftarrow r_s, E_i)}{m(r_T)}$

It is important to note nuances or simplifications exist in the MIRD formalism.[10] As presented it should be clear that source activity and target dose are averaged quantities for a given structure. The beauty of the schema lies in reducing the seemingly complicated task of calculating the absorbed dose of a target region from a nonuniform time variant source region. A second benefit of the MIRD schema is the separation of physical processes from the biological. The relevant physiology is contained in the time-integrated activity (r_s, τ). While the physics is confined in the S-value. Optimization regarding the estimation of internal dosimetry can be completed in an independent multi-step process!

CHAPTER 3

PHANTOM MODELS AND S-VALUE CALCULATIONS

3.1 Background

It is instructive to outline two approaches regarding internal dosimetry. Both methodologies are based on MIRD formalism. The first methodology is model based and hence it is not by definition personalized. The development of model based approaches are due to a multitude of factors. First without knowledge of source distributions, targets tissue sizes, and shapes one cannot define a dosimetric problem. Furthermore the geometric distance and attenuation between source and target pairs need to be defined to access radiation toxicity.

Radiation burden is a necessary assessment at the genesis of drug development. During the early stages of the developing field of nuclear medicine computational processes were prohibitive due to the lack of computing power. Additionally for the comparison of radiation dose an independent model needed to be developed.

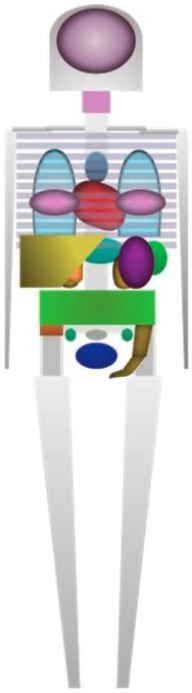

Figure 3.1: Cristy Eckerman Phantom

Phantom Development

Early anatomical models were known as stylized phantoms, and were used to evaluate ionizing radiation deposition in organs from both internal and external exposures. These phantoms were based upon mathematical expressions representing planes, and surfaces (cylindrical, conical, elliptical or

spherical).[11] These constructs were used to describe the shape and position of idealized human organs. One of the earliest widely adopted anatomical models was created by Fisher and Snyder.[12] This phantom dubbed Reference Man (International Commission on Radiation Units and Measurements (ICRP)) was created to represent the average adult worker of the western hemisphere. Although the ICRP didn't directly design the phantom, they collected data on people's bodies and organs. The phantom was created to reflect the reference data termed reference man (50 percentile values).[13] The two creators then ran Monte Carlo simulations, and used their results to determine S-values for a number of source and target organ pairs. This early phantom contained both male and female organs for completeness if not correctness. By 1987 Cristy and Eckerman published results that added new organs to the Fisher-Snyder phantom. Moreover they included pediatric phantoms for several ages (1, 5, 10 and 15 years).[14] The age values were a proxy for the geometric changes during childhood and were meant to be approximate in nature. To accomplish this goal the researchers studied how organ placement and size varied with age. In 1995 Stabin and colleagues created an adult female phantom that was widely adopted. Many researchers had previously used the 15 year old (Cristy-Eckerman) to approximate females. Although hermaphrodite phantoms were still in use, it should be mentioned that Kramer et. al. in 1982 created separate male and female phantoms. Additionally Stabin created three additional female phantoms at various gestational periods due to the importance of fetal dosimetry in radiological protection.[15] The aforementioned models had organ masses and volumes in accordance with ICRP data of former Reference Man (ICRP-23, 1975). ICRP-89 updated the historical values of ICRP-23.[16] It should be noted organ mass values are based upon European and North American populations.

Note

the organ mass reported by ICRP varies from that reported by three Asian countries.[16] The variation in mass by definition will play a role in dosimetric calculations. One can see that ICRP's reference mass value is typically within the mass distribution range for the aforementioned countries hence it was deemed sufficient for general radiation protection standards. Important improvement have been made regarding computational models due to the advancements in imaging and computers. Anatomical models can be based upon computed tomography, magnetic resonance or other high resolution scans of individuals.[17] The advantage of voxelized images is they replace the previous stylized phantoms with the complexity of realistic human anatomy. In general voxelized human subjects do not conform to previous reference data contained in ICRP 23 or 89. Authors have shown the organ shapes of mathematical phantoms present an over-simplification influencing energy deposition and deviating substantially from voxel models.[18]

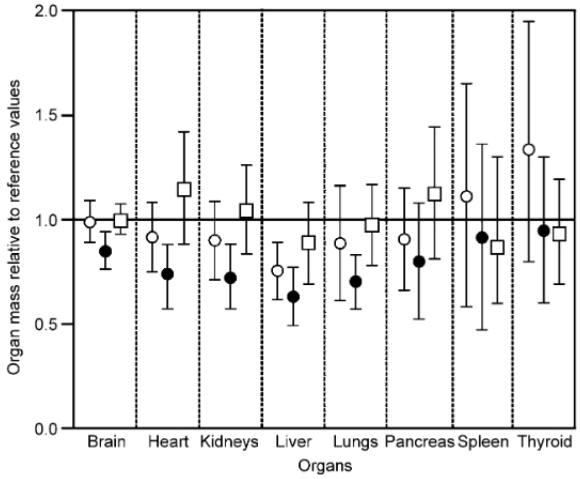

Figure 3.2: Normalized comparison of organ masses (mean $\pm$ 1 SD) for adult males from three Asian countries compared with the ICRP reference values of Publication 89 (ICRP values=1.0). $\circ, China; \bullet, India; \square, Japan (IAEA, 1998)$.

In terms of internal dosimetry the influencing parameters include the relative position of source to target organs for penetrating radiation (cross-fire effect). Non-penetrating radiation organ mass has been shown to play a pivotal role. ICRP 110 developed reference phantoms by a multi-step process of scaling and segmenting anatomical imaging. The resulting phantoms represented characteristics of ICRP's reference data with realistic anatomical information.[19] Realistic reference phantoms: an ICRP/ICRU (**ICRU!** (**ICRU!**)) joint effort, a report of adult reference computational phantoms. Improvements upon the accuracy and details of tomographic phantoms have continued in recent years.

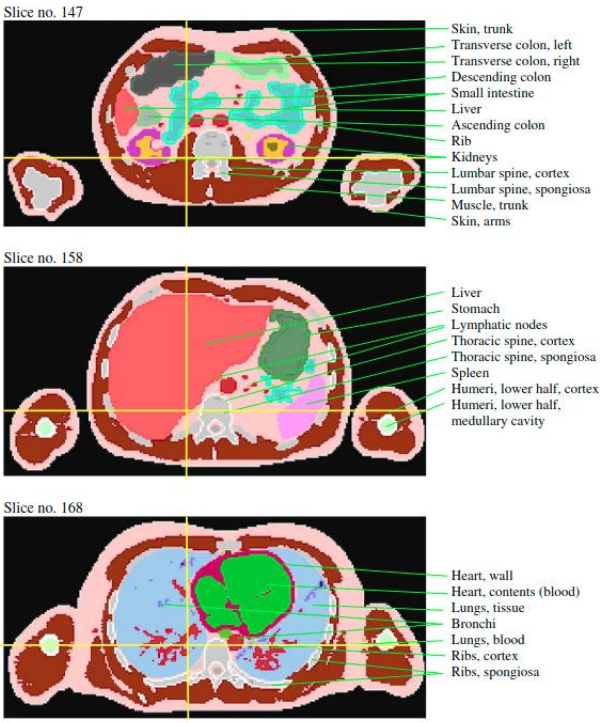

Figure 3.3: ICRP 110 Computational Male Axial Images

However voxelized phantoms have several limitations.[20] Some imported structures are smaller than acquisition voxels and require models rather than direct segmentation. Anatomical voxel sizes are governed by the imaging acquisition system, hence they are limited. A voxel size in any one dimension is on the order of millimeters, whereas some structures require micrometer resolution.

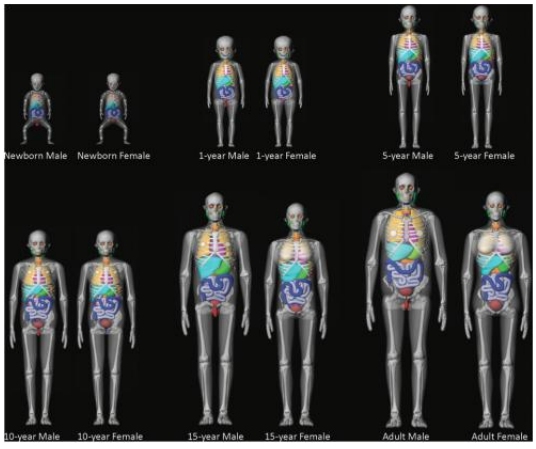

Figure 3.4: Hybrid Phantoms Introduced by University of Florida.

These structures may involve the lining of tissues like the gastrointestinal (alimentary) track, known to be very radio-sensitive. The benefits of mathematical phantoms are somewhat

overlooked, these phantoms can be flexible with respect to organ position and deformation compared to voxel phantoms. However as computational methods have increased voxelized phantoms can provide ideal characteristics for computation and can be linked naturally to imaging. To obtain the optimal attributes of both phantom types, hybrid phantoms based on non-uniform B-spline (NURBS) and mesh surfaces have been created.[3] These phantoms have the flexibility of complex adjustments (deformations) while maintaining anatomical realism. For simulation purposes the phantoms can be converted back into voxels. However this generation of phantoms provide for the independent scalability of segmented tissues. Modern mesh phantoms have replaced their voxelized predecessors in many instances. Phantom anatomies can be deformed to depict humans standing or sitting for example. Finally these phantoms allow one to sculpt non-referenced phantoms using the reference phantom as an anatomical template.[21] As impressive as this phantom technology has become it is important to remember it has been primarily on radiation protection and not individual patients.

Dosimetry Programs

Headwinds

Multiple dosimetry software solutions exist in nuclear medicine at the time present time. None are typically utilized for patient care in diagnostics and are only rarely implemented in therapeutics. In fact the term dose in nuclear medicine is often used interchangeably with activity!

Presently one of the most commonly used programs to aid in passive dose assessments (protocol creations) is SNMMI's Dose Tool (Society of Nuclear Medicine and Molecular Imaging (SNMMI)), this web application does not provide or show organ-level dosimetry (Although the dose assessment seems to be partly based OLINDA/EXE).[7] Radiopharmaceutical therapies studies are commonly conducted by the FDA based on activity, although dosimetry may be investigated in early phases of the study. The physician prescription or written directives are typically based on the prescribed activity and compared to the delivered activity. As use of agents continue to rise interest in individual radiation burden has followed, increasingly radiation safety officers are asked to estimate these values by clinicians and patients.

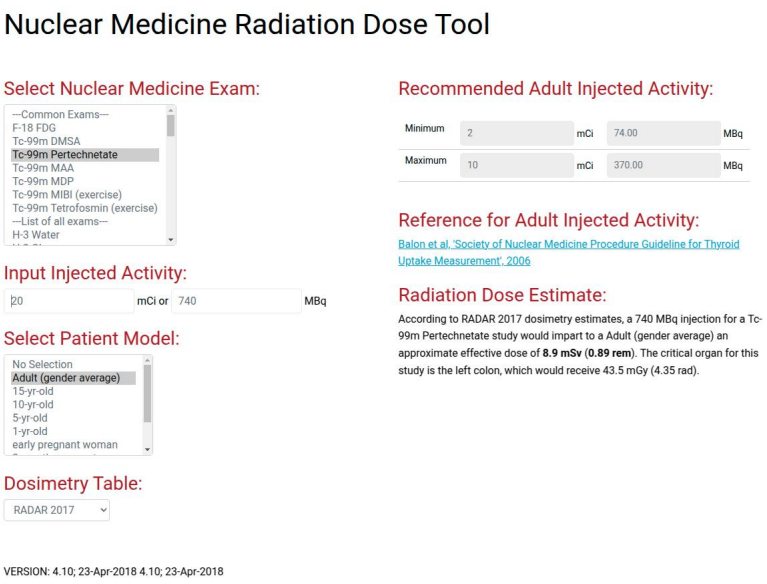

Figure 3.5: Nuclear Medicine Radiation Dose Tool SNMMI.

3.2 Model Based Dosimetry

Several organ level dosimetry based software solutions exist, which follow MIRD formalism. They leverage phantoms or computational models to represent standardized humans. As previously discussed these models utilize equations, voxels, and surfaces to depict anatomical geometry with respect to organs. Typically one can calculate the transport of radiation from a source organ to that of a target organ provided the energy and particle type (SAF). Radionuclide emissions or decay information is provided by ICRP 107. The ICRP document contains radionuclide information regarding half-lives, decay chains, particle types, energies and yields.

S-values for phantoms can be derived in an efficient manner from SAF tables calculated for various phantoms combined with emission data (energy and yields) from ICRP 107. Biokinetic models for radiopharmaceuticals have also been tabulated, the latest and most comprehensive collection is found in ICRP 128, which identifies source organs as well as TIAC values for various agents.[22] Note tissue weighting factors have been provided in ICRP 103.[23] The tissue weighting factors are used to ”weight” the contribution of individual organs and tissues to the detrimental effects of radiation. These values do not account for deterministic effects or high radiation exposures, but are a measure of stochastic effects such as cancer. Results were never intended to be representative of individuals but provide reference values for radiation safety. Furthermore it allows one to relate in a meaningful way phantoms doses of various agents.

OLINDA/EXE 2.0

OLINDA/EXE stands for ”Organ Level Internal Dose Assessment and Exponential Modeling” is the latest version, note 1.0 and MIRDOSE were based on the SAFs calculated from the ORNL (various versions) of stylized phantoms mentioned earlier. The latest version uses NURBS phantoms based on reference organ masses defined in ICRP 89.[7] TIAC for the various source regions are typically entered by the user, the software and its predecessors have been used in drug development (dosimetry) for diagnostics and therapeutics. OLINDA/EXM 2.0 is commercially available through Hermes (Hermes Medical Solution). Hermes also has a voxel dosimetry software solution based upon dose point kernel methods(S-voxel).

MIRDcalc

The program includes the SAF library calculated from the ICRP pediatric and adult voxel phantoms.[24] It contains decay data obtained from ICRP Publication 107. A total of 81 source and 43 target regions and five spherical tumor models were included in the SAF library.

NCINM 2.0

National Cancer Institute dosimetry system for Nuclear Medicine (NCINM) is an organ-level dose and effective dose calculator for patients undergoing nuclear medicine procedures.[25][26] The S-values are derived for UF/NCI hybrid phantoms as well as ICRP voxel phantoms for 68 source regions and 55 target regions. The thin radio-sensitive layers of the alimentary tract utilizes the SAF from ICRP Publication 133. A user can either manually input biokinetic data or kinetic data for 105 radio-pharmaceuticals can automatically (default) populate time integrated activity curve (TIAC) for source regions.

Models versus Patient Imaging

The risk regarding near term toxicities if not care, without optimization has led to greater attention and reimbursement mechanisms for personalized dosimetry in radionuclide therapy. Early methods relied on anatomical models, and S-value calculations for both diagnostics and therapeutics. At the time of this writing U.S. Food and Drug Administration (FDA) approved methods exist for therapy model based dosimetry involving phantoms or pre-calculated dose tables (OLINDA, Rapid 3D-RD-S, etc..).[27] Additionally voxel dosimetry software has been recently released (MIM-MRT, Hermes, Voximetry-Torch, etc..) for therapies which utilizes the anatomical imaging of the treated patient.[27][28] Note both can provide organ level dose estimates. Therapy dosimetry programs of all types allow or require the use physiological imaging to provide biokinetic information.[29] Such methods can provide more accurate dosimetry estimates compared to model based dosimetry. Model based methods may fail to consider individual variability either biokinetically or anatomically. Patient-specific dosimetry in it's most pure form requires expensive imaging data, intelligent oversight and extensive computation time.

3.3 Gap Identified

A large divide could soon exist between personalized dosimetry conducted in a manner similar to external beam and the historical model based practices. It is unreasonable to expect valuable time and treasure to be allocated to improving diagnostic organ dose estimates. In large part at present time RPT is in the process of this same justification. Personalization of model based techniques might be a cost effective bridge to greater adoption of dosimetry in medicine. The current methods of personalization being explored with commercial software is typically post administration. One would hope an estimated dose could be provided to the clinician and patient prior to the administration. If the organ exposure is expected to be prospective it cannot necessarily rely on image acquisition for anatomical or physiological information. Furthermore, from a radiation safety or epidemiological perspective one would like to be able to determine these estimates retroactively, when some imaging details cannot be expected to be available.

Existing Methods of Extension and Personalization

Although size variance may seem obvious this aspect is only accounted for by creation of phantoms associated with pediatric growth.[30] It should be pointed out during puberty the single greatest predictor of variation (size) is likely age, at adulthood this is clearly no longer true. The Mirdcalc platform additionally allows one to blends S-values between phantoms.[24] This can be utilized to account for gaps in the spectrum of phantoms. However, Mirdcalc at the time of this review does not extend this feature to adult phantoms. At present time no phantom of a larger size exists past the average adult.

A common simplification used in radionuclide dosimetry is that emissions from a radionuclide can be divided into penetrating or non-penetrating radiation. This can greatly simplify the math, this concept has been used extensively to estimates of tumor dose (modeled as a sphere) in codes like OLINDA/EXE.[7] Electrons are often considered non-penetrating and photons as penetrating radiation, but this can be an oversimplification. The assumption is dependent on the energy of the

radiation as well as the size of the source region. For electrons, the absorbed fraction is ≈ 1 if the mass of the sphere is typically more than ≈ 20 g and the electron energy is less than ≈ 1 MeV.[31] Hence the simplification is essentially true at an organ level or for a significant lesion. For photons, the absorbed fraction is less than 0.1 if the mass of the sphere is less than 100 g and if the photon energy is larger than 50 keV.[31] The approximation of considering photons as penetrating radiation is valid in most pre-clinical situations, but as the mass increases, the approximation becomes inappropriate.

Note the calculation of absorbed dose with MIRD formalism uses tabulated S-values of a phantom. As has been previously mentioned the patient's anatomy is being treated mathematically and physically the same as that of the phantom, via the S-values. To apply the same architecture of calculation but include patient specific attributes, some suggest scaling the S-values.[32] The S-values can be scaled to the mass of each patient's target organ. due to the inverse dependency of the absorbed dose to the mass of the target region. The organ mass is typically determined with the use of advanced imaging (Computed Tomography (CT) or Magnetic Resonance Imaging (MRI)). The anatomical size approximately equals the physiological size if the entire organ is functioning in a like manner and has uptake. Note one can write an expression for scaling the phantom S-value for a patient's organ (x) using the following expression.[32]

$$S_{patient_x} \approx S_{phantom_x} \frac{m_{phantom_x}}{m_{patient_x}} \tag{3.1}$$

As mentioned earlier the approximation relies on the arduous task of determining mass of every organ and then scaling each S-value one by one! A more crude and less often used method involves replacing the organ masses with total masses. Note the approximation would assume each organ mass varies proportionally with total mass.

3.3.1 NCINM to Evaluate Existing Methods

NCINM is a mature example of model based internal dosimetry. Early adaptations such as MIRDose [33] were based on unrealistic phantoms which resulted in inaccuracies when compared to realistic phantoms.

It is instructive to exam

S-value scaling using organ mass on sophisticated mature phantoms like those utilized by NCINM. This exercise can be conducted through the use of NCINM's phantom library by comparing adult values with those representative of 15 year olds. Furthermore many common radiopharmaceuticals along with biokinetic and source organ information is contained in NCINM. A calculation was made for a common agent Tc-99m Furisfosmin, at an administered activity 30 mCi. This agent is utilized in cardiac stress testing. Male and Female phantoms (15 yr Adult) were compared, note biokinetics was held constant for comparison (default values). Absorbed doses for selected target organs are reported below, additionally the effective dose is shown based on ICRP-103 (tissue weighting factors).

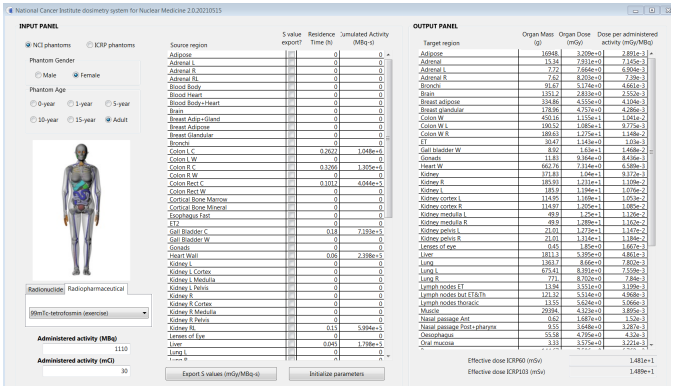

Figure 3.6: The graphical user interface of NCINM

Table 3.1: A selection of Organ Doses resulting from a typical cardiac stress test (exercise only) applied to various sized phantoms - NCINM Model (Normalized with respect to Adult Male)

Organ Doses and Dose Ratio				
Organ	Adult Male	15 yr Male	Adult Female	15yr Female
U. Bladder	13mGy	15.2mGy (1.17)	14.2mGy (1.09)	15.7mGy (1.21)
Kidney	13.1mGy	14.6mGy (1.11)	14.2mGy (1.08)	15.6mGy (1.19)
G. Bladder	20.5mGy	22.4mGy (1.09)	24.0mGy (1.17)	25.1mGy (1.22)
Heart	6.21mGy	7.30mGy (1.18)	7.60mGy (1.22)	8.32mGy (1.34)
Colon	13.2mGy	14.7mGy (1.11)	15.6mGy (1.18)	16.1mGy (1.22)
Liver	7.18mGy	8.18mGy (1.14)	8.50mGy (1.18)	9.21mGy (1.28)
Eff Dose	13.3mSv	15.6mSv	16.4mSv	17.6mSv

Table 3.2: Liver mass for various sized phantoms (NCINM) - Units (grams)

Liver Masses of NCINM Phantoms				
Organ	Adult Male	15 yr Male	Adult Female	15 yr Female
Liver	2362.2	1779	1811.3	1652

Table 3.3: Liver mass for various sized phantoms normalized to Adult Male (NCINM) - Units (grams)

Organ Masses Normalized to Adult Male				
Organ	Adult Male	15 yr Male	Adult Female	15 yr Female
Liver	1	0.75311	0.76679	0.69935

One can see that by utilizing Equation 3.1 in conjunction with Tables 3.1 and 3.3, one can calculate the expected liver dose of the adult male based on another phantom's S-value scaled with

respect to organ mass. If we utilize the 15 year old phantom and scale the S-value accordingly we would find a predicted S-value of 8.18 mGy * 0.75311 = 6.16 mGy. Note this results in a low estimate of approximately 14 percent, as one can calculate by comparing to the S-value for the adult male in Table 3.1. Note this estimate and it's associated error was found by utilizing organ masses (which may or may not be available in clinical practice). It should be noted a similar error would have resulted ($\approx 14\%$) if no correction was made (opposite direction). Interestingly by scaling we underestimate the value by the same amount as the original overestimation.

3.3.2 Path Forward

In order to achieve improved personalization applicable at the time of treatment or to estimate at a later date one must use very basic patient information. Typical information available would center around height, weight, sex and age. However in some instances lab values may also be available that may provide greater insight regarding biokinetic models. The first step necessary in adjusting model based values is proving variation exists. One could argue the extension fails on the promise of personalization because the estimate's uncertainty or accuracy is unacceptable. Personalization ideally would ensure patient attributes are considered in the dose estimate, although it must be understood it is still an estimate. Dosimetry will be utilized to a greater extent if the values are respective of patient characteristics. It is much easier to extend or modify the results of a model if the model is closer to ground truth.

It is important to examine absorbed dose variances at the tissue level based on perturbations of patient variables. It is paramount to first isolate factors that are individual in nature. Some of the factors previously mentioned uptake, kinetics, and geometric constitution all vary between individuals. These factors can be extracted from patients and might be sufficient to extend the complexity of computational models such as NCINM.

It is the goal of this research to apply Monte Carlo techniques to conduct personalized dosimetry on patient images for a number of diagnostic and therapeutic agents to determine organ dose S-values with respect geometric properties. The S-values will be directly calculated for select

target organs on patient by patient basis. The results can be benchmarked by NCINM phantom S-values.

The ultimate goal of this work is to transform phantom dosimetry into more personalized dosimetry accounting for radiation type and energy and anatomical characteristics. In computed tomography a similar transformation took place starting with the dose to an acrylic phantom of various sizes Computed Tomography Dose Index volume (CTDIvol). This value can be transformed to one that approximates a patient's dose due to their size. The personalization is termed Size Specific Dose Estimate (SSDE) which makes use of the patient's effective diameter, at a particular location. In a similar vein this research will not provide for personal radionuclide dosimetry, but it will be more personalized than existing models.

Based on the experiments conducted the second portion of this research involves optimization or rather minimization of the difference between adjusted phantom estimates and personal organ dosimetry. The minimization will based on alterations of the S-values used in the modeling of dosimetry. To minimize S-value difference and hence organ dosimetry difference correlations must be found with respect to patient attributes.

As it was first introduced in 1975, mass ratio scaling is still in use even though phantom and computational processes have improved tremendously this correction is still utilized almost 50 years later! Although the corrections mentioned are fairly straight forward and the technique would be the same across all target and organ combinations, this is not a likely outcome. Careful analysis may provide an answer or fit that is varied based on radionuclide. Furthermore, the correction applied at S-value level will vary accordingly between the tissue combinations.

CHAPTER 4

PURPOSE AND SPECIFIC AIMS

Purpose

The goals of this research is multi-factorial with respect to patient specific S-values and by proxy dosimetry. One stated goal is to determine the range of patient variation of organ S-values. This will be accomplished by acquiring imaging data of individual patients along with basic patient characteristics. The images will be segmented to create anatomical (computational) models. These models will be used in a Monte Carlo construct Monte Carlo N-Particle (MCNP) to simulate radiation transport for several radioisotopes. The results of the simulation will allow for the calculation of S-values directly. A second goal is to benchmark the variation for select organs against those calculated by NCINM which represents a modern nuclear medicine dosimetry system. Third, this research will investigate the variation if found can be correlated with patient attributes. A final objective is to explore methodologies that would extend the validity and results of modern phantoms to approach personalized S-values as a proof of concept.

Specific Aims

1. Patient Images
    - Analyze data regarding patient characteristics
    - Review image characteristics for simulation
2. Segmentation and verification
    - Automatic Segmentation
        - TotalSegmentater
    - Organs and Structures

- Organ Volumes and Masses

3. Radionuclides of Interest
    - Diagnostic and Therapeutic Agents
        - Important Radionuclide and Distinguishing Properties
4. Monte Carlo Simulation
    - Overview
    - MCNP6
        - Material Card
        - Lattice File
        - Source Definition
        - Tallies
    - Calculation of S-values
5. NCINM Simulation for Radionuclides Studied (Phantom)
    - Obtain organ mass values per phantom
    - Obtain organ S-values for each studied emitter
6. Analysis
    - Benchmark S-value results to NCINM models
    - Explore variation for organ S-values
    - Possible correlations between patient S-values and personal characteristics
    - Discuss possible methods to personalize phantom S-values

CHAPTER 5

MATERIAL, METHODS AND INTERMEDIATE RESULTS

5.1 Patient Data

Patient Image Origin

To evaluate the variances between the S-values of patients and phantoms, one needs diagnostic images. The gold standard modality of anatomical imaging is computed tomography. Fifty-six patient computed tomography exams were made available by the NIH. The patient images were de-identified prior, meaning all information that could link to a specific individual were expunged. The images are clinical exams most involve the Chest, Abdomen and Pelvis (CAP) of persons due to clinical indications. These images are assumed to be ordered by a physician for the individual's benefit. The subsequent analysis and use of these image datasets provided no direct harm or benefit for the individual patients. The patient data has been deemed to be exempt by the **IRB!** (**IRB!**).

Patient Characteristics Review

Along with the images basic patient characteristics was also included such as sex, age, height, and weight. Ideally the parameters would span through a range of values representative of patients found in the clinic.

Furthermore it would also be optimal if the only one characteristic under investigation would be altered at a time. The second request is outside of reality and the first can only be accomplished with a large cohort of patients. Although the number of patients in this study are not trivial, it cannot be claimed that they are perfectly representative. The female patients studied as shown in Table 5.1 range in age from 21 to just 41 years of age. Therefore this dataset skews young respective to published studies of patients undergoing nuclear medicine procedures.[34] The male patients to a lesser degree scale younger than expected patients. Note in Figure 5.1 and Figure 5.2 the patient attributes have been normalized to the distribution's mean value. Additionally the figures display patient characteristics in the form of a box plot. A Box plot is a visual representation of the five-number summary of a data set. The minimum, first quartile (Q1), median (Q2), third quartile (Q3), and maximum. The box itself represents the interquartile range (IQR), which is the middle 50% of the data, while the whiskers extend from the box to the minimum and maximum values.

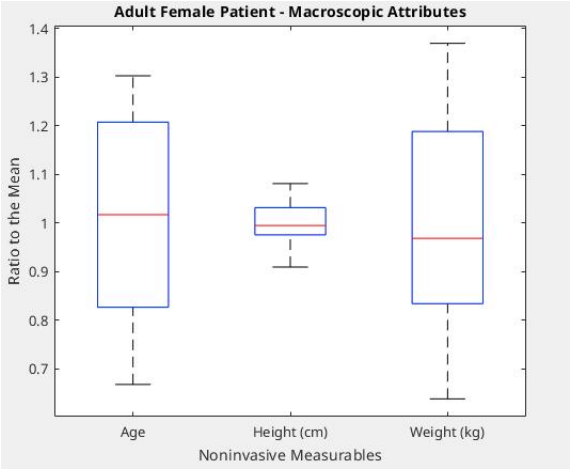

Figure 5.1: Female Patient Attributes

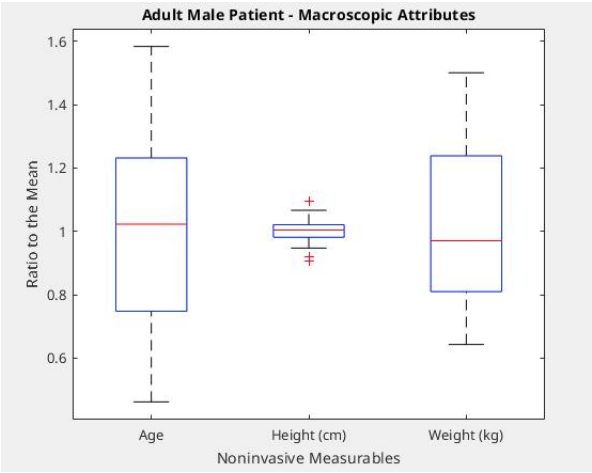

Figure 5.2: Male Patient Attributes

In either case the male and female subjects do seem to represent the expected range of height, weight and Body Mass Index (BMI) values required to study their influence on patient organ dose.[35] Note BMI is a derived quantity which can be calculated as follows $BMI = \frac{weight}{height^2}$ in units kg/m^2.

Image Properties

The images of these patients were obtained in high resolution axial images 512 x 512 matrices in the x-y plane. In this plane the resolution was typically submillimeter. However in the z-direction, along the bed of the scanner the resolution was more modest typically 5 mm (reconstruction). High and low BMI female patients are depicted in figures 5.3 and 5.4. One can see the BMI correlates quite well with the effective diameter of the patients. In figure 5.5, one can see quite easily qualitatively the size difference between M20 (BMI = 40 kg/m^2 and M14 (BMI 18 kg/m^2).

It should be noted that the images utilized are realistic even in manners that are inconvenient to this study. The most notable difficulty is with respect to the absence of expected organs. Based on the subsequent segmentation and review of the clinical images the absence of some organs were noted. To the extent possible the clinical patients with these abnormal presentations were included, however problematic and absent organs were removed from analysis. A final disclosure is the model of anatomy was acquired of patients in a supine position.

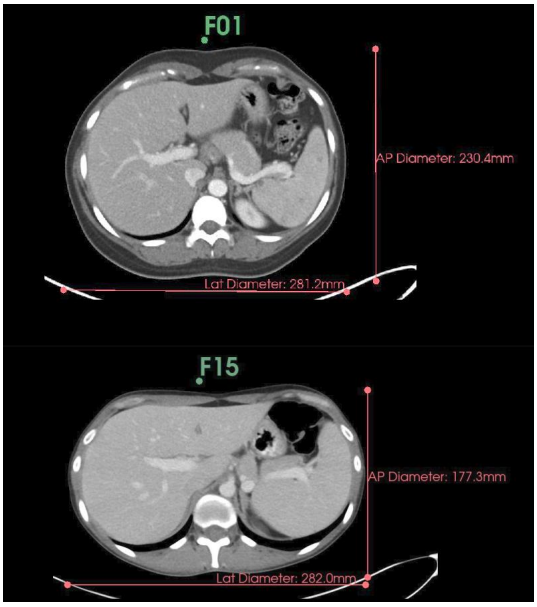

Figure 5.3: CT image mid liver (axial) of patients F01 - 36.38 BMI and F15 - 16.05 BMI

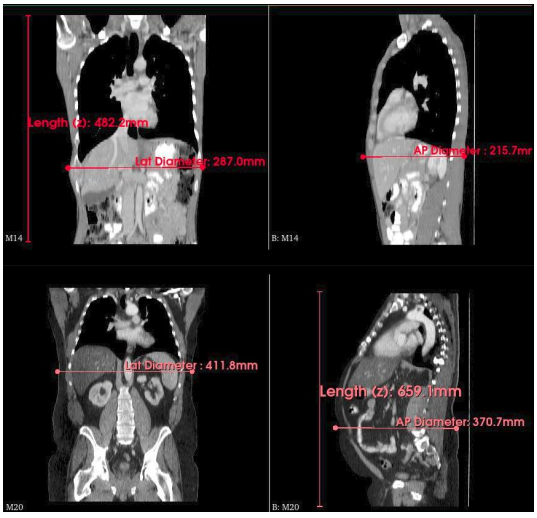

Figure 5.4: CT images of two male patients,low BMI (M14 18 kg/m^2) and with a high BMI (M20 39.8 kg/m^2)

Table 5.1: Female patient properties

Female Patient Attributes				
ID	Age	Height (cm)	Weight (kg)	BMI (kg/m^2)
1	22	161	94.3	36.38
2	27	158.9	78.6	31.13
3	26	155.3	61.3	25.42
4	38	166.3	81.8	29.58
5	40	160	56.2	21.95
6	24	162	94	35.82
7	25	171.5	66.7	22.68
8	33	175.6	68.6	22.25
9	36	159.8	84.5	33.09
10	21	170.5	60.7	20.88
11	22	168	69.9	24.77
12	31	163	64	24.09
13	30	172.7	64.6	21.66
14	36	162	87.5	33.34
15	26	165.4	43.9	16.05
16	40	160.3	91.8	35.73
17	36	176.1	82.5	26.6
18	35	153.7	63.8	27.01
19	38	170.4	79.8	27.48
20	39	167.3	58	20.72
21	38	158.1	75.4	30.17
22	33	158.9	45	17.82
23	27	154	48.6	20.49
24	28	166.2	48.7	17.63
25	29	161.2	53	20.4
26	41	153.2	66.6	28.38
27	39	166.3	86.1	31.13
28	23	168	57.4	20.34
29	37	152.6	80	34.35
30	24	148.1	51.9	23.66

Table 5.2: Male Patient Properties

Male Patient Attributes				
ID	Age	Height (cm)	Weight (kg)	BMI (kg/m^2)
1	56	173	108	36.1
2	26	160	54	21.1
3	55	184	111	32.8
4	39	177	104	33.2
5	55	162	78	29.7
6	57	180	86	26.5
7	59	174	84	27.7
8	50	179	98	30.6
9	24	179	75	23.4
10	36	180	79	24.4
11	22	177	63	20.1
12	21	173	63	21
13	72	172	69	23.3
14	28	178	57	18
15	51	176	71	22.9
16	34	167	68	24.4
17	34	188	65	18.4
18	70	173	95	31.7
19	58	169	68	23.8
20	50	178	126	39.8
21	41	177	86	27.5
22	46	193	104	27.9
23	45	176	90	29.1
24	47	171	70	23.9
25	60	182	105	31.7
26	46	185	105.8	30.9

Table 5.3: Female Image Properties

Female Image Properties						
ID	X	Y	Z	Vx(cm)	Vy(cm)	Vz(cm)
1	512	512	120	0.08203	0.08203	0.5
2	512	512	131	0.09766	0.09766	0.5
3	512	512	123	0.09766	0.09766	0.5
4	512	512	129	0.09766	0.09766	0.5
5	512	512	128	0.08594	0.08594	0.5
6	512	512	125	0.09766	0.09766	0.5
7	512	512	129	0.0875	0.0875	0.5
8	512	512	133	0.09043	0.09043	0.5
9	512	512	132	0.08984	0.08984	0.5
10	512	512	133	0.08613	0.08613	0.5
11	512	512	141	0.08984	0.08984	0.5
12	512	512	592	0.07031	0.07031	0.1
13	512	512	133	0.07031	0.07031	0.5
14	512	512	121	0.07812	0.07812	0.5
15	512	512	129	0.07812	0.07812	0.5
16	512	512	125	0.09766	0.09766	0.5
17	512	512	142	0.09766	0.09766	0.5
18	512	512	123	0.09219	0.09219	0.5
19	512	512	134	0.09766	0.09766	0.5
20	512	512	127	0.09375	0.09375	0.5
21	512	512	124	0.09375	0.09375	0.5
22	512	512	120	0.07422	0.07422	0.5
23	512	512	127	0.08203	0.08203	0.5
24	512	512	127	0.08203	0.08203	0.5
25	512	512	126	0.07812	0.07812	0.5
26	512	512	122	0.07812	0.07812	0.5
27	512	512	123	0.08164	0.08164	0.5
28	512	512	127	0.08203	0.08203	0.5
29	512	512	131	0.09766	0.09766	0.5
30	512	512	118	0.07031	0.07031	0.5

Table 5.4: Male Image Properties

Male Image Properties						
ID	X	Y	Z	Vx(cm)	Vy(cm)	Vz(cm)
1	512	512	136	0.08984	0.08984	0.5
2	512	512	116	0.06836	0.06836	0.5
3	512	512	135	0.08984	0.08984	0.5
4	512	512	148	0.07812	0.07812	0.5
5	512	512	138	0.08594	0.08594	0.5
6	512	512	141	0.08203	0.08203	0.5
7	512	512	123	0.08594	0.08594	0.5
8	512	512	86	0.08594	0.08594	0.5
9	512	512	143	0.07812	0.07812	0.5
10	512	512	95	0.07031	0.07031	0.5
11	512	512	128	0.07812	0.07812	0.5
12	512	512	72	0.07031	0.07031	0.5
13	512	512	56	0.07422	0.07422	0.5
14	512	512	98	0.0625	0.0625	0.5
15	512	512	74	0.07031	0.07031	0.5
16	512	512	127	0.08203	0.08203	0.5
17	512	512	103	0.07031	0.07031	0.5
18	512	512	127	0.08594	0.08594	0.5
19	512	512	121	0.08047	0.08047	0.5
20	512	512	131	0.09766	0.09766	0.5
21	512	512	87	0.09434	0.09434	0.5
22	512	512	154	0.09375	0.09375	0.5
23	512	512	133	0.08203	0.08203	0.5
24	512	512	87	0.07031	0.07031	0.5
25	512	512	136	0.08789	0.08789	0.5
26	512	512	151	0.09766	0.09766	0.5

5.2 Determination of Radionuclide and Organ Selection

Radionuclide imaging normally centers around photon emitters that are not consider toxic. Tissues that are near and far from uptake organs are exposed to ionizing radiation. The impact of lower exposures falls into the realm of epidemiology and health physics. Typically only after many years and large groups of people have been observed can the effect of low ionizing radiation be realized and quantified.[36]

Diagnostic Radionuclides

Many diagnostic procedures may be repeated on a given individual. The practice of repeated procedures compounds issues with excessive dose practices and estimation inaccuracies. Precision medicine implies that the risk to benefit relationship is understood and conveyed to the patient and provider.

Tc-99m

To determine which radio-pharmaceuticals would be most beneficial to analyze, a compelling reason must be identified. Some studies that are repeated routinely in nuclear medicine are cardiac studies. These exams also have a relatively high administered activity. The use of nuclear cardiology might have long term implications, furthermore other competing technologies such as stress echo exists along with cardiac computed tomography. The majority of these exams use Tc-99m as the radioisotope. Furthermore it is important to remember in nuclear medicine, 80 percent of all exams performed utilize Tc-99m.Hence it is important to study Tc-99m emissions if one is interested in general nuclear medicine dosimetry.

F-18

A consistent area of growth in nuclear studies has centered around positron emission tomography. Fluorodeoxyglucose (FDG) is the most widely used agent in positron emission tomography

(PET). The positron emitter utilized by this drug is F-18, it is unique in that the positron dose is locally significant, but it subsequently leads to high energy photon emissions. This property contrasts nicely when compared with relatively weak gamma and beta emitters. A PET agent because of its emission profile I believe will add significantly to this research. It might reveal dependencies of personalized organ doses with patient characteristics differently than the other agents. FDG has played a leading role in inflammation, infection and cancer detection and monitoring. FDG accumulates in the body in proportion to glucose metabolism. Organs and tissues with high glycolytic rates like the brain generally will have high accumulation. It is cleared by via the patient's urine. Neurology has increasingly made use of agents like Flutemetamol (F-18 radioisotope) to provide insight and quantify the amyloid burden of patients.[37] Around forty percent of Flutemetamol activity is cleared through the renal pathway, the highest absorbed doses are typically found in the bladder wall, kidneys and liver.[38] Flurpiridaz was first approved by the FDA for diagnosing coronary artery disease in September of 2024, it provides higher diagnostic accuracy than the agents used in conjunction with SPECT imaging. One study found the organ receiving the largest mean absorbed dose was the kidneys at 0.24 rem/mCi, followed by the heart wall at 0.18 rem/mCi.[39] PET imaging is clearly expanding, however one isotope is clearly dominant and should be included in this study due to continued utilization.

Radionuclide Therapy

Radionuclide therapy because of both efficacy and toxicity concerns greatly favor personalized dosimetry. Models may seem inadequate since most do not allow lesion delineation. However, their relative importance regarding dosimetry and the aspect of self-dose make them worthy of study. Additionally nuclear medicine dosimetry programs may provide insight with respect to the toxicity of targeted agents, if not tumor dosimetry.

Lu-177

In recent years the approval of two Lu-177 based agents has greatly expanded RPT in scope and number. Lutathera (Lutetium Dotatate) is used to treat neuroendocrine tumors. The dose is administered in 200 mCi fractions two months apart for a total of four administrations. The administrations are delivered as infusions with an administration time of approximately thirty minutes. Note this therapy requires a concurrent administration of amino acids that must be started approximately thirty minutes prior to Lutathera and lasts approximately three hours to reduce the kidney dose.[40][41] In 2022 a second Lu-177 based agent trade name Pluvicto was approved by the FDA.[42] This therapy also known as Lu-177 PSMA (Prostate Specific Membrane Antigen) is prescribed to treat metastatic castration resistant prostate cancer. Lu-177 is known to be a therapeutic isotope because of the emission of beta particles with a maximum energy of approximately 497 keV. However Lu-177 also emits low energy gamma rays that allow post therapy imaging. Both have the potential to contribute to cross-fire effects. Although tumors are not organs and cannot be included in this research, however clearance pathways can be studied to assess toxicity. A large percentage of both radiopharmaceuticals are eliminated via the renal process, which may lead to toxicity.[43] The kidneys have been recognized as dose-limiting organs for therapeutic radiopharmaceuticals, with a historical cumulative absorbed dose limit of 23Gy. This limit is based on external beam radiation therapy (EBRT).[44] Over the course of multiple fractions, facilities have claimed to approach or exceed 23 Gy for the kidneys.[45]

I-131

One of the earliest therapeutic radionuclides is I-131. Sodium Iodide (I-131) therapy has been use to for many years to treat diseases of the thyroid including hyperthyroidism types of thyroid cancer. It works by targeting and destroying thyroid cells which highly absorb iodine. I-131 emits beta particles with a maximal energy of 606 keV (89% abundance, as well as others) and 364 keV gamma rays (81% abundance as well as others). These emissions make it interesting in comparison to Lu-177 because it also emits high energy photons, this could make it's S-values

dependence on patient characteristics quite different. Furthermore I-131 is uniquely interesting in terms of MIRD formalism because it has a strong uptake by an organ (similar to targeted radiopharmaceutical therapies and tumors).[46] The dose toxicity of I-131 has been mapped to renal clearance rates by researchers to aid in dose optimization.[47]

5.3 Segmentation of Patient Images and Mass Determination

Segmentation

Image segmentation can be thought of as the partitioning of a media into regions based upon some shared characteristic. In medical imaging the segmentation process has been utilized for disease diagnosis, treatment planning, and monitoring of disease progression.[48] Manual segmentation has has been considered the gold standard for delineating anatomical structures, but this process is both time and labor-intensive. Furthermore manual segmentation in medical imaging may require an expert level of knowledge that is hard to justify. Manual segmentation also relies on a human factor that is varied and hard to quantify. A general purpose medical autosegmentation software solution has been desired for some time. Researchers from the University Hospital Basel (Switzerland) developed a ready-to-use segmentation toolkit that enables automatic segmentation for most of the major anatomic structures based on CT images called TotalSegmentator.[49]

TotalSegmentator

TotalSegmentator is a deep learning segmentation model. The model is publicly available (including its training data), furthermore it segments most anatomically relevant structures throughout the body. It is based on a robust final dataset created by sampling retrospectively 1204 CT examinations from 2012 to 2020 from the University Hospital Basel (Picture Archiving and Communication System (PACS)). A total of 104 anatomic structures are automatically segmented if they are present in the image. Segmentation was supervised by two expert body imaging physicians. To speed the process further, they used an iterative learning approach in which the model was originally trained then corrected after 20, 100 and 1204 patients to provide a ground truth model. The model is available as an extension using 3D slicer, furthermore it can be used in batch mode with programs such as python and matlab. Additionally totalsegmentator can be accessed as an online service by uploading imaging files.

Implementation

It is important to define volumetric characteristics of the patient images to prepare simulations. Totalsegmentator has become well know in last couple of years, but earlier the model was less known and accessible. A batch code or script was created to apply Totalsegmentator to the aforementioned patient images (Nifti fortmat). The results from automatic segmentation leads to masks for 104 tissues in the human body.

	Segment	Voxel count	Volume (LM) [mm3]	**Volume (LM) [cm3]**
1	spleen	60285	202833	202.833
2	right kidney	47852	161001	161.001
3	left kidney	57617	193856	193.856
4	gallbladder	2204	7415.5	7.4155
5	liver	388302	1.30647e+06	1306.47
6	stomach	39132	131662	131.662
7	aorta	34038	114523	114.523
8	inferior vena cava	13996	47090.4	47.0904
9	portal vein	6030	20288.3	20.2883
10	pancreas	23835	80194.4	80.1944
11	right adrenal gland	349	1174.23	1.17423
12	left adrenal gland	743	2499.87	2.49987
13	superior lobe of left lung	182295	613343	613.343
14	inferior lobe of left lung	183933	618854	618.854
15	superior lobe of right lung	149563	503214	503.214
16	middle lobe of right lung	69559	234036	234.036
17	inferior lobe of right lung	221715	745974	745.974

Figure 5.5: A selection of volumetric data from F01, courtesy of 3D slicer

Additionally volumetric data for each patient and tissue was obtained in terms of pixels. Using knowledge of pixel size in each dimension (x,y,z) for the datasets the organ volumes for each patient were determined. The organ volumes were then multiplied by tissue density (user defined, not Hounsfield based) to determine organ masses that are used directly in S-value calculations. This work was typically accomplished using the MATLAB programming language. Importantly the organ segmentation masks are the early basis of the geometry model used in Monte Carlo simulation. The masks or segmentation files were converted to a binary voxel format from arrays (nrrd) in preparation for their eventual implementation with MCNP.

TotalSegmentators Known Issues

The automatic segmentation software has been shown to perform well even when presented with atypical anatomy. These challenges include tissues that are missing (splenectomy), displaced (bowels displaced by inguinal hernia), or duplicated (transplant kidney). However failures do exist cases, such as missing small parts of the colon or iliac arteries and mixing up neighboring vertebrae and ribs. These issues should not be consequential if the organ is neither a source or target organ.

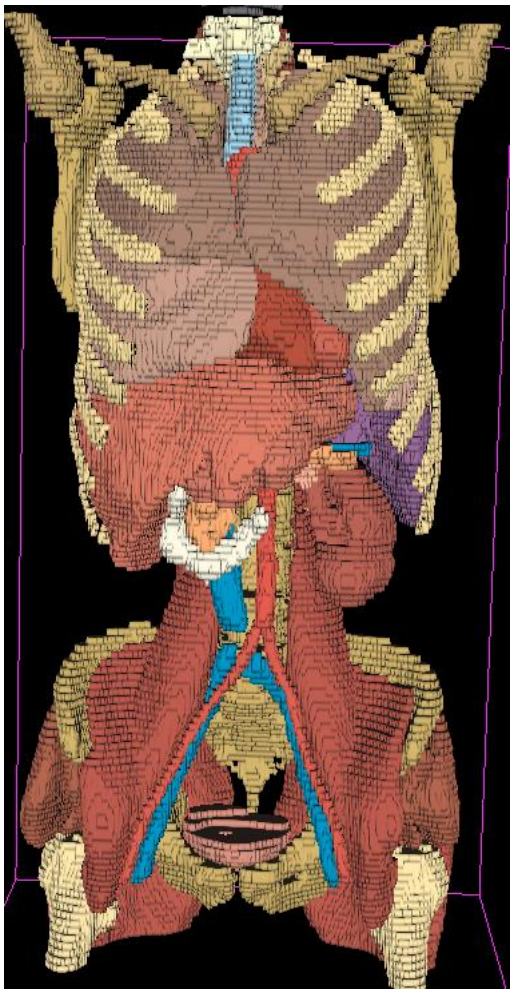

Figure 5.6: Organ segmentation of M9, with the removal of obscuring organs to visualize vessel discontinuity and absence of right kidney. Courtesy of 3D slicer

Model Results and Target Organ Selection

Based on the model created and a review of the original patient images, several items were noted. To calculate S-values, the organ must be present in the model! Several organs were missing, some were due to the patient population for instance a number of the patients based on images and totalsegmentator had underwent cholecystectomies (gall bladder removals). Because this was quite a few patients this organ was removed from consideration. Additionally the adrenal glands were not identifiable by totalsegmentator, although they were believed to be present albeit difficult to discern. Note the thyroid was not contained in the images, the bladder was missing on many subjects also due to the organ being outside the scan length. As noted earlier totalsegmentator struggles with the intestines creating a model and deciding where the small intestines end and the colon begins is not reliable. Furthermore the esophagus while consistently modeled it was not contained, its volume could not be reliably related to patient macroscopic attributes. Tissues with similar challenges were also excluded. Note although these organs S-values were not calculated, their information was still very much used for radiation transport in the simulation.

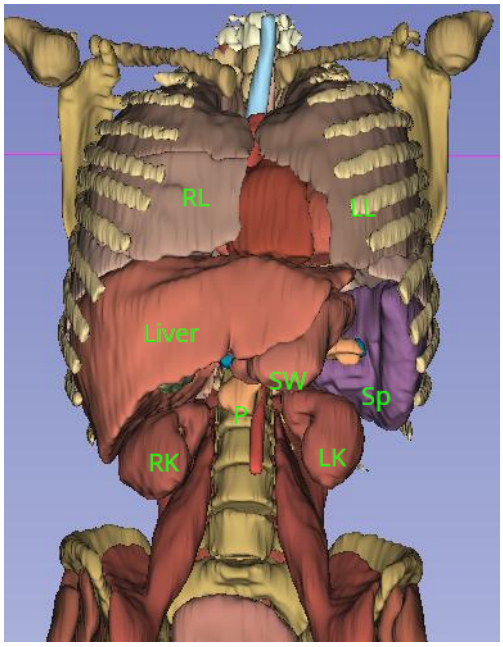

Figure 5.7: Organ segmentation of F15, with the removal of obscuring organs to label and visualize organs that will have S-values calculated. Courtesy of 3D slicer

5.3.1 Simulation

1. Radionuclides
    - Tc-99m, F-18, Lu-177, I-131
2. Source Organs
    - Right Kidney
    - Left Kidney

    These organs are important because they are integral to the removal of radiopharmaceuticals. Hence they are consistently source organs, and in some radiopharmaceutical therapies they are the dose limiting organs. Both are included as source organs and not independently because we may not know a priori that a kidney has been removed.
3. Target Organs
    - Spleen

    Its location is in the left upper quadrant of the abdomen above the left kidney. It also can become large due to various conditions, the prevalence of these conditions increases with age.
    - Right Kidney

    This organ allows for the study of self dose, and can be directly compared to the left kidney for a sanity check.
    - Left Kidney

    This organ allows for the study of self dose, and can be directly compared to the right kidney for a sanity check.

- Liver

  This organ is a large organ and can greatly vary in size. Additionally the right lobe of the liver is in close contact with the right kidney.

- Pancreas

  The pancreas is located in front of the left kidney and spleen.

- Left Lung

  Located within the chest and anterior filling the rib cage, this organ while large is distant from the kidneys in this analysis. A sanity check allows for it to be compared with the Right Lung

- Right Lung

  Located within the chest and anterior filling the rib cage, this organ while large is distant from the kidneys in this analysis. A sanity check allows for it to be compared with the Left Lung

5.4 Monte Carlo Simulation

5.4.1 Overview

Monte Carlo (MC) method is a modeling tool, capable of achieving a close adherence to reality, concerning the analysis of complex systems. Generally it is a method for estimation of the solution of mathematical problems by means of random numbers or probabilities. It is very useful for complex problems which cannot be resolved in closed form. A physical process comprises individual probabilistic events that are simulated sequentially. These events are governed by probability distributions statistically sampled to describe the total process.
Therefore, a large number of trials are required to describe adequately the physical phenomenon. Considering particle interaction, this method follows every single particle emitted from a source to its death (absorption, escape, etc.). Probability distributions are randomly sampled to determine the outcome at each step of every particle life, using transport data. In the MC method, solutions are obtained by simulating individual particles and recording some aspects of their average behavior rather than solving an explicit equation.
Radiation transport is one of the areas that has greatly benefited from Monte Carlo methods. Furthermore basic research has provided interaction cross sections that it utilizes in the modeling of radiation transport. It is not possible to directly measure internal radiation emitted, transported and absorbed in patients, hence Monte Carlo methods have historically been utilized. In the MIRD schema the use of these methods is typically hidden from end user. However tables of S-values for source and target organ pairs of phantom models are based on MC results.

5.4.2 MCNP 6.2 and Implementation

The Monte Carlo simulations conducted in this work utilize MCNP 6.2 which is a general-purpose, continuous-energy, generalized-geometry, time-dependent, Monte Carlo radiation transport code. It is supported and maintained by Los Alamos National Laboratory (LANL). The software is exported, controlled and distributed by Radiation Safety

Information Computational Center (RSICC) wich provided the aforementioned version.[50] The software was tested and installed on a Linux workstation (CPU AMD Ryzen 9 16 core processor, with 32 GB of RAM), this setup was used to conduct all simulations.

The software models radiation transport through varied media and can record properties during the simulation such as current, flux and energy deposition.[51] The program allows for structures to be modeled based on geometrical constructs know as combinatorial geometry. These constructs can be simple or more complex like the previously introduced stylized human phantoms. The structures (known as cells) must be defined in terms of composition and density. Furthermore the source of radiation must also be described. The source requires dimension, location along with particle emission type, energy and trajectory. Once these items are in place various experiments can be simulated.

Units of MCNP

The unit of interest with respect to length in MCNP, must be in centimeters. Energy units in the software must be provided in terms of MeV. Mass is in the form of grams, and density is given by g/cm^3. Note the input variables in for the simulation were provided in these units.

Details

It should be noted MCNP relies on adherence to a particular format. Furthermore at the heart of the transport code beyond it's design is cross-sectional data libraries. These libraries contain information about the probability of various interactions between the particle and the media, which may even include the production of secondary particles. To initialize a simulation or computational experiment a series of cards and elements must be completed. Through the process of describing the methods of implementation used in this work, MCNP will be briefly introduced.

Geometry

The geometry of the simulation space must be defined. As previously mentioned one can utilize simple geometric shapes along with material properties. However in more complicated geometries alternative methods are better suited. Due to the repetitive nature of human anatomy many elements (voxels) have the same properties, but are not well represented by large geometric shapes. The patient CT datasets were partitioned by totalsegmentator into 104 volumes representing various organs and other tissues. The segmentation process provided tags for the various tissues along with volumetric data, the data was saved as a binary file for each patient. In addition to the tag information, basic geometric data with respect to the resolution and matrix of the images was also utilized to create an accurate simulation. MCNP allows for the creation of a lattice geometry consisting of a single rectangular parallelepiped, appropriately established. A bounding "window" is defined in the higher universe, it is filled by the lattice universe. The lattice is filled with other cells that contain the appropriate material information. To accomplish the lattice build a MATLAB code was modified to read in both image properties (matrix and resolution) and the aforementioned binary file for each patient. Additionally densities for each of the 104 volumes was hard coded to match either soft tissue, air, bone, or lung values in g/cm^3. Furthermore these tissues were also identified as one of the four corresponding materials as defined by the materials card. The material card contains information of the composition of each material. To accomplish this goal each material has a unique material number, since each material is a mixture by nature additional details are needed. The first detail is the elemental composition, for instance Hydrogen is represented as 1000, where 1 represents its atomic number and the remaining three digits relate to its isotope. The second detail for each isotope is its mass fraction of the mixture. In the end each material contains a list of isotopes with corresponding mass fractions, this information will govern the cross sections utilized in radiation transport in these mediums. Furthermore the separate density information will help determine how likely or often an interaction will occur in the various volumes.

Source

Additionally utilizing the binary file created by totalsegmentator a geometric representation of the source term was realized. Each patient has a unique representation of a radiation source in their simulation. The left and right kidneys of each patient were chosen as source organs. A MATLAB script opened the patient binary file and looped over the two source organs tagging these voxels and saving a source file that was later called by the main MCNP code. The MATLAB file hence defines the kidney elements as source positions that will be randomly sampled during MCNP simulation. It should be noted additional details are needed for a complete source definition (SDEF Card). The particle type was run independently for both photons and electrons emissions for each isotope studied. ICRP 107 can be used to provide nuclear decay data for dosimetric calculations, hence this is the source of information regarding decay properties for Tc-99m, F-18, Lu-177 and I-131.[52] ICRP 107 contains additional information regarding isotopes however only the energy and yield data was used in this simulation. The document separately lists photons and beta emissions, it should be pointed out the beta emission energies are provided in terms of their mean energy. The values are appended to the end of the main MCNP input file for each isotope studied. The appended values refer to source specification (SI) which corresponds to the isotopes energies and source probabilities (SP) which corresponds to the yield. The location of the source (particle) radiation was contained to the patient's kidneys and the direction was isotropic in nature. To keep the same S-value calculation and simulation format the positrons emitted by F-18 were modeled as an electrons. Note prior versions of MCNP before MCNP6 used electrons to model some aspects of positron transport due to their similarities, the annihilation is simulated as the production of photons. It should be noted no significant difference was observed between the electron / photons analog results and positron transport. Energies and yields for this conversion were provided by ICRP 107.

Mode and Termination

MCNP can be used to track the interaction of various particle types. A declaration of the problem mode has to be declared. The mode used in this research was (p,e), which denotes that both photons and electrons will be transported in the simulation, regardless of the initial particle type. Two types of terminations exist in the transport process. The first is the termination of an individual random walk. In the simulation, this process is governed by the lower energy limit of 1 keV for both electrons and photons. Below the 1 keV limit the particle was treated as absorbed at its location. No strict guidance was used with respect to probabilities although in general this can be implemented in the form of a "Cut" card. A second termination is the end of the simulation of all histories. During the simulation for all particle types, patients and isotopes the number of particle histories (NPS) was set to 10^7, which was found to provide sufficient statistical accuracy (Appendix A).

Tally and Relative Error

Tallying is the process of measuring parameters of interest. F8 tally is a surface-crossing estimator in a cell that models a physical detector. The source cell is first credited with the energy times the weight of the source particle, which in this simulation is taken to be unity. When a particle crosses a surface, the energy times the weight is subtracted from the account of the cell it is leaving and is added to the cell it is entering. At the end of the history the result in each tally cell is divided by the source weight. The *F8 tally can be used for photons and electrons to calculate energy deposition on a surface or in a cell. Note if no tracks entered the cell no energy would be imparted. In this simulation the *F8 tallies were conducted for the following organs spleen, left kidney, right kidney, liver, stomach, pancreas, left lung and right lung. Note simulations were conducted twice per patient per radionuclide to simulate both photon and electron emissions. For each tally, MCNP not only calculates the sample mean $\overline{x}$, but several

other statistics the most import is the relative error R defined as

$$R \equiv \frac{S_{\overline{x}}}{\overline{x}} \tag{5.1}$$

5.5 NCINM Values for Isotopes of Interest and Reference Phantoms

To understand how to optimize NCINM it is instructive to investigate its computational basis. Specific-absorbed fractions were calculated using MCNPX, a well vetted Monte Carlo radiation transport code. The phantoms that are used for comparison and to extend NCINM were collaboratively developed by the National Cancer Institute and the University of Florida. Multiple pediatric phantoms exist in male and female form simulating infants to teenagers, however only a single adult phantom exists per sex respectively. Phantom anatomy match reference data from ICRP 89, tissue densities were also obtained from ICRP 89 and ICRU 46. As previously mentioned NCINM has a total of 68 source organs and 55 target tissues, following the guidance of ICRP 110. Specific-absorbed fractions (SAF) were calculated for multiple combinations of source and target regions across an energy spectrum ranging from 10 keV to 6 MeV for both electron and photons, 25 energies in total. The SAF $\Phi(\mathrm{r}_t \leftarrow \mathrm{r}_s)$ was obtained by dividing the absorbed fraction by m_t (the blood mass of each tissue, ICRP-89). The S-value is then obtained by taking SAF for a source region r_s and a target region r_t and multiplying by the energy and probability respectively. $S(r_t \leftarrow \mathrm{r}_s) = \sum_i E_i Y_i \Phi(\mathrm{r}_t \leftarrow \mathrm{r}_s, E_i)$, E_i and Y_i are energies and yields of the i^{th} nuclear transformation of the radionuclide. The probabilities Y_i and energies E_i were obtained via ICRP 107.[52] Note in NCINM the contributions from daughter nuclei are ignored.

Table 5.5: A selection of target organs masses for the adult NCINM phantoms - Units $(grams)$

NCINM Organ Mass Values (grams)		
Organ	Male	Female
Spleen	228.93	187.8
Right Kidney	219.33	185.93
Left Kidney	219.44	185.9
Liver	2362.2	1811.3
Stomach	187.45	159.91
Pancreas	173.2	144.672
Left Lung	876.36	675.41
Right Lung	1030	771

Phantom Organ Mass

To understand a patient's S-value variance for the target organs studied it is important to consider their mass variation with respect to a phantom comparisons. To accomplish this goal the mass values for NCINM's adult male and female phantoms were compiled. The mass values in grams for the two phantoms are shown in table 5.5.

Isotope S-values for Adult NCINM Phantoms

S-values for organs of interest for both diagnostic isotopes Tc-99m and F-18 for both the NCINM's male and female phantoms are shown Table 5.6. Furthermore therapeutic isotopes Lu-177 and I-131 are displayed in Table 5.7. These S-values will provide a benchmark for patient comparison. The comparison is useful for characterizing the patient's S-value distribution. Furthermore when used in conjunction with patient properties, the potential may exist to extend NCINM's values to approach personalization. It is instructive prior to exploring the variation of patient S-values to examine the variation seen in phantom S-values. Table 5.8 depicts the S-values for four NCINM phantoms for the isotope Tc-99m, these phantoms are expected to be similar with respect to complexity and realism. Hence the observed variation should be attributable to the geometric aspects of tissue positioning, shape and size. Some target organs showed a large S-value variation between the phantoms like the lobes of the lung and to a lesser degree the kidneys. However, the spleen by comparison showed little variance. Although these results are not directly based on a individual patients, the experiment may provide useful insight regarding the analysis of patient results.

Table 5.6: A selection of S-values tabulated for select target organs resulting from Tc-99m and F-18 (source organ kidneys) for adult NCINM phantoms - Units $mGy/(MBq * s)$

S-values Diagnostic				
	Tc-99m		F-18	
Organ	Male	Female	Male	Female
Spleen	5.2032e-07	5.13e-07	3.6327e-06	3.6771e-06
Right Kidney	1.16e-05	1.29e-05	1.541e-04	1.732e-04
Left Kidney	1.16e-05	1.3e-05	1.541e-04	1.734e-04
Liver	2.8136e-07	2.7256e-07	1.9261e-06	1.8988e-06
Stomach	3.5745e-07	2.8965e-07	2.4064e-06	1.992e-06
Pancreas	1.0895e-06	1.0973e-06	7.598e-06	7.7272e-06
Left Lung	5.0713e-08	7.44e-08	4.0775e-07	5.8973e-07
Right Lung	4.6664e-08	5.9193e-08	3.835e-07	4.8376e-07

Table 5.7: A selection of S-values tabulated for select target organs resulting from Lu-177 and I-131 (source organ kidneys) for adult NCINM phantoms - Units $mGy/(MBq * s)$

S-values Therapeutic				
	Lu-177		I-131	
Organ	Male	Female	Male	Female
Spleen	1.3691e-07	1.3581e-07	1.4206e-06	1.4277e-06
Right Kidney	7.24e-05	8.16e-05	1.039e-04	1.185e-04
Left Kidney	7.24e-05	8.17e-05	1.38e-04	1.186e-04
Liver	7.222e-08	7.0184e-08	7.5338e-07	7.3922e-07
Stomach	9.2008e-08	7.4609e-08	9.4557e-07	7.7909e-07
Pancreas	2.8799e-07	2.9023e-07	2.9823e-06	3.0246e-06
Left Lung	1.3092e-08	1.9265e-08	1.5429e-07	2.2394e-07
Right Lung	1.1948e-08	1.5246e-08	1.4425e-07	1.82e-07

Table 5.8: A selection of S-values for select target organs resulting from Tc-99m (source organ kidneys) applied to various sized phantoms - Units $mGy/(MBq * s)$

S-values and Ratio				
Organ	Adult Male	15 yr Male	Adult Female	15 yr Female
Spleen	5.2032e-07	5.5561e-07	5.1309e-07	5.8688e-07
Spleen Ratio	1	1.0678	0.9861	1.1279
Right Kidney	1.16e-05	1.38e-05	1.29e-05	1.45e-05
Right Kidney Ratio	1	1.1897	1.1121	1.25
Left Kidney	1.16e-05	1.38e-05	1.3e-05	1.45e-05
Left Kidney Ratio	1	1.1897	1.1207	1.25
Liver	2.8136e-07	2.7674e-07	2.7256e-07	3.1838e-07
Liver Ratio	1	0.98358	0.96872	1.1316
Stomach	3.5745e-07	4.5253e-07	2.8965e-07	3.6208e-07
Stomach Ratio	1	1.266	0.81032	1.013
Pancreas	1.0895e-06	1.1995e-06	1.0973e-06	1.2957e-06
Pancreas Ratio	1	1.101	1.0072	1.1893
Left Lung	5.0713e-08	9.2493e-08	7.44e-08	1.0579e-07
Left Lung Ratio	1	1.8239	1.4671	2.0861
Right Lung	4.6664e-08	7.7374e-08	5.9193e-08	8.4685e-08
Right Lung Ratio	1	1.6581	1.2685	1.8148

CHAPTER 6

RESULTS AND ANALYSIS

6.1 Patient Organ Masses

6.1.1 Overview and Determination

The patient images were segmented by totalsegmentator, which resulted in 104 tissues. These volumes were used to create a sophisticated simulation geometry. The variation of volumes that are neither source or target organs certainly may impact the transport of radiation. However these volume variations do not directly impact the S-value calculations for the target organs. Furthermore slight inconsistencies in totalsegmentator should not significantly impact the validity of this research study. As has been previously shown the volumetric data for the various structures was one of the outputs of totalsegmentator, as displayed in Figure 5.5. The number of voxels associated with each structure multiplied by the voxel size ($V_x * V_y * V_z$, units cm^3) as recorded in Table 5.3 and 5.4 was utilized. This provided a volume for each target organ of every patient. Next the volumes were multiplied by a set density for each target organ, the resulting target organ masses are displayed in Table 6.1 and 6.2. These target mass values are used explicitly to calculate S-values. The S-value which was previously introduced in chapter 2, is shown below highlighting its dependence on target organ's mass.

$$S(r_T \leftarrow r_s) = \sum{}_i E_i Y_i \Phi(r_T \leftarrow r_s, E_i), E_i \tag{6.1}$$

Where Φ is also known as the specific absorbed fraction (SAF), which is inversely dependent upon the $m(r_T)$.

$$SAF = \Phi(r_T \leftarrow r_s, E_i) = \frac{\phi(r_T \leftarrow r_s, E_i)}{m(r_T)} \tag{6.2}$$

6.1.2 Patient Variation

To study variations in the mass of the organs of subjects, a comparison was made to the phantom mass values tabulated in Table 5.5. A summary of the results depicted in Figures 6.1 and 6.2 follows.

Spleen

The mass ratio for spleens of females was found to be greater than one, whereas the male cohort was found to be slightly less than the phantom analog. Both datasets show a strong variation in mass, which is not surprising.

Kidneys, Liver, and Lung

Both datasets show the kidney's mean values are slightly less than normalization, furthermore the variance is modest. The same can be said for the liver and the lobes of the lung.

Stomach and Pancreas

The stomach mass was relatively high with a great deal of variance which was expected. On the other hand the pancreas's mean was low with respect to phantom models, but the mass of the organ did not vary greatly between patients.

Exclusions

As previously mentioned even when certain volumes were found to be absent, unless they were directly involved in the calculation the patient was kept for simulation. It should be noted when the target volume was not fully imaged (scanner range) the organ S-values were removed from consideration. Male subject (M5) did not have a left kidney, this target organ S-value was removed, however the rest of the S-values for this subject were retained (even though the left kidney is a source organ). In a similar manner male patients (M9 and M16) were found to have an absent right kidney, the same process was followed. However male patient (M13) had source

organs (kidneys) not fully imaged, and this led to the resulting S-values for all organs being removed.

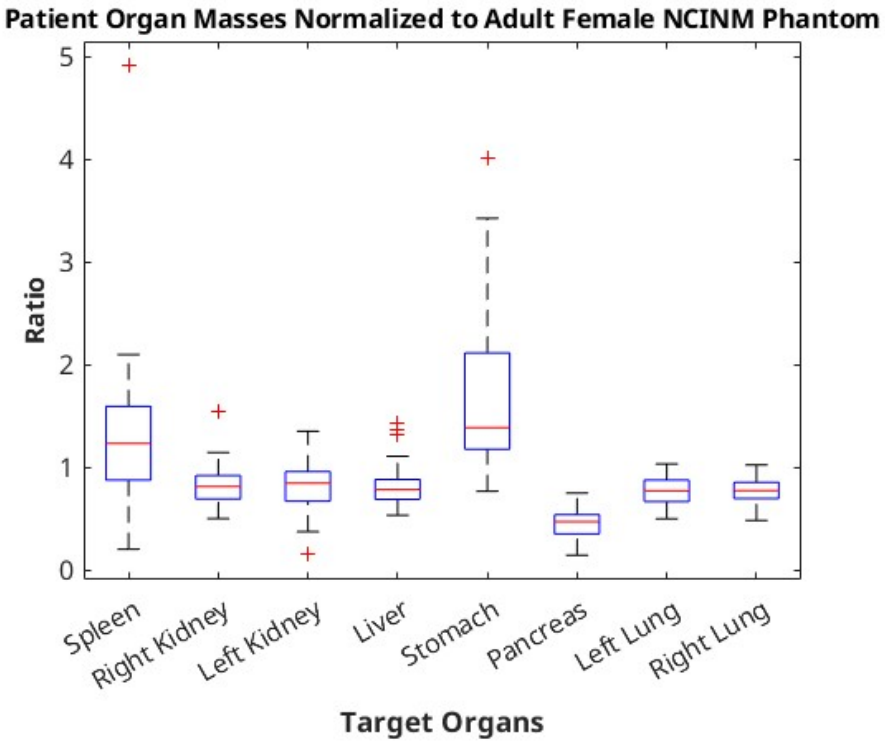

Figure 6.1: Female Patient Organ Masses Normalized with respect to NCINM Adult Female Phantom

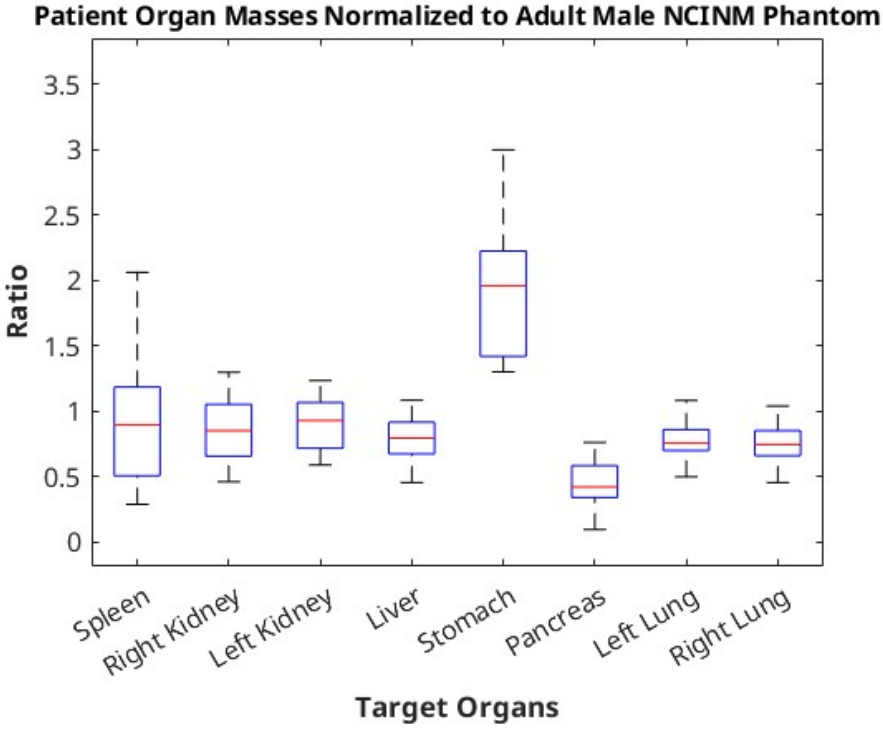

Figure 6.2: Male Patient Organ Masses Normalized with respect to NCINM Adult Male Phantom

Table 6.1: Select Female Organ Mass Values

Female Orgam Mass Values (grams)								
	Spleen	R. Kidney	L. Kidney	Liver	Stomach	Pancreas	L. Lung	R. Lung
f01	210.9	167.4	201.6	1359	136.9	83.4	364.7	439
f02	922.3	212.5	251.3	2587	546.2	84.34	421.6	548.7
f03	299.2	156.2	171.4	1419	338	77.92	463.5	541.8
f04	332.6	193.8	202.4	2372	280.3	79	451.5	507.7
f05	37.72	162.8	69.2	1200	139.4	20.72	617.5	729.5
f06	236.7	170.6	161	1182	188.7	56.67	336.3	488.4
f07	121.5	111.1	107.6	1451	547.6	75	540.1	632.2
f08	202.6	134	134.4	1545	215.4	79.65	572.9	651.9
f09	250	183.7	178	1772	244.4	48.98	519.1	590.2
f10	325.6	144	153.1	1735	205.2	55.17	525.9	603.5
f11	293.4	191.2	175.9	1547	132.5	58.76	488.7	600.6
f12	202.4	123.5	129.8	1368	366.4	72.85	584.4	631.8
f13	147.9	171	164	1568	221.7	69.23	654.3	756.4
f14	176.7	164.1	201.7	1881	140.3	108.2	449.6	518.8
f15	340.7	146.1	119.6	1330	139.2	39.87	522.2	562.2
f16	160.3	157.5	168.1	1506	642.6	88.9	697.6	788.7
f17	190.1	122.2	113.5	1417	259.8	71.4	602.3	675.7
f18	80.03	194.4	184.8	1247	347	69.88	479.5	501.4
f19	259.4	130.6	133.8	1363	227.8	79.62	564.2	699.2
f20	136.6	137.5	27.69	1218	220.7	43.67	591.5	621.6
f21	357.5	146.2	162.1	1597	194.3	68.79	440	543.5
f22	130	128.7	129	1129	150	55.31	650.9	745.4
f23	164.3	93.12	106	1194	122.5	31.68	606.6	658.1
f24	283	118.7	124.4	1288	210.8	51.08	342.6	370.9
f25	196.3	122.6	119.5	1213	188.1	66.42	615.8	777.1
f26	394.1	167.1	162.8	2006	221.4	47.63	424.2	538.2
f27	334.3	195.2	202.2	2459	301.6	75.92	479.1	561.7
f28	226.2	287.1	240.1	1264	269.7	67.34	372.1	418
f29	237.8	131.6	152.5	1520	430.8	44.47	475.3	535.5
f30	274.8	93.21	127.6	962.4	352.9	50.81	558.6	619.3

Table 6.2: Select Male Organ Mass Values

Male Orgam Mass Values (grams)								
	Spleen	R. Kidney	L. Kidney	Liver	Stomach	Pancreas	L. Lung	R. Lung
m01	270.4	218.3	233.2	2453	369.6	71.78	666.6	732.5
m02	117.7	119.4	129.7	1081	269.6	50.22	439	470.3
m03	393.9	230.8	238.7	1964	494	100.9	1134	1255
m04	159	214.9	217.8	1586	402.1	74.4	678.6	781.6
m05	256.3	285	1.604	1587	562.5	90.16	494.5	662.7
m06	218.2	187.5	195.4	1872	244.2	112.2	661.1	807.2
m07	377.3	170.9	180.8	1944	394.3	109.5	1019	1047
m08	244.8	207.3	209	2025	411.6	94.37	615.8	770.4
m09	341.9	0	255.4	1749	247	63.2	649.9	663.5
m10	237.6	168.2	175.5	1884	355.4	89	735.4	808.2
m11	66.47	271.1	157.2	1938	257.8	60.28	706.9	774.6
m12	205.3	175	177.1	1818	301.2	105.9	507.6	624
m13	157.8	0	8.915	1603	413.4	16.92	559.3	661.1
m14	84.41	169.1	158.2	1740	253.2	22.24	745.7	840.3
m15	113.7	238.6	255.3	2128	462.3	56.53	665.5	766.9
m16	73.98	0.4825	267.2	1888	325	41.23	629.6	688.1
m17	112.4	146.6	162.1	1467	254.6	53.48	890.4	922.4
m18	170.3	194.4	204.3	2322	355.8	84.14	811.1	910.6
m19	71.99	139.2	132.2	1605	429.1	72.09	714.1	893.2
m20	472.6	260.3	271.5	4899	367.5	128	614.9	744.8
m21	266.2	101.6	253.7	2567	687.8	62.54	448.9	371
m22	277.2	200.1	212.2	2298	442.1	73.34	950.5	1073
m23	188.6	232.6	223.9	2424	245.4	132.3	631.2	763.7
m24	193.2	148.8	136.8	1359	368.9	71.59	682.7	738.9
m25	349.4	236.4	218.7	1530	286.6	104.4	784.3	875.3

CHAPTER 7

PATIENT SPECIFIC ORGAN S-VALUES - TABLES

S-value Calculation

Typically as has been previously shown S-values are normally derived from the specific absorbed fractions (SAF) and absorbed fractions $\phi(r_T \leftarrow r_s$. The dependency is shown below.

$$S(r_T \leftarrow r_s) = \sum{}_i E_i Y_i \Phi(r_T \leftarrow r_s, E_i) \tag{7.1}$$

$$SAF = \Phi(r_T \leftarrow r_s, E_i) = \frac{\phi(r_T \leftarrow r_s, E_i)}{m(r_T)} \tag{7.2}$$

However, in this computational experiment, the S-values were directly calculated from the Monte Carlo simulations as reported by Lamart et al.[53] An analysis was separately conducted for photons and electrons. This exercise provided the energy deposition in each tallied organ r_T per emitted particle (photon or electron). Hence $E_\gamma(r_T)$ and $E_\beta(r_T)$ (MeV/particle) for photons and electrons. The energy deposition per particle must be multiplied by either the total photon Y_γ or electron Y_β yield per decay. Furthermore their product must be summed and divided by the target organ mass M_T. Using in a house MATLAB program the output files of tallies for the various target organs were acquired along with the relative error for each tally. A second routine calculated the S-values for each patient and isotope via the equation below in the units (mGy/(MBq·s)).

$$S(r_T \leftarrow r_s) = 1.602 * 10^{-4} \frac{1}{M(r_T)} (E_\gamma(r_T) Y_\gamma + E_\beta(r_T) Y_\beta) \tag{7.3}$$

Note the electron and photon yields are shown in table 7.1. The male and female S-values are furthermore displayed for each isotope.

Table 7.1: Total photon and electron yield per disintegration for selected isotopes

Total photon and electron yield per disintegration		
Isotope	**Electron Yield**	**Photon Yield**
Tc-99m	5.52	6.47
F-18	0.967	1.93
Lu-177	2.27	1.55
I-131	1.76	1.83

For each tally, MCNP not only calculates the sample mean $\overline{x}$, but several other statistics. The most important of these statistics is the relative error R defined below.

$$R = S_{\overline{x}}/\overline{x} \tag{7.4}$$

Where $S_{\overline{x}}$ the standard deviation of the tally mean and $\overline{x}$ is the mean. In a similar manner to the calculation for S-values which is a weighted sum of the photon and electron components, one can determine the relative simulation S-value error in a similar fashion. One can obtain a weighted error for the simulation of the S-values through the use of the relative error and the deposited energy for each particle in two terms $R_{E_\gamma}(r_T) * E_\gamma(r_T)$ and $R_{E_\beta}(r_T) * E_\beta(r_T)$. The relative error and deposited energy can be used to determine $\Delta S(r_T \leftarrow r_s)$ written in units of (mGy/(MBq·s)).

$$\Delta S(r_T \leftarrow r_s) = 1.602 * 10^{-4} \frac{1}{M(r_T)} (R_{E_\gamma}(r_T) E_\gamma(r_T) Y_\gamma + R_{E_\beta}(r_T) E_\beta(r_T) Y_\beta) \tag{7.5}$$

The relative error in the S-value then can be determine as shown in the equation below. The relative S-value error for all isotopes and target organs was found to be less than 1 percent, values are tabulated in Appendix A.

$$R_S = \frac{\Delta S(r_T \leftarrow r_s)}{S(r_T \leftarrow r_s)} \tag{7.6}$$

Table 7.2: Female Patients Specific S-values **Tc-99m**

S-values Female Tc-99m ($mGy/(MBq * s)$)								
	Spleen	R. Kidney	L. Kidney	Liver	Stomach	Pancreas	L. Lung	R. Lung
f01	7.33e-07	1.11e-05	1.11e-05	3.95e-07	3.71e-07	8.87e-07	1.46e-07	9.95e-08
f02	3.81e-07	9.01e-06	8.88e-06	3.11e-07	4.29e-07	6.69e-07	6.3e-08	6.66e-08
f03	4.27e-07	1.2e-05	1.2e-05	3.56e-07	2.69e-07	7e-07	8.13e-08	8.2e-08
f04	6.49e-07	1.04e-05	1.04e-05	3.36e-07	3.58e-07	8.28e-07	1.25e-07	7.98e-08
f05	1.21e-06	1.75e-05	1.59e-05	6.1e-07	7.54e-07	8.6e-07	1.31e-07	1.35e-07
f06	6.18e-07	1.22e-05	1.2e-05	3.81e-07	4.01e-07	7.29e-07	1.39e-07	1.02e-07
f07	8.35e-07	1.79e-05	1.77e-05	6.51e-07	4.68e-07	1.01e-06	1.09e-07	1.33e-07
f08	6.51e-07	1.45e-05	1.45e-05	3.61e-07	2.88e-07	7.68e-07	9.51e-08	6.47e-08
f09	3.94e-07	1.14e-05	1.13e-05	4.01e-07	2.92e-07	6.52e-07	9.16e-08	7.99e-08
f10	6.6e-07	1.34e-05	1.36e-05	4.52e-07	3.28e-07	7.37e-07	1.02e-07	7.87e-08
f11	6.18e-07	1.13e-05	1.12e-05	4.96e-07	3.66e-07	7.81e-07	9.61e-08	1.09e-07
f12	9.14e-07	1.56e-05	1.55e-05	5.99e-07	5.02e-07	9.35e-07	1.72e-07	1.53e-07
f13	8.47e-07	1.23e-05	1.21e-05	4.82e-07	4.47e-07	8.28e-07	1.27e-07	9.74e-08
f14	6.11e-07	1.08e-05	1.1e-05	3.29e-07	4.2e-07	7.42e-07	1.09e-07	7.71e-08
f15	6.23e-07	1.51e-05	1.47e-05	5.15e-07	4.4e-07	7.93e-07	1.17e-07	9.7e-08
f16	7.91e-07	1.24e-05	1.25e-05	3.82e-07	2.95e-07	6.07e-07	9.76e-08	1.2e-07
f17	6.53e-07	1.66e-05	1.62e-05	4.31e-07	3.91e-07	7.22e-07	8.45e-08	8.16e-08
f18	5.95e-07	1.08e-05	1.09e-05	3.96e-07	3.45e-07	7.97e-07	1.22e-07	9.16e-08
f19	6.35e-07	1.46e-05	1.45e-05	4.19e-07	3.62e-07	7.37e-07	1.06e-07	1.18e-07
f20	2.55e-07	2.37e-05	1.93e-05	5.85e-07	2.99e-07	6.82e-07	8.73e-08	1.12e-07
f21	6.75e-07	1.3e-05	1.31e-05	4.96e-07	3.54e-07	7.93e-07	1.17e-07	1.15e-07
f22	1.04e-06	1.51e-05	1.51e-05	6.12e-07	5.51e-07	1.03e-06	1.86e-07	1.27e-07
f23	1.09e-06	1.89e-05	1.9e-05	5.12e-07	4.54e-07	1.18e-06	1.55e-07	1.13e-07
f24	8.69e-07	1.61e-05	1.61e-05	5.47e-07	5.39e-07	1.09e-06	1.31e-07	1.09e-07
f25	9.16e-07	1.61e-05	1.6e-05	5.22e-07	4.98e-07	1.02e-06	1.49e-07	1.01e-07
f26	7.47e-07	1.23e-05	1.23e-05	4.45e-07	3.49e-07	8.12e-07	1.06e-07	1.07e-07
f27	6.61e-07	1.04e-05	1.04e-05	3.25e-07	3.57e-07	8.14e-07	1.13e-07	7.65e-08
f28	5.54e-07	8.23e-06	8.08e-06	4.29e-07	4.07e-07	7.45e-07	1.19e-07	1.01e-07
f29	6.54e-07	1.39e-05	1.41e-05	4.33e-07	3.34e-07	8.75e-07	1.26e-07	1.21e-07
f30	8.62e-07	1.73e-05	1.78e-05	5.22e-07	3.99e-07	1.04e-06	1.42e-07	1.45e-07

Table 7.3: Male Patients Specific S-values **Tc-99m**

S-values Male Tc-99m ($mGy/(MBq * s)$)								
	Spleen	R. Kidney	L. Kidney	Liver	Stomach	Pancreas	L. Lung	R. Lung
m01	2.98e-07	9.64e-06	9.61e-06	2.36e-07	2.14e-07	4.21e-07	7.85e-08	6.19e-08
m02	1.01e-06	1.66e-05	1.68e-05	5.07e-07	3.87e-07	8.53e-07	1.59e-07	1.15e-07
m03	3.7e-07	9.42e-06	9.39e-06	2.51e-07	2.25e-07	5.12e-07	7.32e-08	5.38e-08
m04	6.99e-07	1.04e-05	1.02e-05	4.11e-07	3.34e-07	7.29e-07	1.31e-07	1.05e-07
m05	1.15e-07	1.58e-05	-	5.29e-07	1.32e-07	3.67e-07	5.58e-08	1.05e-07
m06	3.92e-07	1.12e-05	1.12e-05	2.81e-07	2.07e-07	4.7e-07	8.85e-08	7.22e-08
m07	4.94e-07	1.23e-05	1.23e-05	3.38e-07	2.56e-07	4.42e-07	8.53e-08	7.69e-08
m08	4.5e-07	1.06e-05	1.05e-05	3.19e-07	2.56e-07	5.49e-07	8.35e-08	7.97e-08
m09	9.7e-07	-	1.75e-05	1.45e-07	3.92e-07	6.05e-07	1.17e-07	5.38e-08
m10	5.28e-07	1.26e-05	1.25e-05	4.11e-07	3.48e-07	6.79e-07	8.49e-08	7.74e-08
m11	7.61e-07	1.04e-05	9.98e-06	4.45e-07	4.31e-07	7.41e-07	1.27e-07	1.07e-07
m12	7.89e-07	1.24e-05	1.24e-05	4.63e-07	3.54e-07	7.03e-07	1.45e-07	1.35e-07
m13	-	-	-	-	-	-	-	-
m14	9.82e-07	1.34e-05	1.31e-05	4.2e-07	5.4e-07	9.44e-07	1.43e-07	1.21e-07
m15	4.24e-07	9.08e-06	9.04e-06	3.2e-07	3.4e-07	5.74e-07	8.27e-08	7.67e-08
m16	1.5e-06	-	1.69e-05	1.4e-07	6.64e-07	7.31e-07	2.14e-07	6.99e-08
m17	8.4e-07	1.39e-05	1.39e-05	5e-07	4.7e-07	7.33e-07	1.54e-07	9.73e-08
m18	4.99e-07	1.09e-05	1.09e-05	2.85e-07	2.3e-07	5.22e-07	1.15e-07	7.83e-08
m19	4.31e-07	1.56e-05	1.53e-05	3.3e-07	2.92e-07	5.71e-07	8.57e-08	1.02e-07
m20	4.24e-07	8.38e-06	8.31e-06	2.15e-07	2.66e-07	4.22e-07	1.1e-07	7.63e-08
m21	7.37e-07	1.15e-05	1.25e-05	2.53e-07	4.28e-07	5.71e-07	8.88e-08	5.18e-08
m22	5.69e-07	1.07e-05	1.06e-05	3.18e-07	3.03e-07	6.1e-07	1e-07	9.58e-08
m23	4.97e-07	9.69e-06	9.63e-06	3.18e-07	2.58e-07	4.92e-07	8.49e-08	7.79e-08
m24	6.62e-07	1.49e-05	1.48e-05	4.33e-07	3.8e-07	7.09e-07	9.67e-08	9.39e-08
m25	3.63e-07	9.79e-06	9.63e-06	2.89e-07	1.96e-07	4.31e-07	7.43e-08	6.77e-08

Table 7.4: Female Patients Specific S-values **F-18**

S-values Female F-18 ($mGy/(MBq * s)$)								
	Spleen	R. Kidney	L. Kidney	Liver	Stomach	Pancreas	L. Lung	R. Lung
f01	6.16e-06	0.000136	0.000136	3.2e-06	2.92e-06	6.9e-06	1.25e-06	8.82e-07
f02	3.11e-06	0.000109	0.000109	2.45e-06	3.36e-06	5.08e-06	5.59e-07	5.92e-07
f03	3.54e-06	0.000149	0.00015	2.87e-06	2.09e-06	5.4e-06	7.29e-07	7.4e-07
f04	5.37e-06	0.000127	0.000127	2.66e-06	2.72e-06	6.43e-06	1.07e-06	7.02e-07
f05	1.06e-05	0.000215	0.000203	4.98e-06	6.12e-06	6.72e-06	1.15e-06	1.19e-06
f06	5.2e-06	0.00015	0.000149	3.08e-06	3.21e-06	5.84e-06	1.21e-06	9.06e-07
f07	6.98e-06	0.000222	0.000221	5.19e-06	3.65e-06	7.71e-06	9.39e-07	1.12e-06
f08	5.49e-06	0.000181	0.000182	2.93e-06	2.29e-06	6.09e-06	8.37e-07	6.06e-07
f09	3.25e-06	0.000139	0.000139	3.17e-06	2.26e-06	4.93e-06	7.97e-07	7.08e-07
f10	5.47e-06	0.000166	0.000167	3.66e-06	2.58e-06	5.61e-06	9.04e-07	7.11e-07
f11	5.1e-06	0.000137	0.000137	4e-06	2.86e-06	6.13e-06	8.47e-07	9.54e-07
f12	7.64e-06	0.000193	0.000193	4.79e-06	3.9e-06	7.2e-06	1.46e-06	1.28e-06
f13	7.09e-06	0.00015	0.000149	3.85e-06	3.45e-06	6.45e-06	1.1e-06	8.56e-07
f14	5.18e-06	0.000134	0.000136	2.66e-06	3.24e-06	5.81e-06	9.64e-07	6.99e-07
f15	5.19e-06	0.000186	0.000184	4.17e-06	3.39e-06	6.06e-06	1.05e-06	8.8e-07
f16	6.66e-06	0.000152	0.000154	3.07e-06	2.3e-06	4.66e-06	8.35e-07	1.02e-06
f17	5.49e-06	0.000207	0.000204	3.52e-06	3.09e-06	5.78e-06	7.6e-07	7.47e-07
f18	5.05e-06	0.000133	0.000133	3.19e-06	2.74e-06	6.31e-06	1.07e-06	8.23e-07
f19	5.37e-06	0.000183	0.000182	3.36e-06	2.79e-06	5.79e-06	9.31e-07	1.03e-06
f20	2.09e-06	0.000295	0.000257	4.76e-06	2.34e-06	5.31e-06	7.69e-07	1e-06
f21	5.56e-06	0.00016	0.000161	3.96e-06	2.73e-06	6.05e-06	1.03e-06	1e-06
f22	8.7e-06	0.000188	0.000188	4.93e-06	4.24e-06	8.04e-06	1.59e-06	1.09e-06
f23	9.26e-06	0.000238	0.00024	4.21e-06	3.54e-06	9.37e-06	1.36e-06	9.97e-07
f24	7.28e-06	0.0002	0.0002	4.4e-06	4.26e-06	8.58e-06	1.17e-06	9.99e-07
f25	7.66e-06	0.0002	0.0002	4.21e-06	3.89e-06	7.8e-06	1.28e-06	8.98e-07
f26	6.12e-06	0.000151	0.000151	3.51e-06	2.66e-06	6.06e-06	9.11e-07	9.15e-07
f27	5.45e-06	0.000127	0.000127	2.57e-06	2.68e-06	6.26e-06	9.66e-07	6.64e-07
f28	4.61e-06	9.89e-05	9.79e-05	3.44e-06	3.22e-06	5.69e-06	1.05e-06	9.02e-07
f29	5.44e-06	0.000172	0.000175	3.46e-06	2.57e-06	6.81e-06	1.09e-06	1.04e-06
f30	7.21e-06	0.000216	0.000221	4.25e-06	3.13e-06	8.14e-06	1.23e-06	1.25e-06

Table 7.5: Male Patients Specific S-values **F-18**

S-values Male F-18 ($mGy/(MBq * s)$)								
	Spleen	R. Kidney	L. Kidney	Liver	Stomach	Pancreas	L. Lung	R. Lung
m01	2.59e-06	0.000111	0.000111	1.96e-06	1.71e-06	3.3e-06	6.82e-07	5.62e-07
m02	8.91e-06	0.000194	0.000195	4.29e-06	3.19e-06	7e-06	1.42e-06	1.07e-06
m03	3.14e-06	0.000108	0.000108	2.04e-06	1.77e-06	4.19e-06	6.46e-07	4.88e-07
m04	6.03e-06	0.000118	0.000117	3.32e-06	2.63e-06	5.86e-06	1.12e-06	8.96e-07
m05	9.72e-07	0.00018	-	4.45e-06	1.04e-06	2.81e-06	5.05e-07	9.35e-07
m06	3.31e-06	0.000129	0.000129	2.28e-06	1.62e-06	3.71e-06	7.7e-07	6.39e-07
m07	4.24e-06	0.000142	0.000142	2.78e-06	2.03e-06	3.43e-06	7.38e-07	6.68e-07
m08	3.92e-06	0.000121	0.000121	2.62e-06	2.1e-06	4.5e-06	7.44e-07	7.18e-07
m09	8.36e-06	-	0.0002	1.2e-06	3.14e-06	4.88e-06	1.05e-06	5.12e-07
m10	4.43e-06	0.000144	0.000144	3.38e-06	2.7e-06	5.34e-06	7.61e-07	7e-07
m11	6.6e-06	0.000118	0.000115	3.66e-06	3.43e-06	5.85e-06	1.11e-06	9.54e-07
m12	6.76e-06	0.000142	0.000142	3.81e-06	2.83e-06	5.54e-06	1.25e-06	1.17e-06
m13	-	-	-	-	-	-	-	-
m14	8.66e-06	0.000153	0.000151	3.46e-06	4.36e-06	7.75e-06	1.26e-06	1.09e-06
m15	3.72e-06	0.000104	0.000104	2.69e-06	2.83e-06	4.7e-06	7.61e-07	7.02e-07
m16	1.32e-05	-	0.000193	1.12e-06	5.36e-06	5.82e-06	1.86e-06	6.29e-07
m17	7.26e-06	0.00016	0.00016	4.2e-06	3.86e-06	6.01e-06	1.36e-06	8.83e-07
m18	4.25e-06	0.000125	0.000125	2.34e-06	1.81e-06	4.17e-06	9.92e-07	6.82e-07
m19	3.77e-06	0.00018	0.000179	2.78e-06	2.41e-06	4.68e-06	7.8e-07	9.17e-07
m20	3.57e-06	9.57e-05	9.55e-05	1.71e-06	2.06e-06	3.29e-06	9.45e-07	6.56e-07
m21	6.39e-06	0.000135	0.000143	2.08e-06	3.42e-06	4.47e-06	8.1e-07	4.97e-07
m22	4.89e-06	0.000122	0.000122	2.58e-06	2.35e-06	4.76e-06	8.78e-07	8.31e-07
m23	4.26e-06	0.000111	0.000111	2.6e-06	2.03e-06	3.86e-06	7.56e-07	6.89e-07
m24	5.68e-06	0.000172	0.000171	3.61e-06	3.06e-06	5.67e-06	8.67e-07	8.44e-07
m25	3.08e-06	0.000112	0.000111	2.39e-06	1.59e-06	3.48e-06	6.68e-07	6.13e-07

Table 7.6: Female Patients Specific S-values **Lu-177**

S-values Female Lu-177 ($mGy/(MBq * s)$)								
	Spleen	R. Kidney	L. Kidney	Liver	Stomach	Pancreas	L. Lung	R. Lung
f01	2.45e-07	6.52e-05	6.51e-05	1.22e-07	1.09e-07	2.79e-07	4.62e-08	2.9e-08
f02	1.22e-07	5.19e-05	5.18e-05	9.47e-08	1.36e-07	2.11e-07	1.83e-08	1.93e-08
f03	1.37e-07	7.32e-05	7.32e-05	1.1e-07	7.79e-08	2.17e-07	2.37e-08	2.44e-08
f04	2.11e-07	6.07e-05	6.07e-05	1.02e-07	1.04e-07	2.66e-07	4e-08	2.3e-08
f05	5.36e-07	0.000104	0.000103	1.96e-07	2.38e-07	2.58e-07	4.04e-08	3.98e-08
f06	2.07e-07	7.25e-05	7.24e-05	1.18e-07	1.21e-07	2.33e-07	4.53e-08	3.07e-08
f07	2.84e-07	0.00011	0.00011	2.06e-07	1.4e-07	3.18e-07	3.17e-08	3.85e-08
f08	2.16e-07	8.93e-05	8.93e-05	1.12e-07	8.46e-08	2.5e-07	2.86e-08	1.89e-08
f09	1.23e-07	6.65e-05	6.64e-05	1.22e-07	8.47e-08	1.92e-07	2.7e-08	2.33e-08
f10	2.15e-07	8.08e-05	8.08e-05	1.42e-07	9.53e-08	2.21e-07	3.08e-08	2.29e-08
f11	2.01e-07	6.55e-05	6.55e-05	1.56e-07	1.07e-07	2.51e-07	2.82e-08	3.22e-08
f12	3.05e-07	9.47e-05	9.47e-05	1.89e-07	1.51e-07	3e-07	5.32e-08	4.57e-08
f13	2.86e-07	7.18e-05	7.17e-05	1.5e-07	1.34e-07	2.71e-07	3.97e-08	2.83e-08
f14	2.03e-07	6.56e-05	6.56e-05	1.01e-07	1.25e-07	2.36e-07	3.27e-08	2.26e-08
f15	2.04e-07	9.04e-05	9.02e-05	1.62e-07	1.28e-07	2.41e-07	3.72e-08	2.86e-08
f16	2.68e-07	7.38e-05	7.38e-05	1.19e-07	8.75e-08	1.86e-07	2.92e-08	3.69e-08
f17	2.17e-07	0.000102	0.000102	1.35e-07	1.17e-07	2.33e-07	2.47e-08	2.41e-08
f18	1.99e-07	6.34e-05	6.34e-05	1.21e-07	1.03e-07	2.57e-07	3.72e-08	2.67e-08
f19	2.11e-07	9.06e-05	9.06e-05	1.31e-07	1.06e-07	2.4e-07	3.36e-08	3.81e-08
f20	8.93e-08	0.000145	0.000143	1.84e-07	9.1e-08	2.17e-07	2.77e-08	3.41e-08
f21	2.2e-07	7.79e-05	7.79e-05	1.55e-07	1.03e-07	2.44e-07	3.44e-08	3.36e-08
f22	3.6e-07	9.3e-05	9.29e-05	1.94e-07	1.61e-07	3.38e-07	6.29e-08	3.86e-08
f23	3.84e-07	0.00012	0.00012	1.64e-07	1.32e-07	4.03e-07	4.82e-08	3.33e-08
f24	2.98e-07	9.86e-05	9.86e-05	1.7e-07	1.61e-07	3.49e-07	3.91e-08	3.21e-08
f25	3.09e-07	9.9e-05	9.89e-05	1.64e-07	1.46e-07	3.28e-07	4.7e-08	2.94e-08
f26	2.45e-07	7.28e-05	7.28e-05	1.37e-07	1.01e-07	2.44e-07	3.09e-08	3.1e-08
f27	2.15e-07	6.05e-05	6.05e-05	9.82e-08	1.03e-07	2.59e-07	3.49e-08	2.19e-08
f28	1.8e-07	4.58e-05	4.57e-05	1.31e-07	1.22e-07	2.24e-07	3.66e-08	2.96e-08
f29	2.16e-07	8.45e-05	8.45e-05	1.35e-07	9.71e-08	2.75e-07	3.79e-08	3.61e-08
f30	2.85e-07	0.000108	0.000109	1.66e-07	1.16e-07	3.39e-07	4.25e-08	4.56e-08

Table 7.7: Male Patients Specific S-values **Lu-177**

S-values Male Lu-177 ($mGy/(MBq * s)$)								
	Spleen	R. Kidney	L. Kidney	Liver	Stomach	Pancreas	L. Lung	R. Lung
m01	9.8e-08	5.32e-05	5.32e-05	7.43e-08	6.56e-08	1.35e-07	2.43e-08	1.89e-08
m02	3.64e-07	9.62e-05	9.62e-05	1.68e-07	1.2e-07	3.03e-07	5.14e-08	3.61e-08
m03	1.21e-07	5.13e-05	5.12e-05	7.85e-08	6.85e-08	1.74e-07	2.26e-08	1.64e-08
m04	2.42e-07	5.57e-05	5.56e-05	1.31e-07	1.02e-07	2.45e-07	4.17e-08	3.21e-08
m05	3.58e-08	8.41e-05	-	1.73e-07	3.93e-08	1.11e-07	1.64e-08	3.19e-08
m06	1.3e-07	6.27e-05	6.27e-05	8.84e-08	6.28e-08	1.52e-07	2.76e-08	2.21e-08
m07	1.64e-07	6.83e-05	6.83e-05	1.08e-07	7.86e-08	1.39e-07	2.6e-08	2.36e-08
m08	1.5e-07	5.78e-05	5.77e-05	1.02e-07	7.89e-08	1.82e-07	2.54e-08	2.42e-08
m09	3.3e-07	-	9.43e-05	4.29e-08	1.19e-07	2.03e-07	3.73e-08	1.6e-08
m10	1.74e-07	6.99e-05	6.99e-05	1.33e-07	1.06e-07	2.3e-07	2.56e-08	2.33e-08
m11	2.76e-07	5.62e-05	5.6e-05	1.43e-07	1.33e-07	2.48e-07	4.28e-08	3.38e-08
m12	2.74e-07	6.83e-05	6.82e-05	1.5e-07	1.07e-07	2.3e-07	4.5e-08	4.12e-08
m13	-	-	-	-	-	-	-	-
m14	3.56e-07	7.35e-05	7.33e-05	1.35e-07	1.75e-07	3.58e-07	4.83e-08	3.79e-08
m15	1.45e-07	4.88e-05	4.87e-05	1.02e-07	1.07e-07	1.9e-07	2.57e-08	2.32e-08
m16	5.42e-07	-	9e-05	4.18e-08	2.11e-07	2.6e-07	7.22e-08	2.14e-08
m17	2.95e-07	7.78e-05	7.78e-05	1.64e-07	1.47e-07	2.51e-07	5.32e-08	2.98e-08
m18	1.71e-07	6.03e-05	6.03e-05	9.03e-08	6.99e-08	1.76e-07	3.72e-08	2.38e-08
m19	1.49e-07	8.84e-05	8.83e-05	1.06e-07	9.05e-08	1.89e-07	2.68e-08	3.23e-08
m20	1.39e-07	4.53e-05	4.52e-05	6.62e-08	8.15e-08	1.35e-07	3.59e-08	2.31e-08
m21	2.52e-07	6.74e-05	6.77e-05	7.99e-08	1.35e-07	1.87e-07	2.72e-08	1.58e-08
m22	1.92e-07	5.84e-05	5.83e-05	9.99e-08	9.18e-08	1.96e-07	3.18e-08	2.99e-08
m23	1.67e-07	5.27e-05	5.27e-05	1.01e-07	7.76e-08	1.58e-07	2.58e-08	2.38e-08
m24	2.26e-07	8.41e-05	8.4e-05	1.4e-07	1.18e-07	2.33e-07	2.98e-08	2.85e-08
m25	1.2e-07	5.29e-05	5.28e-05	9.18e-08	6.05e-08	1.37e-07	2.38e-08	2.08e-08

Table 7.8: Female Patients Specific S-values **I-131**

S-values Female I-131 ($mGy/(MBq * s)$)								
	Spleen	R. Kidney	L. Kidney	Liver	Stomach	Pancreas	L. Lung	R. Lung
f01	2.41e-06	9.54e-05	9.55e-05	1.25e-06	1.13e-06	2.73e-06	4.82e-07	3.35e-07
f02	1.21e-06	7.65e-05	7.62e-05	9.57e-07	1.32e-06	2.02e-06	2.11e-07	2.23e-07
f03	1.38e-06	0.000106	0.000106	1.12e-06	8.16e-07	2.13e-06	2.75e-07	2.8e-07
f04	2.1e-06	8.9e-05	8.91e-05	1.04e-06	1.07e-06	2.54e-06	4.12e-07	2.64e-07
f05	4.25e-06	0.000151	0.000146	1.95e-06	2.4e-06	2.62e-06	4.41e-07	4.52e-07
f06	2.04e-06	0.000106	0.000105	1.2e-06	1.25e-06	2.31e-06	4.68e-07	3.44e-07
f07	2.74e-06	0.000158	0.000158	2.04e-06	1.43e-06	3.05e-06	3.59e-07	4.29e-07
f08	2.15e-06	0.000129	0.000129	1.14e-06	8.89e-07	2.42e-06	3.2e-07	2.27e-07
f09	1.27e-06	9.76e-05	9.74e-05	1.24e-06	8.81e-07	1.94e-06	3.04e-07	2.68e-07
f10	2.14e-06	0.000117	0.000118	1.43e-06	1.01e-06	2.22e-06	3.45e-07	2.67e-07
f11	2e-06	9.61e-05	9.61e-05	1.57e-06	1.12e-06	2.42e-06	3.21e-07	3.61e-07
f12	3e-06	0.000137	0.000137	1.88e-06	1.53e-06	2.85e-06	5.62e-07	4.95e-07
f13	2.78e-06	0.000105	0.000105	1.51e-06	1.35e-06	2.55e-06	4.24e-07	3.25e-07
f14	2.02e-06	9.51e-05	9.58e-05	1.04e-06	1.27e-06	2.3e-06	3.68e-07	2.64e-07
f15	2.03e-06	0.000131	0.000131	1.63e-06	1.33e-06	2.39e-06	4e-07	3.32e-07
f16	2.61e-06	0.000107	0.000108	1.2e-06	8.99e-07	1.83e-06	3.2e-07	3.91e-07
f17	2.15e-06	0.000147	0.000146	1.37e-06	1.21e-06	2.26e-06	2.88e-07	2.8e-07
f18	1.97e-06	9.3e-05	9.32e-05	1.24e-06	1.07e-06	2.49e-06	4.1e-07	3.1e-07
f19	2.1e-06	0.00013	0.00013	1.32e-06	1.09e-06	2.29e-06	3.57e-07	3.95e-07
f20	8.32e-07	0.00021	0.000194	1.86e-06	9.2e-07	2.1e-06	2.96e-07	3.81e-07
f21	2.18e-06	0.000113	0.000114	1.55e-06	1.07e-06	2.4e-06	3.92e-07	3.81e-07
f22	3.42e-06	0.000134	0.000134	1.93e-06	1.67e-06	3.18e-06	6.2e-07	4.19e-07
f23	3.64e-06	0.000171	0.000172	1.64e-06	1.39e-06	3.73e-06	5.22e-07	3.79e-07
f24	2.85e-06	0.000142	0.000142	1.72e-06	1.67e-06	3.41e-06	4.45e-07	3.76e-07
f25	3.01e-06	0.000143	0.000143	1.65e-06	1.53e-06	3.11e-06	4.96e-07	3.41e-07
f26	2.4e-06	0.000106	0.000106	1.37e-06	1.04e-06	2.41e-06	3.48e-07	3.47e-07
f27	2.13e-06	8.88e-05	8.89e-05	1e-06	1.05e-06	2.49e-06	3.71e-07	2.51e-07
f28	1.8e-06	6.82e-05	6.78e-05	1.34e-06	1.26e-06	2.24e-06	4.01e-07	3.42e-07
f29	2.13e-06	0.000122	0.000123	1.35e-06	1.01e-06	2.69e-06	4.15e-07	3.98e-07
f30	2.82e-06	0.000155	0.000157	1.67e-06	1.22e-06	3.23e-06	4.7e-07	4.8e-07

Table 7.9: Male Patients Specific S-values **I-131**

S-values Male I-131 ($mGy/(MBq * s)$)								
	Spleen	R. Kidney	L. Kidney	Liver	Stomach	Pancreas	L. Lung	R. Lung
m01	1.01e-06	7.79e-05	7.79e-05	7.64e-07	6.73e-07	1.32e-06	2.64e-07	2.14e-07
m02	3.5e-06	0.000138	0.000139	1.68e-06	1.24e-06	2.78e-06	5.49e-07	4.06e-07
m03	1.22e-06	7.54e-05	7.54e-05	7.97e-07	6.97e-07	1.65e-06	2.48e-07	1.85e-07
m04	2.37e-06	8.23e-05	8.19e-05	1.31e-06	1.04e-06	2.32e-06	4.34e-07	3.44e-07
m05	3.76e-07	0.000125	-	1.74e-06	4.05e-07	1.12e-06	1.92e-07	3.56e-07
m06	1.29e-06	9.1e-05	9.12e-05	8.95e-07	6.37e-07	1.46e-06	2.99e-07	2.44e-07
m07	1.66e-06	9.97e-05	9.96e-05	1.09e-06	7.96e-07	1.36e-06	2.84e-07	2.56e-07
m08	1.53e-06	8.48e-05	8.47e-05	1.02e-06	8.2e-07	1.77e-06	2.84e-07	2.73e-07
m09	3.27e-06	-	0.000139	4.64e-07	1.23e-06	1.93e-06	4.03e-07	1.93e-07
m10	1.73e-06	0.000102	0.000102	1.32e-06	1.06e-06	2.13e-06	2.91e-07	2.66e-07
m11	2.6e-06	8.27e-05	8.14e-05	1.43e-06	1.35e-06	2.32e-06	4.32e-07	3.65e-07
m12	2.65e-06	9.99e-05	9.98e-05	1.49e-06	1.11e-06	2.2e-06	4.82e-07	4.48e-07
m13	-	-	-	-	-	-	-	-
m14	3.39e-06	0.000107	0.000107	1.36e-06	1.72e-06	3.1e-06	4.89e-07	4.16e-07
m15	1.44e-06	7.21e-05	7.21e-05	1.05e-06	1.1e-06	1.85e-06	2.91e-07	2.66e-07
m16	5.2e-06	-	0.000134	4.35e-07	2.11e-06	2.33e-06	7.22e-07	2.4e-07
m17	2.84e-06	0.000113	0.000113	1.64e-06	1.51e-06	2.38e-06	5.29e-07	3.36e-07
m18	1.67e-06	8.8e-05	8.81e-05	9.16e-07	7.12e-07	1.66e-06	3.86e-07	2.62e-07
m19	1.46e-06	0.000128	0.000127	1.08e-06	9.4e-07	1.84e-06	2.97e-07	3.51e-07
m20	1.4e-06	6.67e-05	6.66e-05	6.69e-07	8.12e-07	1.31e-06	3.67e-07	2.51e-07
m21	2.5e-06	9.65e-05	9.98e-05	8.11e-07	1.34e-06	1.78e-06	3.08e-07	1.87e-07
m22	1.91e-06	8.56e-05	8.53e-05	1.01e-06	9.28e-07	1.89e-06	3.39e-07	3.19e-07
m23	1.66e-06	7.74e-05	7.74e-05	1.02e-06	7.93e-07	1.53e-06	2.89e-07	2.62e-07
m24	2.23e-06	0.000122	0.000122	1.41e-06	1.2e-06	2.24e-06	3.33e-07	3.22e-07
m25	1.21e-06	7.8e-05	7.76e-05	9.34e-07	6.19e-07	1.37e-06	2.56e-07	2.33e-07

CHAPTER 8

BENCHMARKING AND S-VALUE VARIATION

8.1 Tc-99m Comparison

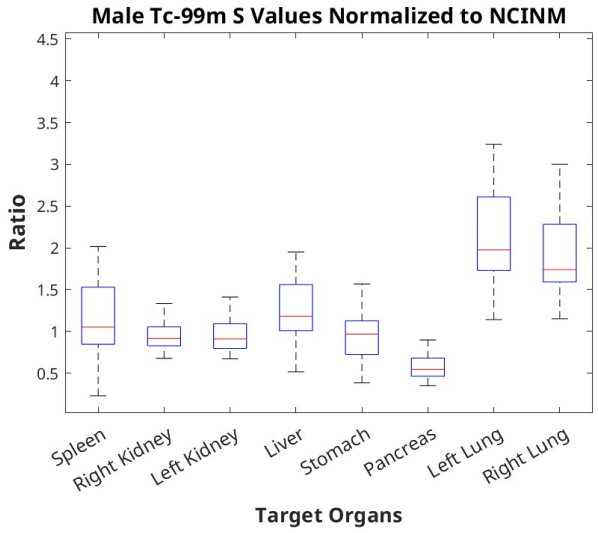

Figure 8.1: Male Patient Specific S-values Normalized to NCINM (Tc-99m)

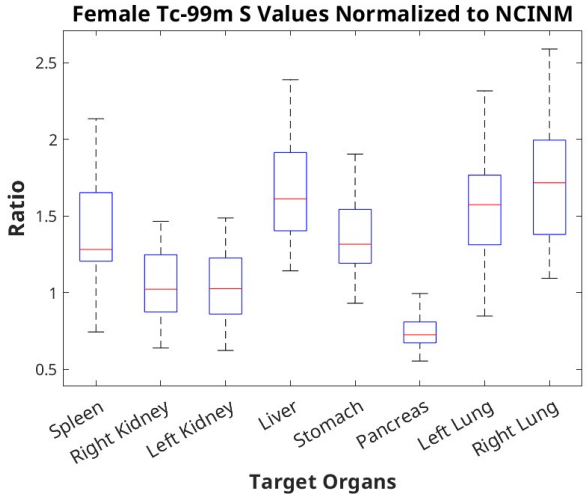

Figure 8.2: Female Patient Specific S-values Normalized to NCINM (Tc-99m)

The patient S-values calculated (Table 7.2 → 7.9) can be compared against those provided by NCINM (Table 5.6 and 5.7) for the appropriate isotope. Benchmarking can be accomplished by normalizing the patient S-values to that of the corresponding NCINM phantom value for each organ and isotope. Several characteristics are worth considering when analyzing the results. One should not necessarily expect that the phantom S-values to be central to the patient distribution. However one would expect actual patient populations would vary to a phantom at least as much as NCINM phantoms varied with respect to one another which was depicted in Table 5.8.

Male Patients

The variation in S-values for the target organs was a factor of 5 (between max divided by min) for the spleen and stomach. However, a more modest factor of 2 is evident in the kidneys which were source organs. Note the range is independent of normalization to the NCINM model. The normalized distribution of the target organ S-values can be seen in the associated bar plot. The spleen, kidneys, liver and the stomach all contained the phantom model value within the distribution, and were generally well mannered with respect to the phantom value. Although the S-values for the pancreas enjoyed little distributional variance, the distribution was lower than that of the phantom model. While the lobes of the lungs had higher than expected S-values.

Female Patients

The variation of in S-values for the target organs were similar to that of the male cohort with the exception of lower variance in stomach and liver. The NCINM phantom values were well within the source organ's (kidneys) distribution. The stomach and to a lesser extent the spleen were in fair agreement with the phantom models albeit slightly higher. The liver and lungs S-values were underreported by the phantom model. However the pancreas was found to be lower than predicted by NCINM.

8.2 F-18 Comparison

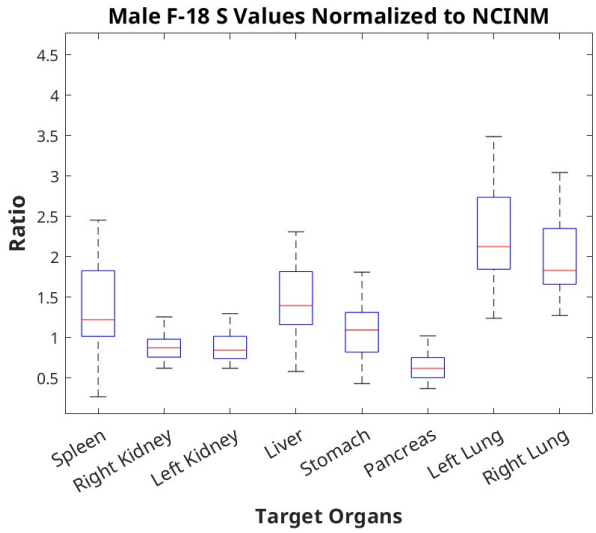

Figure 8.3: Male Patient Specific S-values Normalized to NCINM (F-18)

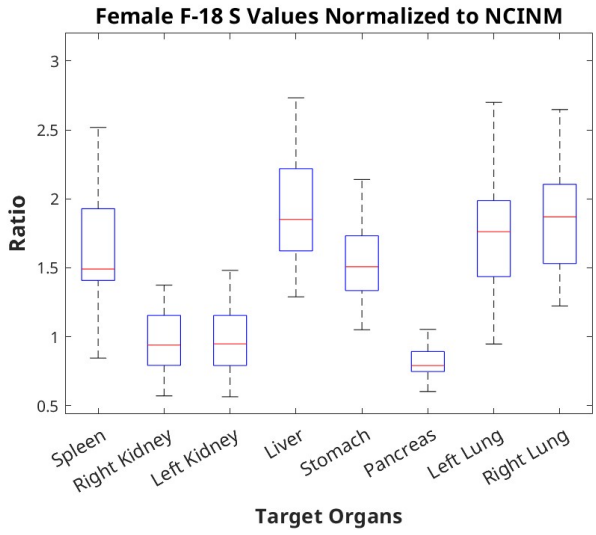

Figure 8.4: Female Patient Specific S-values Normalized to NCINM (F-18)

Male Patients

Although the actual S-values are completely different the variation seen in the organs for the cohort of patients were found to be similar to that of Tc-99m. In contrast to the Tc-99m results the kidney distribution was lower than predicted by the NCINM model, this was even more so for the pancreas. The spleen, liver and stomach had greater variation, but overlapped with respect to phantom results. The patient values for the lung were higher than the model predicted.

Female Patients

The distribution and variation for F-18 were similar to Tc-99m, although the pancreas and lungs compared slightly more favorably.

8.3 Lu-177 Comparison

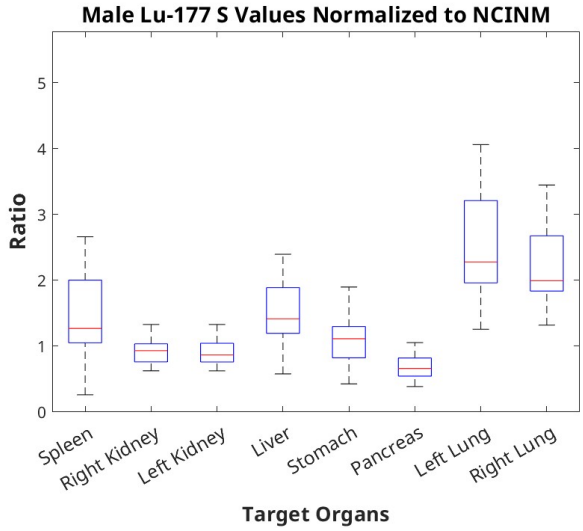

Figure 8.5: Male Patient Specific S-values Normalized to NCINM (Lu-177)

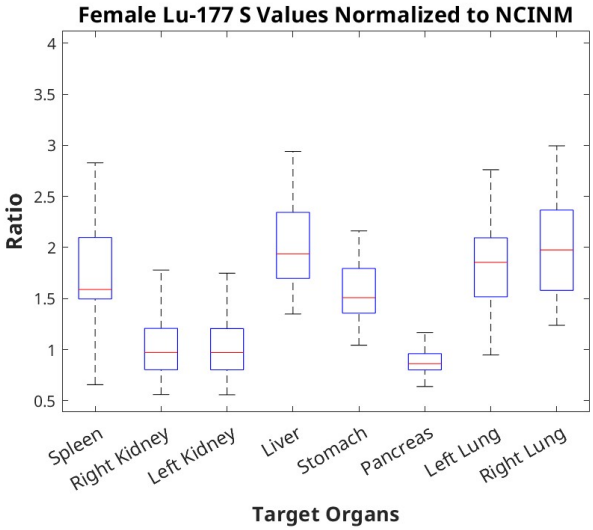

Figure 8.6: Female Patient Specific S-values Normalized to NCINM (Lu-177)

Male Patients

Similar distribution to the other isotopes. However less variation was noted overall with the exception of the spleen.

Female Patients

The distribution was similar and largely unaffected by the change of isotope. The only noteworthy anecdote was a slight increase in the variance of the spleen.

8.4 I-131 Comparison

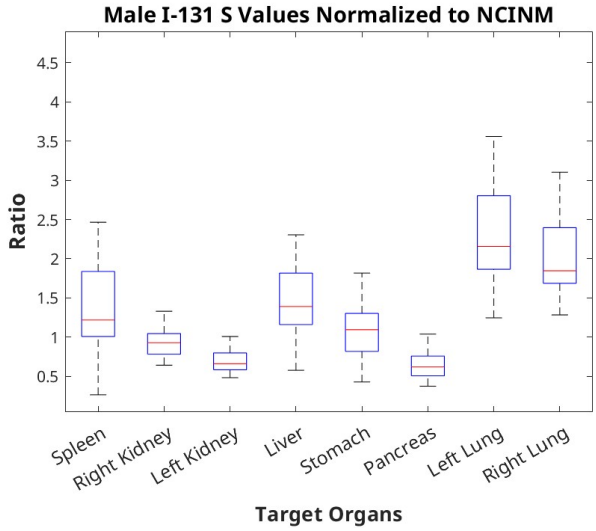

Figure 8.7: Male Patient Specific S-values Normalized to NCINM (I-131)

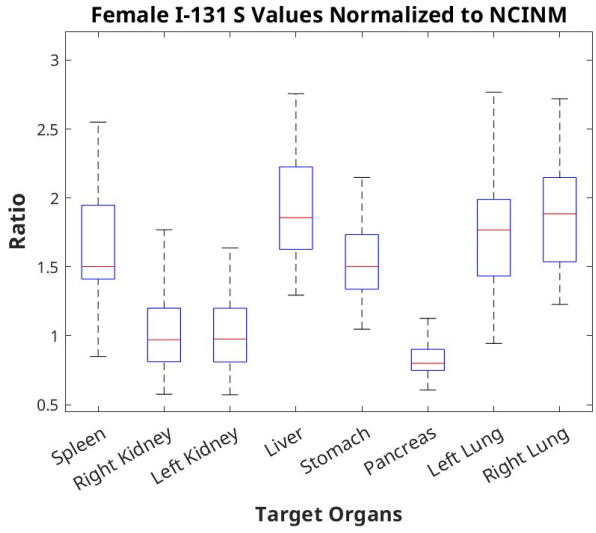

Figure 8.8: Female Patient Specific S-values Normalized to NCINM (I-131)

Male Patients

The left kidney
was lower than other isotopes
otherwise distribution was similar
to previous results. The variance of
the S-values were again remarkably
consistent for all evaluated isotopes.

Female Patients

No noteworthy variation
in the distribution with respect
to other isotopes was realized.

CHAPTER 9

PATIENT ATTRIBUTE CORRELATION WITH S-VALUES: AN EXTENSION OF NCINM MODEL

9.1 Tc-99m

It is the goal of this work to investigate if patient attributes known prior to therapy correlate with organ S-values. To investigate this inquiry the patient specific S-values were plotted versus the patient's corresponding age, height, weight and BMI. To de-emphasize the influence of outliers to the data's distribution, a MATLAB routine was employed to "clean" the data. The program removed outliers based on the Median Absolute Deviation (MAD), which first involved the determination of median ($\tilde{X}$). Next the residuals or deviations from the median was calculated.

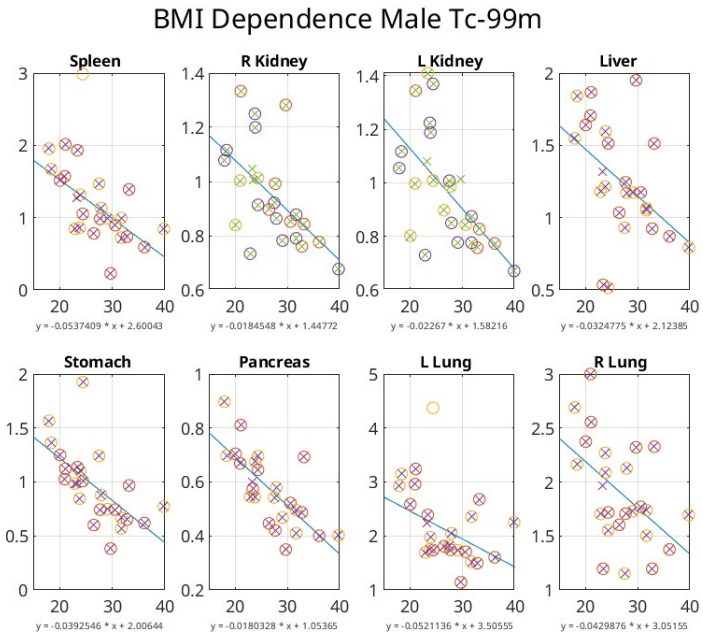

Figure 9.1: Male Patient's S-value Dependence (Tc-99m) on BMI

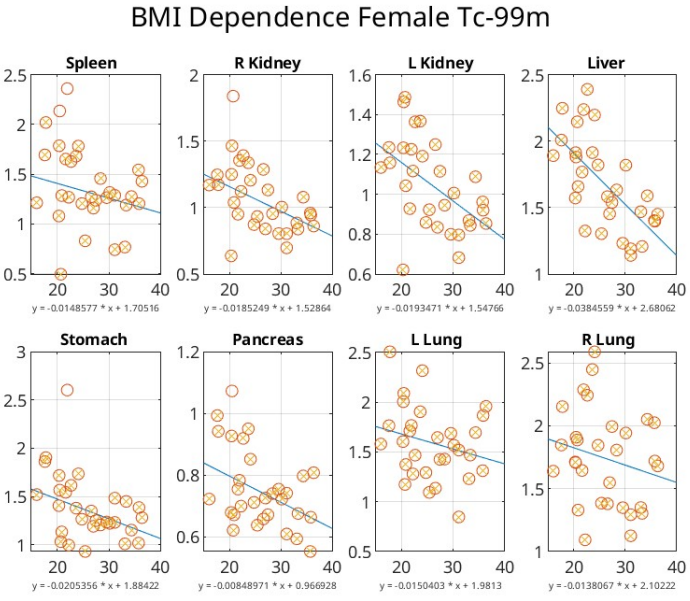

Figure 9.2: Female Patient's S-value Dependence (Tc-99m) on BMI

MAD is defined as the median of absolute value of the differences, which is MAD =

median$(X_i - \tilde{X})$. It should be noted that the purge of outliers was only with respect to the determination of the fitting parameters, all S-value data was kept in the final analysis. A linear polynomial fit was determined for each distribution. The fit function was applied to the distribution previously normalized with respect to the NCINM model. Armed with the fit function, S-values for patients based on attributes can be applied to the NCINM models. An review of the NCINM's extended model was conducted based on patient's BMI. The distribution was determined by normalizing the patient specific S-values with the new model. The percent reduction of the Interquartile Range (IQR) was

$$Ratio = \frac{S(j,k)}{S_m(j,k)} \tag{9.1}$$

Where S(j,k) is the S-value of the j^{th} patient and k^{th} organ, and S_m is the extended model value for the same patient and organ.

Male Patients

Several attributes had explanatory insight into the distribution. Age dependence was seen in the organs of the spleen, stomach and pancreas. Whereas height only correlated well with the source organs (kidneys). The patient's BMI and to lesser degree weight correlated best with organ S-value variance. The BMI correlation although prevalent with all organs was especially strong in spleen, stomach and pancreas. A graph of S-values versus BMI is shown, along with a linear polynomial fit. Note similar graphs were conducted for participant age, height and weight.(Appendix B, C and D)

Female Patients

The dependence of the S-values with respect to BMI was most prominent in the liver, kidneys and stomach. The other organs displayed less correlation. A graph of S-values versus BMI is shown, along with a linear polynomial fit. Note similar graphs were conducted for participant age, height

and weight.(Appendix B, C and D)

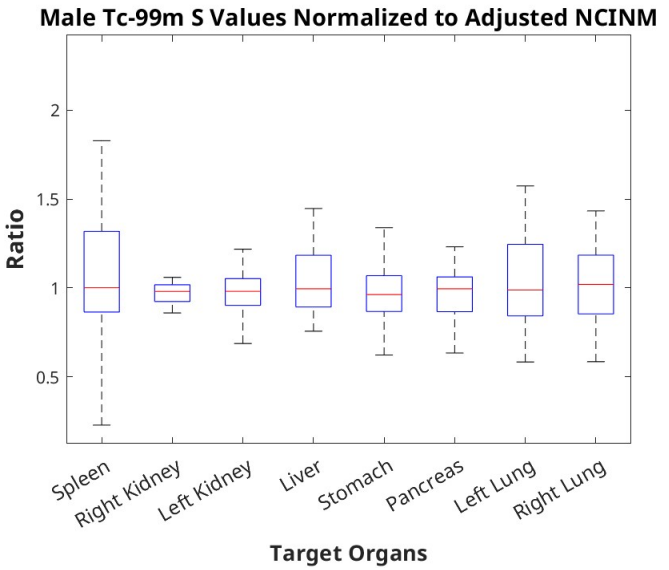

Figure 9.3: Male Patient Specific S-values Normalized to an Extended NCINM Model (Tc-99m)

Male Patients

IQR Reduction

- Spleen ↓ 35%
- Right Kidney ↓ 62%
- Left Kidney ↓ 49%
- Liver ↓ 54%
- Stomach ↓ 56%
- Pancreas ↓ 18%
- Left Lung ↓ 56%
- Right Lung ↓ 56%

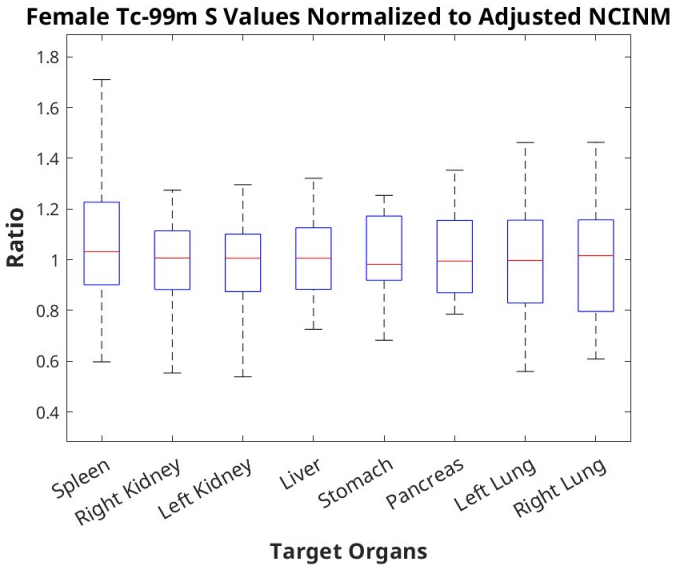

Figure 9.4: Female Patient Specific S-values Normalized to an Extended NCINM Model (Tc-99m)

Female Patients

IQR Reduction

- Spleen ↓ 27%
- Right Kidney ↓ 38%
- Left Kidney ↓ 38%
- Liver ↓ 53%
- Stomach ↓ 28%
- Pancreas ↓ -%
- Left Lung ↓ 28%
- Right Lung ↓ 41%

9.2 F-18

Male Patients

The data was highly correlated with BMI, especially the spleen and stomach. The patient's weight seemed to be related to the kidney S-values. Age also performed well in the stomach and spleen this probably indicates that BMI is related to patient age.

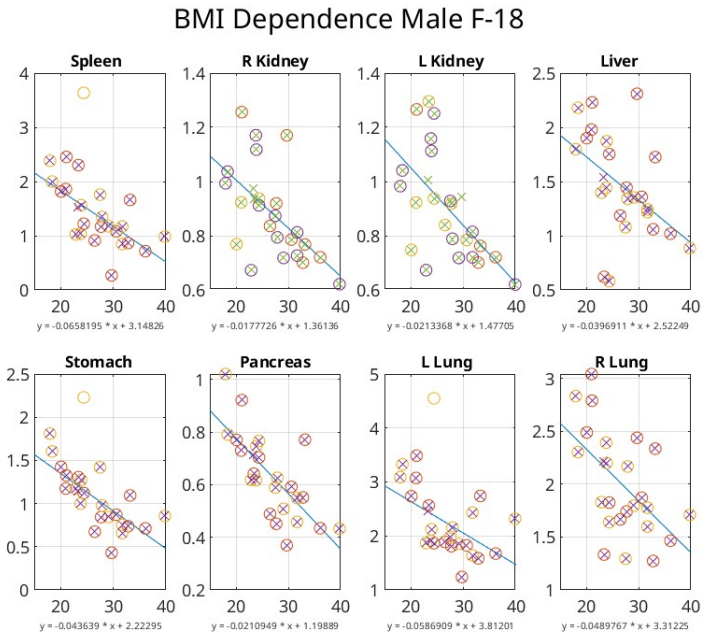

Figure 9.5: Male Patient's S-value Dependence (F-18) on BMI

Female Patients

The liver, kidney and stomach were most highly correlated with BMI. The weight seemed to display a similar correlation as BMI with respect to the patient specific S-values. Height did seem to be correlated with lung S-values.

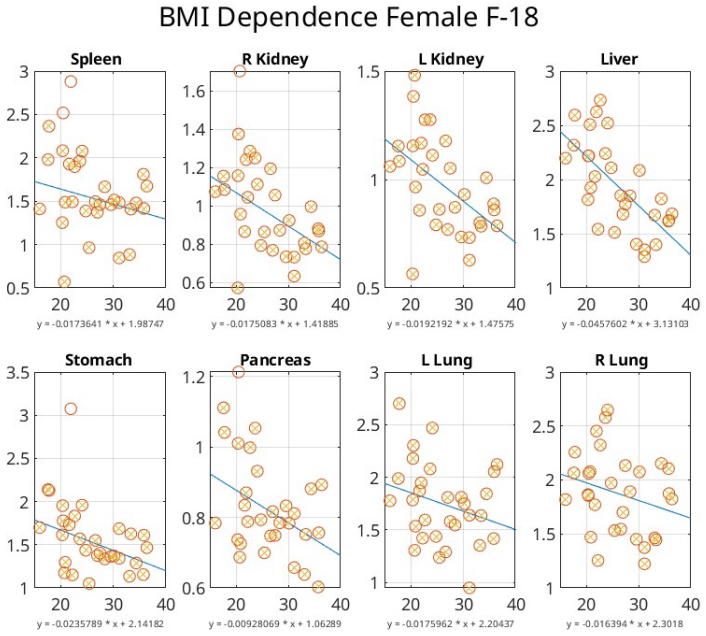

Figure 9.6: Female Patient's S-value Dependence (F-18) on BMI

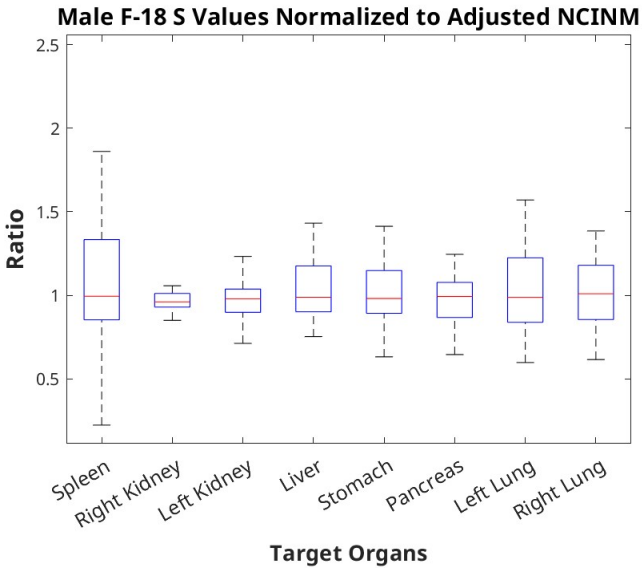

Figure 9.7: Male Patient Specific S-values Normalized to an Extended NCINM Model (F-18)

Male Patients

IQR Reduction

- Spleen ↓ 44%
- Right Kidney ↓ 65%
- Left Kidney ↓ 50%
- Liver ↓ 63%
- Stomach ↓ 55%
- Pancreas ↓ 22%
- Left Lung ↓ 58%
- Right Lung ↓ 55%

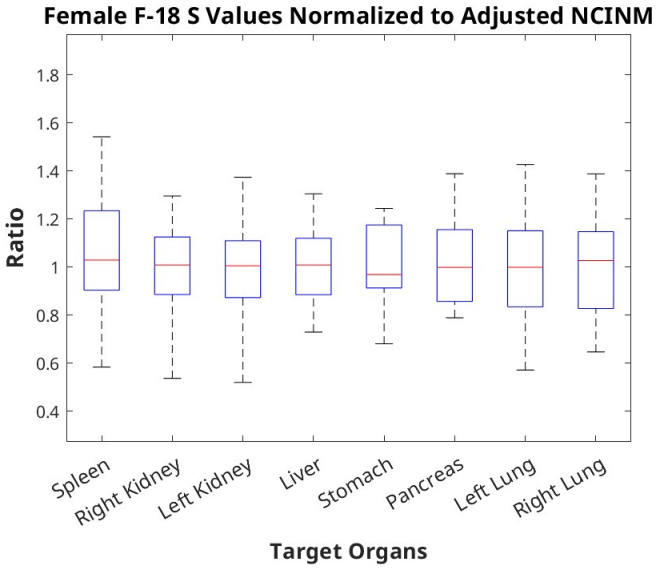

Figure 9.8: Female Patient Specific S-values Normalized to an Extended NCINM Model (F-18)

Female Patients

IQR Reduction

- Spleen ↓ 36%
- Right Kidney ↓ 34%
- Left Kidney ↓ 35%
- Liver ↓ 61%
- Stomach ↓ 34%
- Pancreas ↓ -%
- Left Lung ↓ 43%
- Right Lung ↓ 44%

9.3 Lu-177

Male Patients

The patient's BMI strongly correlated with spleen and stomach values. The weight and height however seemed to be related to the kidney variance.

Female Patients

The distribution was similar to earlier results, with little additional insight with respect to additional correlations between organ S-values and patient attributes.

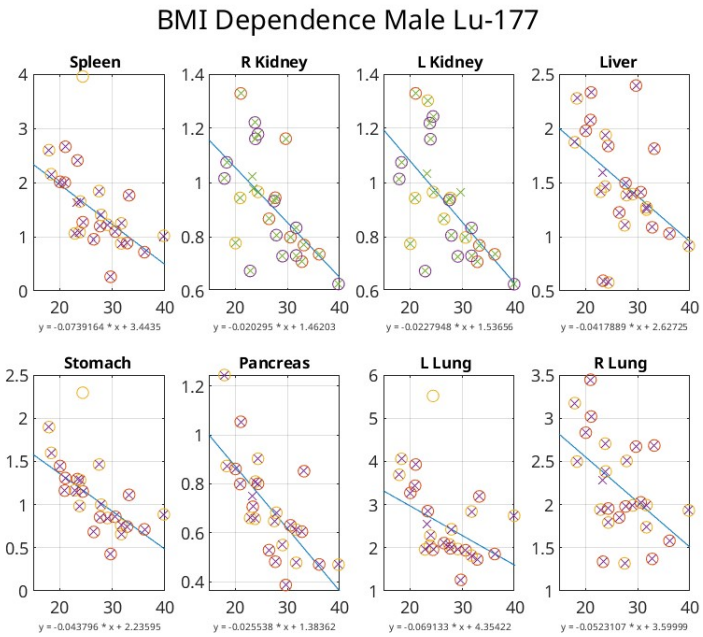

Figure 9.9: Male Patient's S-value Dependence (Lu-177) on BMI

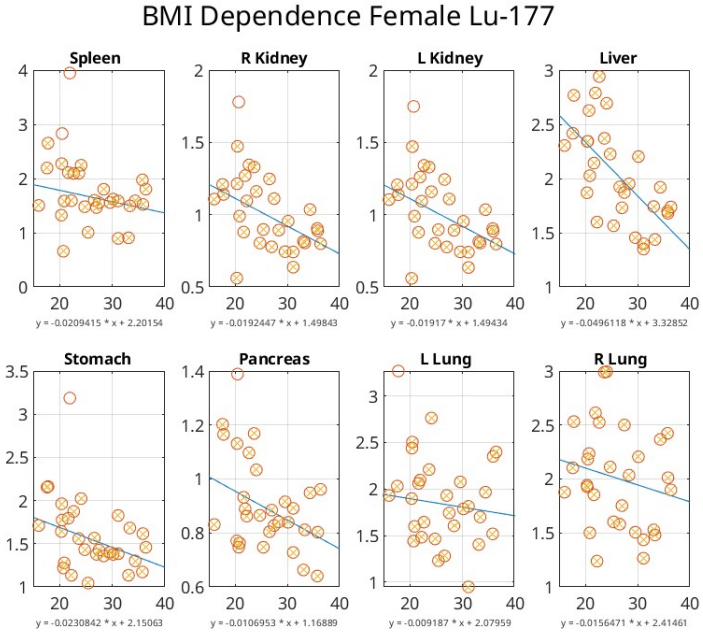

Figure 9.10: Female Patient's S-value Dependence (Lu-177) on BMI

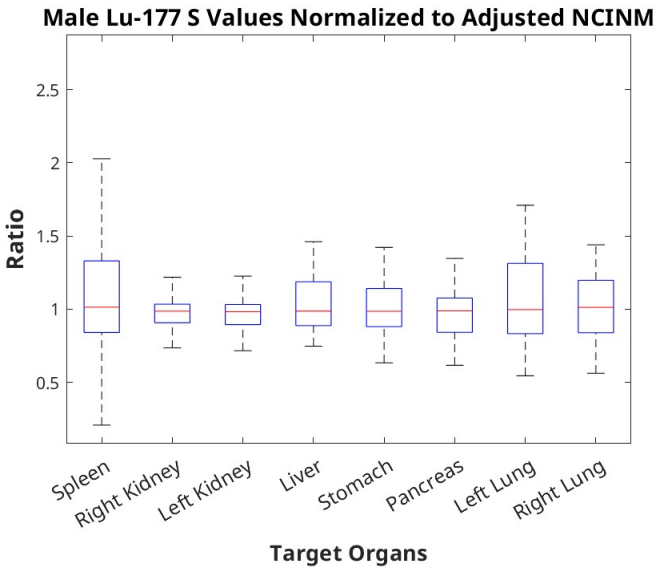

Figure 9.11: Male Patient Specific S-values Normalized to an Extended NCINM Model (Lu-177)

Male Patients

IQR Reduction

- Spleen ↓ 51%
- Right Kidney ↓ 58%
- Left Kidney ↓ 54%
- Liver ↓ 62%
- Stomach ↓ 52%
- Pancreas ↓ 23%
- Left Lung ↓ 62%
- Right Lung ↓ 60%

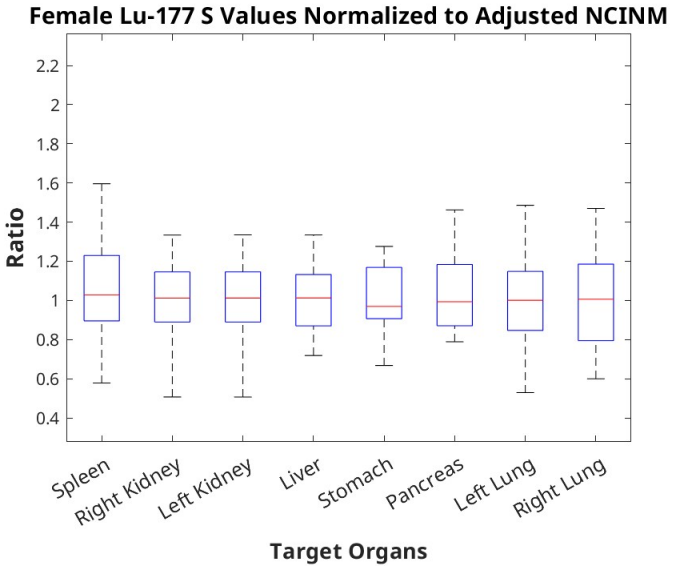

Figure 9.12: Female Patient Specific S-values Normalized to an Extended NCINM Model (Lu-177)

Female Patients

IQR Reduction

- Spleen ↓ 44%
- Right Kidney ↓ 37%
- Left Kidney ↓ 36%
- Liver ↓ 59%
- Stomach ↓ 40%
- Pancreas ↓ -%
- Left Lung ↓ 48%
- Right Lung ↓ 50%

9.4 I-131

Male Patients

BMI and weight were well correlated with the distributions. Height seemed again to be correlated with kidney variances.

Female Patients

The BMI correlated best with the kidneys, liver and stomach organs. It was noted height was weakly correlated with the lung values.

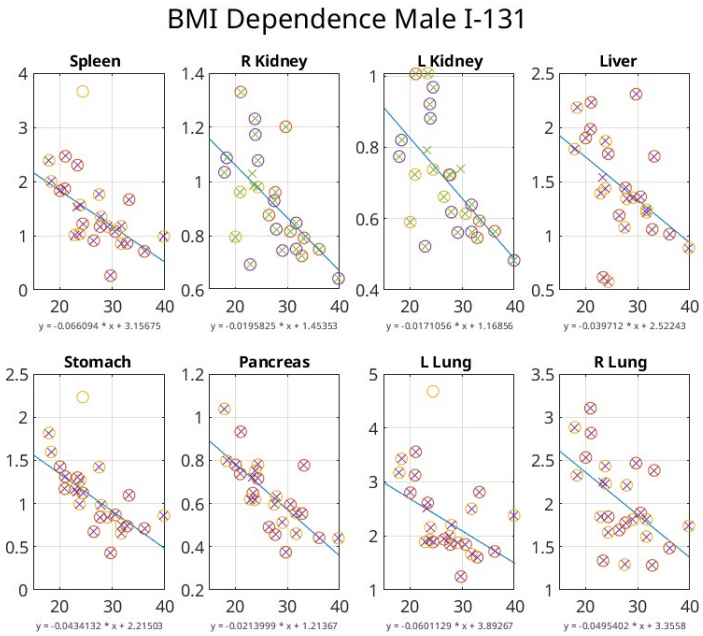

Figure 9.13: Male Patient's S-value Dependence (I-131) on BMI

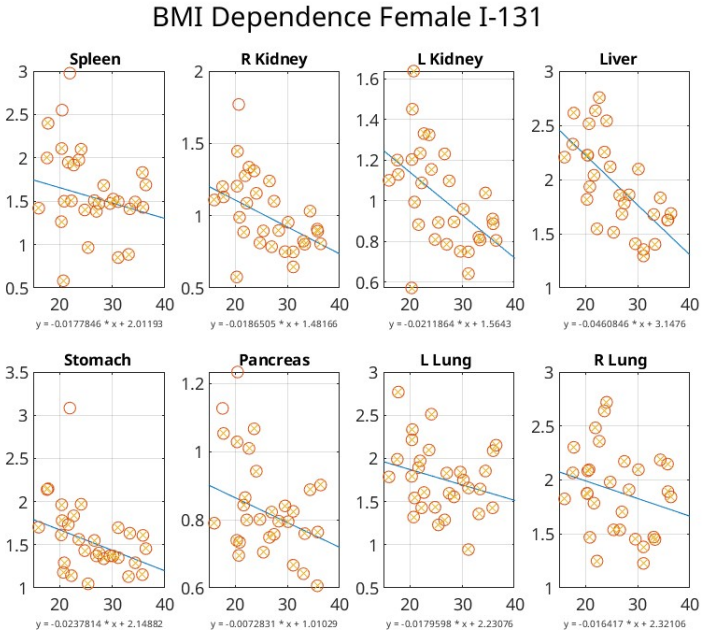

Figure 9.14: Female Patient's S-value Dependence (I-131) on BMI

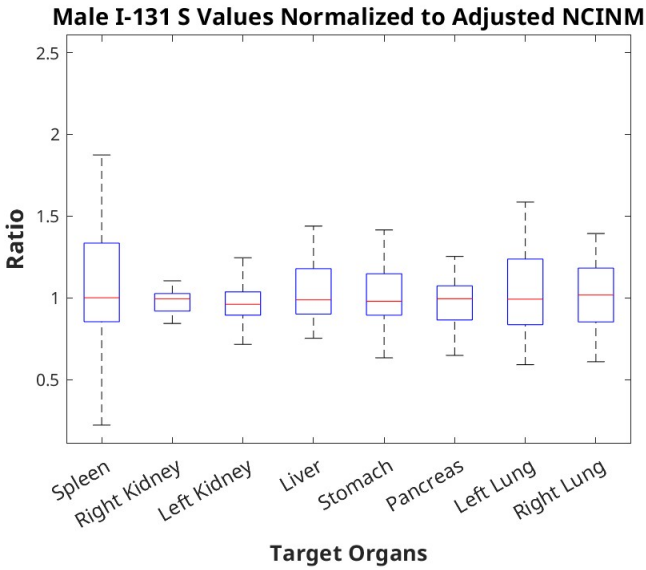

Figure 9.15: Male Patient Specific S-values Normalized to an Extended NCINM Model (I-131)

Male Patients

IQR Reduction

- Spleen ↓ 45%
- Right Kidney ↓ 64%
- Left Kidney ↓ 36%
- Liver ↓ 63%
- Stomach ↓ 54%
- Pancreas ↓ 24%
- Left Lung ↓ 58%
- Right Lung ↓ 56%

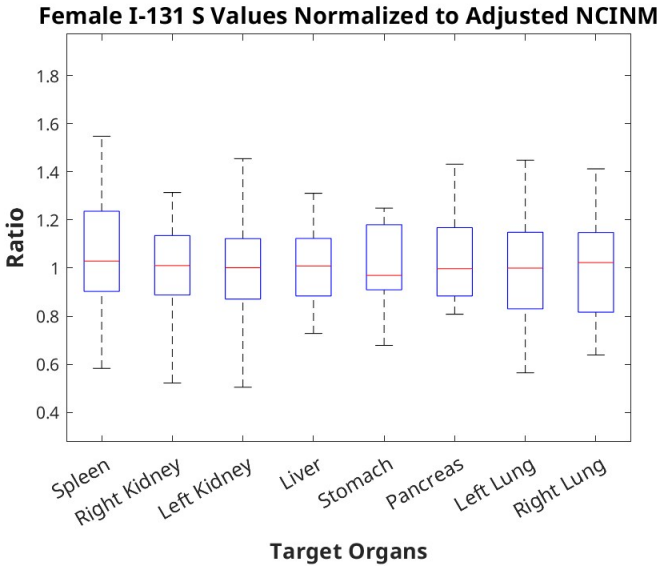

Figure 9.16: Female Patient Specific S-values Normalized to an Extended NCINM Model (I-131)

Female Patients

IQR Reduction

- Spleen ↓ 38%
- Right Kidney ↓ 36%
- Left Kidney ↓ 36%
- Liver ↓ 60%
- Stomach ↓ 32%
- Pancreas ↓ -%
- Left Lung ↓ 43%
- Right Lung ↓ 46%

CHAPTER 10

DISCUSSION AND NEXT STEPS

10.1 Variation and Benchmarking

The variation of patient S-values, highlight the original reasoning for the creation multiple anatomical models. Historically these phantoms have been focused on size differences between pediatric and adult patients. One can see in some instances the variation among adults rival that of the former. It should be noted the variation in S-values was also seen when comparing various phantom models as shown in Table 5.8.

The patient S-values were normalized to the appropriate phantom for the given radionuclide. Using the normalized S-values, one can see a similar trend in the data which reveals the variation between patients is largely independent of isotope. It should be noted the variation between the minimum and maximum S-values for patients ranged from two-fold to a five-fold factor! The variation was found to be more moderate with respect to the kidneys and pancreas. The results varied more widely for the spleen, and to a lesser extent the lungs.

Benchmarking the S-values with NCINM revealed in most cases the phantoms were contained within the patient's distribution if not centered. Two notable exceptions, the lungs were high with respect to the models and the pancreas was low. Note the image acquisition process created some uncertainty especially related to the lung volume and their relative placement. Patients are generally imaged during inhalation breathe holds or to a lesser degree expiratory holds to reduce motion and to evaluate certain conditions. This can certainly affect the mean distance from source organs. It was shown in the phantom analysis the lungs can vary significantly. The pancreas mass distribution for patients was low with respect to the corresponding phantom mass, this may help explain the low normalized S-values. Additionally although reasonable efforts were made, the complexity of the patient models might be a factor. The complexity is in reference to possibly

more sophisticated and detailed simulated structures of the NCINM phantom models versus the patient models. Alternatively the phantom model may fail to approximate typical values seen in nature, thus leading to values outside of the distribution. Ensuring the phantom models closely resemble actual patients is paramount. Patient data shouldn't be seen as a replacement for the phantoms, but they should be used to validate these models. If accurate models exist, they can be used as tools. These tools may allow for intelligent comparisons between various diagnostic and therapeutic protocols.

10.2 NCINM Model Extension

Some patient attributes were found to be correlated with S-values. The correlation was found to vary with respect to the source and target pair. The correlation analysis was conducted in a multistep process. First the S-values were normalized to the appropriate phantom model as was previously introduced. The data was "cleaned" using a median absolute deviation (MAD). The cleaned S-values were used to fit a linear polynomial with the patient attributes as the independent variable. These patient attributes included age, height, weight, and BMI. A plot of S-values (all patients) versus attributes was made that included the visible linear fit. Using the linear fit created which resulted from studying the BMI correlation, an extended model was created. The extended model allows for personalization of the NCINM phantom results.

$$Ratio = \frac{S(j,k)}{S_m(j,k)} \tag{10.1}$$

Where S(j,k) is the S-value of the j^{th} patient and k^{th} organ, and S_m is the extended model value for the same patient and organ.

When applied this leads to two corrections to the distribution. First it scales the models (phantom) to the patient distribution. This may correct for the S-value differences that may occur due to changes in the population averages. Alternatively this may be a result of the phantom's insufficiency regarding realism. Arguably worse it could be caused by overly simplistic or crude

patient simulations. Hopefully neither is true, but this requires further investigation. A second result of the fit is a decrease in the variance between the extended model and the patient simulations. One way to evaluate this item for the population is by reviewing the decrease in the interquartile range. It should be noted these values are affected by the scaling of the distribution (absolute differences). However the IQR was reduced for male patients by 40% to 50% for the spleen, and 50% to 60% for the kidneys, lungs, liver and stomach. The pancreas on the other hand was only reduced by 20%, due partly to scaling (original ratio was less than 1). The female patients distributions were $\approx 10\%$ less reduced.

One reason for the high correlation with BMI and to a lesser degree weight is the location of the organs analyzed. The organs were specific to the trunk region and central to the body. It is believed that the female patients may have a more varied distribution of their mass, therefore BMI and weight may not correlate as highly with the patient's trunk. The patient attributes reported in general are not expected to be independent of one another, hence a combination of these variables was not employed during the initial fit. Subsequent more sophisticated analysis may improve the extension and accuracy of the NCINM model. One for example would expect a stronger correlation with height would be found for distal organ pairs.

10.3 Next Steps

The patient simulations would be improved with more patient data. Furthermore this research would benefit if more of the patient was imaged, one avenue may include PET/CT scans that are often conducted from the patient's eyes to thighs. Second as artificial intelligence segmentation tools are refined greater complexity might be realized. Additionally, it is advisable to explore incorporating the phantom segmentation data in the patient simulation space to ensure the validity of the comparison. A more complex fit should be explored to improve personalization. Beyond anatomical corrections to phantoms, the models could be extended for uptake and clearance based on laboratory values.

References

[1] Byeong-Cheol Ahn. "Personalized Medicine Based on Theranostic Radioiodine Molecular Imaging for Differentiated Thyroid Cancer". In: BioMed Research International 2016 (Apr. 2016). Ed. by Jie Tian, p. 1680464. ISSN: 2314-6133. URL: https://doi.org/10.1155/2016/1680464.

[2] Yuni K. Dewaraja et al. "MIRD pamphlet No. 23: quantitative SPECT for patient-specific 3-dimensional dosimetry in internal radionuclide therapy". eng. In: Journal of nuclear medicine : official publication, Society of Nuclear Medicine 53.8 (Aug. 2012), pp. 1310–1325. ISSN: 0161-5505. URL: https://pubmed.ncbi.nlm.nih.gov/22743252.

[3] Villoing D. et al. "NCINM: organ dose calculator for patients undergoing nuclear medicine procedures". In: Biomedical physics & engineering express (2020).

[4] Mahadevappa Mahesh, Armin J. Ansari, and Fred A. Mettler. "Patient Exposure from Radiologic and Nuclear Medicine Procedures in the United States and Worldwide: 2009–2018". In: Radiology 307.1 (Apr. 2023). ISSN: 1527-1315. DOI: 10.1148/radiol.221263.

[5] Cristina Barca et al. "Expanding Theranostic Radiopharmaceuticals for Tumor Diagnosis and Therapy". In: Pharmaceuticals 15.1 (Dec. 2021), p. 13. ISSN: 1424-8247. DOI: 10.3390/ph15010013.

[6] M. Andersson et al. "DAC-Dose 2.1, an internal dosimetry program for diagnostic nuclear medicine based on the ICRP adult reference voxel phantoms". In: I. EJNMMI research (2017).

[7] Michael Stabin and Adam Farmer. "OLINDA/EXM 2.0: The new generation dosimetry modeling code". In: Journal of Nuclear Medicine 53.supplement 1 (2012), pp. 585–585. ISSN: 0161-5505. eprint: https://jnm.snmjournals.org/content. URL: https://jnm.snmjournals.org/content/53/supplement_1/585.

[8] Stephen A. Graves et al. "Reimbursement Approaches for Radiopharmaceutical Dosimetry: Current Status and Future Opportunities". In: Journal of Nuclear Medicine 62.Supplement 3 (Dec. 2021), 48S–59S. ISSN: 2159-662X. DOI: 10.2967/jnumed.121.262752.

[9] Sven-Erik Strand, Pat Zanzonico, and Timothy K. Johnson. “Pharmacokinetic modeling”. In: Medical Physics 20.2 (Mar. 1993), pp. 515–527. ISSN: 2473-4209. DOI: 10.1118/1.597047.

[10] Wesley E. Bolch et al. “MIRD Pamphlet No. 21: A Generalized Schema for Radiopharmaceutical Dosimetry—Standardization of Nomenclature”. In: Journal of Nuclear Medicine (2009).

[11] X George Xu. “An exponential growth of computational phantom research in radiation protection, imaging, and radiotherapy: a review of the fifty-year history”. In: Physics in Medicine and Biology 59.18 (Aug. 2014), R233–R302. ISSN: 1361-6560. DOI: 10.1088/0031-9155/59/18/r233.

[12] Zhao Peng et al. “A Review of Computational Phantoms for Quality Assurance in Radiology and Radiotherapy in the Deep-Learning Era”. In: Journal of Radiation Protection and Research 47.3 (Sept. 2022), pp. 111–133. ISSN: 2466-2461. DOI: 10.14407/jrpr.2021.00402.

[13] Icrp-23. “Specific Absorbed Fractions for Reference Paediatric Individuals”. In: Annals of the ICRP 52.4 (1975), pp. 9–98. DOI: 10.1177/0146453231210647.

[14] Cristy Eckerman and et al. “Specific absorbed fractions of energy at various ages from internal photon sources: part I Methods ORNL/ TM-8381”. In: (1987).

[15] M Stabin et al. “Mathematical models and specific absorbed fractions of photon energy in the nonpregnant adult female and at the end of each trimester of pregnancy”. In: (May 8, 1995). DOI: 10.2172/91944.

[16] ICRP-89. “Basic Anatomical and Physiological Data for Use in Radiological Protection Reference Values.” In: Annals of the ICRP 89 (2002). Ed. by ICRP.

[17] Nina Petoussi-Henss et al. “The GSF family of voxel phantoms”. In: Physics in Medicine and Biology 47.1 (Dec. 2001), pp. 89–106. ISSN: 1361-6560. DOI: 10.1088/0031-9155/47/1/307.

[18] Kitiwat Khamwan et al. “Re-evaluation of pediatric 18F-FDG dosimetry: Cristy–Eckerman versus UF/NCI hybrid computational phantoms”. In: Physics in Medicine amp; Biology 63.16 (Aug. 2018), p. 165012. ISSN: 1361-6560. DOI: 10.1088/1361-6560/aad47a.

[19] Menzel HG, Clement C, and DeLuca P. “ICRP Publication 110. Realistic reference phantoms: an ICRP/ICRU joint effort. A report of adult reference computational phantoms.” In: Annals of the ICRP 39.2 (Apr. 2009), pp. 3–5. ISSN: 1872-969X. DOI: 10.1016/j.icrp.2009.09.001.

[20] Martin Caon. “Voxel-based computational models of real human anatomy: a review”. In: Radiation and Environmental Biophysics 42.4 (Feb. 2004), pp. 229–235. ISSN: 1432-2099. DOI: 10.1007/s00411-003-0221-8.

[21] Kaoru Sato et al. “Construction of new polygon mesh-type phantoms based on adult Japanese voxel phantoms”. In: PLOS ONE 19.10 (Oct. 2024). Ed. by Sakae Kinase, e0309753. ISSN: 1932-6203. DOI: 10.1371/journal.pone.0309753.

[22] S. Mattsson et al. “ICRP Publication 128: Radiation Dose to Patients from Radiopharmaceuticals: a Compendium of Current Information Related to Frequently Used Substances”. In: Annals of the ICRP 44.2$_s$*uppl* (June 2015), pp. 7–321. ISSN: 1872-969X. DOI: 10.1177/0146645314558019.

[23] J. D. Harrison and C. Streffer. “The ICRP protection quantities, equivalent and effective dose: their basis and application”. In: Radiation Protection Dosimetry 127.1–4 (June 2007), pp. 12–18. ISSN: 1742-3406. DOI: 10.1093/rpd/ncm248.

[24] Adam L. Kesner et al. “MIRD Pamphlet No. 28, Part 1: MIRDcalc—A Software Tool for Medical Internal Radiation Dosimetry”. In: Journal of Nuclear Medicine 64.7 (June 2023), pp. 1117–1124. ISSN: 2159-662X. DOI: 10.2967/jnumed.122.264225.

[25] Daphnée Villoing et al. “Organ dose calculator for diagnostic nuclear medicine patients based on the ICRP reference voxel phantoms and biokinetic models”. In: Biomedical Physics amp; Engineering Express 9.1 (Dec. 2022), p. 015004. ISSN: 2057-1976. DOI: 10.1088/2057-1976/aca543.

[26] Daphnée Villoing et al. “NCINM: organ dose calculator for patients undergoing nuclear medicine procedures”. In: Biomedical Physics amp; Engineering Express 6.5 (July 2020), p. 055010. ISSN: 2057-1976. DOI: 10.1088/2057-1976/aba41e.

[27] Jacek Capala et al. “Dosimetry for Radiopharmaceutical Therapy: Current Practices and Commercial Resources”. In: Journal of Nuclear Medicine 62.Supplement 3 (Dec. 2021), 3S–11S. ISSN: 2159-662X. DOI: 10.2967/jnumed.121.262749.

[28] Yuni K. Dewaraja et al. “A pipeline for automated voxel dosimetry: application in patients with multi-SPECT/CT imaging following 177Lu peptide receptor radionuclide therapy”. In: Journal of Nuclear Medicine (Apr. 2022), jnumed.121.263738. ISSN: 2159-662X. DOI: 10.2967/jnumed.121.263738.

[29] Keamogetswe Ramonaheng et al. “Activity quantification and dosimetry in radiopharmaceutical therapy with reference to 177Lutetium”. In: Frontiers in Nuclear Medicine 4 (Mar. 2024). ISSN: 2673-8880. DOI: 10.3389/fnume.2024.1355912.

[30] D Coleman, K T Griffin, and S A Dewji. “Stylized versus voxel phantoms: quantification of internal organ chord length distances”. In: Physics in Medicine & Biology 68.5 (2023), p. 055020. DOI: 10.1088/1361-6560/acbbb6. URL: https://dx.doi.org/10.1088/1361-6560/acbbb6.

[31] D. L. Bailey et al. Nuclear Medicine Physics: A Handbook for Teachers and Students. Ed. by IAEA. IAEA, Dec. 2014.

[32] Snyder W.S. “S, Absorbed Dose per Unit Cumulated Activity of the Source to the Target Organ”. In: Medical Internal Radiation Dose (MIRD) Committee MIRD Pamphlet 11 (1975).

[33] Michael G. Stabin. “MIRDOSE: Personal Computer Software for Internal Dose Assessment in Nuclear Medicine”. In: Journal of Nuclear Medicine 37.3 (1996), pp. 538–546. ISSN: 0161-5505. eprint: https://jnm.snmjournals.org/content/37/3/538.full.pdf. URL: https://jnm.snmjournals.org/content/37/3/538.

[34] Fred A. Mettler et al. “Population Characteristics and Absorbed Dose to the Population From Nuclear Medicine: United States - 1982”. In: Health Physics 50.5 (May 1986), pp. 619–628. ISSN: 0017-9078. DOI: 10.1097/00004032-198605000-00005.

[35] Sabrina K. Young et al. Assessment and adjustment of body weight measures in scanner data. June 2023. DOI: 10.32747/2023.8054018.ers.

[36] I. Shuryak, R. K. Sachs, and D. J. Brenner. “Cancer Risks After Radiation Exposure in Middle Age”. In: JNCI Journal of the National Cancer Institute 102.21 (Oct. 2010), pp. 1628–1636. ISSN: 1460-2105. DOI: 10.1093/jnci/djq346.

[37] Michel Koole et al. “Whole-Body Biodistribution and Radiation Dosimetry of 18F-GE067: A Radioligand for In Vivo Brain Amyloid Imaging”. In: Journal of Nuclear Medicine 50.5 (Apr. 2009), pp. 818–822. ISSN: 2159-662X. DOI: 10.2967/jnumed.108.060756.

[38] Michio Senda et al. “Biodistribution and radiation dosimetry of Flutemetamol (18F) injection in Japanese healthy volunteers”. In: Journal of Nuclear Medicine 53.supplement 1 (2012), pp. 1510–1510. ISSN: 0161-5505. eprint: https://jnm.snmjournals.org/content. URL: https://jnm.snmjournals.org/content/53/supplement_1/1510.

[39] Jamshid Maddahi et al. “Phase I, First-in-Human Study of BMS747158, a Novel 18F-Labeled Tracer for Myocardial Perfusion PET: Dosimetry, Biodistribution, Safety, and Imaging Characteristics After a Single Injection at Rest”. In: Journal of Nuclear Medicine 52.9 (2011), pp. 1490–1498. ISSN: 0161-5505. DOI: 10.2967/jnumed.111.092528.

eprint: https://jnm.snmjournals.org/content/52/9/1490.full.pdf. URL: https://jnm.snmjournals.org/content/52/9/1490.

[40] Jonathan Strosberg et al. “Phase 3 Trial of 177Lu-Dotatate for Midgut Neuroendocrine Tumors”. In: New England Journal of Medicine 376.2 (Jan. 2017), pp. 125–135. ISSN: 1533-4406. DOI: 10.1056/nejmoa1607427.

[41] Angela Y. Jia et al. “Lutetium-177 DOTATATE: A Practical Review”. In: Practical Radiation Oncology 12.4 (July 2022), pp. 305–311. ISSN: 1879-8500. DOI: 10.1016/j.prro.2022.02.002.

[42] Jaleh Fallah et al. “FDA Approval Summary: Lutetium Lu 177 Vipivotide Tetraxetan for Patients with Metastatic Castration-Resistant Prostate Cancer”. In: Clinical Cancer Research 29.9 (Dec. 2022), pp. 1651–1657. ISSN: 1557-3265. DOI: 10.1158/1078-0432.ccr-22-2875.

[43] Gefei Chen et al. “Lu-177-PSMA dosimetry for kidneys and tumors based on SPECT images at two imaging time points”. In: Frontiers in Medicine 10 (Nov. 2023). ISSN: 2296-858X. DOI: 10.3389/fmed.2023.1246881.

[44] Ken Herrmann et al. “Renal and Multiorgan Safety of177Lu-PSMA-617 in Patients with Metastatic Castration-Resistant Prostate Cancer in the VISION Dosimetry Substudy”. In: Journal of Nuclear Medicine 65.1 (Nov. 2023), pp. 71–78. ISSN: 2159-662X. DOI: 10.2967/jnumed.123.265448.

[45] Mattias Sandström et al. “Kidney dosimetry in 777 patients during 177Lu-DOTATATE therapy: aspects on extrapolations and measurement time points”. In: EJNMMI Physics 7.1 (Dec. 2020). ISSN: 2197-7364. DOI: 10.1186/s40658-020-00339-2.

[46] S. Oliver et al. “Determination of organ doses in thyroid treatments with radioactive iodine by Monte Carlo simulation”. In: Radiation Physics and Chemistry 221 (Aug. 2024), p. 111737. ISSN: 0969-806X. DOI: 10.1016/j.radphyschem.2024.111737.

[47] Brandon A Howard et al. “A practical method of I-131 thyroid cancer therapy dose optimization using estimated effective renal clearance”. In: SAGE Open Medical Case Reports 5 (Jan. 2017). ISSN: 2050-313X. DOI: 10.1177/2050313x17745203.

[48] Jun Ma et al. “Segment anything in medical images”. In: Nature Communications 15.1 (Jan. 2024). ISSN: 2041-1723. DOI: 10.1038/s41467-024-44824-z.

[49] Jakob Wasserthal et al. “TotalSegmentator: Robust Segmentation of 104 Anatomic Structures in CT Images”. In: Radiology: Artificial Intelligence 5.5 (Sept. 2023). ISSN: 2638-6100. DOI: 10.1148/ryai.230024.

[50] Christopher Werner et al. MCNP Version 6.2 Release Notes. Feb. MCNP6.2. DOI: 10.2172/1419730.

[51] III Hughes, Henry Grady, and John Timothy Goorley. Features of MCNP6 Relevant to Medical Radiation Physics. Presentation LA-UR-12-24401. Los Alamos, NM, USA: Los Alamos National Laboratory, 2012. URL: http://permalink.lanl.gov/object/tr?what=info:lanl-repo/lareport/LA-UR-12-24401.

[52] "ICRP Publication 107 Nuclear Decay Data for Dosimetric Calculations". In: Annals of the ICRP 46.3-4 (2008). PMID: 29380630, pp. 1–486. DOI: 10.1177/0146645317734963. eprint: https://doi.org/10.1177/0146645317734963. URL: https://doi.org/10.1177/0146645317734963.

[53] Stephanie Lamart et al. "Comparison of internal dosimetry factors for three classes of adult computational phantoms with emphasis on I-131 in the thyroid". In: Physics in Medicine and Biology 56.22 (Oct. 2011), pp. 7317–7335. ISSN: 1361-6560. DOI: 10.1088/0031-9155/56/22/020.

Appendices

Appendix A

S-value Error Simulations

Table A.1: Female (Tc-99m) S-value Percent Error Simulation

Female (Tc-99m) S-value Percent Error ($\frac{\triangle s}{s} * 100$)								
	Spleen	R. Kidney	L. Kidney	Liver	Stomach	Pancreas	L. Lung	R. Lung
f01	0.25	0.213	0.19	0.134	0.366	0.341	0.403	0.38
f02	0.174	0.201	0.19	0.111	0.197	0.394	0.494	0.421
f03	0.279	0.211	0.201	0.146	0.284	0.377	0.437	0.424
f04	0.209	0.203	0.196	0.111	0.275	0.359	0.39	0.39
f05	0.498	0.169	0.279	0.116	0.293	0.657	0.323	0.261
f06	0.26	0.199	0.21	0.144	0.326	0.472	0.442	0.403
f07	0.314	0.205	0.213	0.103	0.186	0.327	0.337	0.281
f08	0.274	0.206	0.205	0.134	0.345	0.379	0.378	0.405
f09	0.311	0.196	0.203	0.122	0.328	0.469	0.388	0.387
f10	0.209	0.21	0.198	0.115	0.329	0.435	0.36	0.371
f11	0.233	0.196	0.203	0.113	0.381	0.426	0.378	0.328
f12	0.236	0.211	0.205	0.114	0.219	0.348	0.285	0.282
f13	0.274	0.197	0.204	0.113	0.279	0.4	0.32	0.303
f14	0.302	0.217	0.192	0.132	0.351	0.322	0.391	0.4
f15	0.222	0.193	0.218	0.125	0.345	0.494	0.362	0.356
f16	0.276	0.209	0.197	0.134	0.216	0.373	0.343	0.294
f17	0.286	0.205	0.214	0.135	0.283	0.414	0.375	0.342
f18	0.442	0.197	0.202	0.146	0.259	0.389	0.379	0.37
f19	0.248	0.207	0.207	0.135	0.309	0.401	0.375	0.319
f20	0.532	0.155	0.416	0.125	0.349	0.501	0.409	0.331
f21	0.198	0.21	0.198	0.114	0.322	0.386	0.375	0.345
f22	0.275	0.206	0.206	0.125	0.3	0.395	0.279	0.286
f23	0.247	0.22	0.202	0.128	0.362	0.493	0.289	0.314
f24	0.204	0.212	0.205	0.122	0.26	0.392	0.401	0.39
f25	0.238	0.206	0.206	0.124	0.288	0.362	0.307	0.294
f26	0.187	0.198	0.198	0.111	0.308	0.431	0.37	0.333
f27	0.208	0.196	0.196	0.112	0.26	0.361	0.403	0.398
f28	0.275	0.181	0.205	0.133	0.273	0.39	0.415	0.39
f29	0.249	0.211	0.192	0.125	0.227	0.433	0.353	0.331
f30	0.2	0.232	0.188	0.149	0.238	0.4	0.309	0.309

Table A.2: Male (Tc-99m) S-value Percent Error Simulation

Male (Tc-99m) S-value Percent Error ($\frac{\triangle s}{s} * 100$)								
	Spleen	R. Kidney	L. Kidney	Liver	Stomach	Pancreas	L. Lung	R. Lung
m1	0.337	0.208	0.198	0.133	0.309	0.515	0.371	0.392
m2	0.277	0.214	0.206	0.139	0.276	0.456	0.344	0.369
m3	0.251	0.196	0.196	0.142	0.267	0.411	0.308	0.33
m4	0.282	0.194	0.195	0.123	0.242	0.393	0.296	0.305
m5	0.514	0.132	0	0.113	0.318	0.446	0.47	0.313
m6	0.321	0.21	0.2	0.132	0.382	0.384	0.367	0.349
m7	0.225	0.208	0.199	0.123	0.28	0.391	0.288	0.301
m8	0.293	0.197	0.197	0.123	0.279	0.388	0.369	0.321
m9	0.167	0	0.134	0.182	0.282	0.452	0.311	0.42
m10	0.274	0.205	0.199	0.114	0.245	0.38	0.317	0.323
m11	0.422	0.173	0.239	0.112	0.267	0.423	0.308	0.301
m12	0.235	0.197	0.197	0.112	0.263	0.332	0.321	0.291
m13	0	0	0	0	0	0	0	0
m14	0.348	0.197	0.209	0.113	0.245	0.674	0.282	0.275
m15	0.43	0.201	0.194	0.122	0.231	0.501	0.374	0.343
m16	0.29	4.27	0.133	0.186	0.2	0.528	0.251	0.388
m17	0.309	0.21	0.199	0.114	0.265	0.474	0.255	0.284
m18	0.332	0.204	0.198	0.124	0.313	0.431	0.3	0.311
m19	0.529	0.205	0.213	0.134	0.261	0.454	0.343	0.292
m20	0.214	0.201	0.196	0.0977	0.278	0.37	0.344	0.354
m21	0.222	0.283	0.163	0.122	0.176	0.465	0.443	0.56
m22	0.244	0.203	0.197	0.12	0.25	0.405	0.298	0.272
m23	0.311	0.196	0.202	0.111	0.328	0.347	0.359	0.335
m24	0.269	0.2	0.211	0.135	0.244	0.386	0.331	0.324
m25	0.272	0.195	0.203	0.144	0.366	0.423	0.357	0.345

Table A.3: Female (F-18) S-value Percent Error Simulation

Female (F-18) S-value Percent Error ($\frac{\triangle s}{s} * 100$)								
	Spleen	R. Kidney	L. Kidney	Liver	Stomach	Pancreas	L. Lung	R. Lung
f01	0.256	0.0513	0.0491	0.137	0.418	0.373	0.402	0.415
f02	0.17	0.0496	0.0494	0.115	0.212	0.436	0.515	0.447
f03	0.286	0.0497	0.0498	0.147	0.314	0.433	0.446	0.412
f04	0.223	0.0491	0.0493	0.115	0.309	0.394	0.393	0.425
f05	0.479	0.0362	0.0726	0.117	0.307	0.73	0.325	0.284
f06	0.267	0.0486	0.0503	0.157	0.366	0.491	0.437	0.404
f07	0.321	0.0493	0.0489	0.106	0.198	0.372	0.365	0.304
f08	0.278	0.0491	0.0494	0.137	0.39	0.406	0.384	0.414
f09	0.316	0.0493	0.0491	0.126	0.369	0.55	0.41	0.399
f10	0.223	0.05	0.0484	0.116	0.367	0.493	0.385	0.394
f11	0.245	0.0492	0.0492	0.116	0.439	0.468	0.41	0.351
f12	0.235	0.0494	0.0495	0.116	0.24	0.395	0.295	0.3
f13	0.289	0.049	0.0509	0.116	0.323	0.428	0.326	0.324
f14	0.31	0.0577	0.0485	0.136	0.407	0.362	0.404	0.426
f15	0.223	0.048	0.0596	0.126	0.388	0.557	0.37	0.369
f16	0.289	0.0506	0.0489	0.137	0.228	0.432	0.354	0.305
f17	0.288	0.0493	0.0506	0.137	0.312	0.437	0.388	0.367
f18	0.46	0.0492	0.0494	0.147	0.281	0.426	0.376	0.394
f19	0.256	0.0488	0.0487	0.137	0.341	0.418	0.381	0.329
f20	0.55	0.0272	0.0964	0.126	0.389	0.577	0.415	0.343
f21	0.213	0.0501	0.0485	0.116	0.367	0.433	0.391	0.356
f22	0.279	0.0489	0.049	0.127	0.34	0.428	0.279	0.302
f23	0.246	0.0495	0.0481	0.127	0.407	0.528	0.304	0.328
f24	0.204	0.0492	0.0493	0.126	0.29	0.425	0.413	0.424
f25	0.246	0.0491	0.0491	0.127	0.319	0.395	0.307	0.313
f26	0.192	0.0486	0.0486	0.115	0.35	0.502	0.417	0.365
f27	0.223	0.0492	0.0493	0.115	0.307	0.405	0.4	0.416
f28	0.287	0.0485	0.0506	0.136	0.302	0.44	0.429	0.416
f29	0.256	0.0497	0.0484	0.127	0.266	0.51	0.374	0.352
f30	0.213	0.06	0.0474	0.148	0.265	0.438	0.321	0.317

Table A.4: Male (F-18) S-value Percent Error Simulation

Male (F-18) S-value Percent Error ($\frac{\triangle s}{s} * 100$)								
	Spleen	R. Kidney	L. Kidney	Liver	Stomach	Pancreas	L. Lung	R. Lung
m1	0.349	0.0513	0.0489	0.136	0.354	0.573	0.406	0.411
m2	0.29	0.0507	0.0492	0.138	0.302	0.486	0.348	0.373
m3	0.264	0.0495	0.0496	0.146	0.302	0.439	0.313	0.338
m4	0.299	0.0501	0.0497	0.126	0.27	0.427	0.316	0.311
m5	0.557	0.0181	0	0.106	0.354	0.525	0.515	0.329
m6	0.34	0.0502	0.0482	0.146	0.433	0.436	0.376	0.373
m7	0.233	0.0508	0.0485	0.126	0.312	0.452	0.309	0.322
m8	0.298	0.0492	0.0491	0.126	0.301	0.437	0.391	0.348
m9	0.171	0	0.0174	0.192	0.309	0.503	0.334	0.432
m10	0.286	0.0506	0.0484	0.116	0.279	0.419	0.343	0.345
m11	0.441	0.0396	0.0624	0.106	0.292	0.47	0.32	0.314
m12	0.246	0.0489	0.0488	0.116	0.298	0.372	0.332	0.308
m13	0	0	0	0	0	0	0	0
m14	0.344	0.0489	0.0505	0.116	0.275	0.696	0.288	0.282
m15	0.448	0.0501	0.0501	0.126	0.251	0.544	0.372	0.354
m16	0.301	0.962	0.018	0.194	0.22	0.583	0.256	0.403
m17	0.321	0.0502	0.0482	0.117	0.283	0.504	0.257	0.299
m18	0.342	0.0509	0.0488	0.126	0.34	0.482	0.307	0.331
m19	0.557	0.0497	0.049	0.137	0.282	0.489	0.363	0.304
m20	0.223	0.0497	0.0497	0.104	0.323	0.435	0.362	0.373
m21	0.224	0.0741	0.0372	0.126	0.188	0.533	0.432	0.586
m22	0.255	0.0492	0.0489	0.125	0.269	0.467	0.294	0.282
m23	0.33	0.0493	0.0493	0.115	0.381	0.392	0.377	0.36
m24	0.277	0.0478	0.0497	0.137	0.261	0.447	0.341	0.328
m25	0.286	0.0498	0.0493	0.157	0.405	0.463	0.379	0.362

Table A.5: Female (Lu-177) S-value Percent Error Simulation

Female (Lu-177) S-value Percent Error ($\frac{\triangle s}{s} * 100$)								
	Spleen	R. Kidney	L. Kidney	Liver	Stomach	Pancreas	L. Lung	R. Lung
f01	0.529	0.0609	0.0509	0.255	0.561	0.693	0.77	0.491
f02	0.335	0.061	0.051	0.207	0.395	0.798	0.602	0.546
f03	0.544	0.0609	0.0609	0.269	0.387	0.749	0.576	0.657
f04	0.435	0.0609	0.0608	0.206	0.431	0.753	0.791	0.54
f05	1.11	0.0409	0.0811	0.235	0.588	1.12	0.582	0.353
f06	0.545	0.0609	0.0609	0.271	0.572	0.95	0.865	0.664
f07	0.668	0.0608	0.0608	0.199	0.319	0.676	0.442	0.382
f08	0.571	0.0608	0.0608	0.255	0.517	0.795	0.635	0.526
f09	0.578	0.0608	0.0609	0.214	0.484	0.802	0.594	0.561
f10	0.436	0.0609	0.0609	0.224	0.486	0.794	0.642	0.49
f11	0.471	0.0608	0.061	0.226	0.535	0.902	0.595	0.553
f12	0.487	0.0608	0.0608	0.215	0.383	0.744	0.549	0.485
f13	0.599	0.0608	0.0609	0.223	0.507	0.833	0.61	0.42
f14	0.631	0.061	0.0509	0.231	0.658	0.669	0.637	0.512
f15	0.449	0.0509	0.061	0.23	0.487	0.922	0.721	0.556
f16	0.593	0.0609	0.0607	0.256	0.365	0.72	0.58	0.558
f17	0.591	0.0608	0.061	0.244	0.495	0.855	0.517	0.523
f18	0.95	0.0608	0.061	0.264	0.445	0.817	0.641	0.513
f19	0.508	0.0608	0.0608	0.257	0.497	0.819	0.73	0.662
f20	1.16	0.0407	0.111	0.229	0.663	1.06	0.827	0.596
f21	0.414	0.0609	0.0509	0.22	0.447	0.756	0.575	0.474
f22	0.591	0.0608	0.0608	0.235	0.471	0.837	0.594	0.522
f23	0.519	0.0609	0.0509	0.257	0.504	1.11	0.545	0.483
f24	0.437	0.0608	0.0608	0.222	0.46	0.812	0.655	0.516
f25	0.499	0.0608	0.0608	0.246	0.452	0.766	0.591	0.381
f26	0.377	0.0609	0.0609	0.199	0.501	0.795	0.534	0.469
f27	0.432	0.061	0.0608	0.205	0.399	0.758	0.734	0.536
f28	0.557	0.0511	0.061	0.245	0.487	0.722	0.767	0.543
f29	0.523	0.0609	0.0509	0.238	0.337	0.921	0.607	0.572
f30	0.422	0.0611	0.0508	0.277	0.326	0.856	0.522	0.608

Table A.6: Male (Lu-177) S-value Percent Error Simulation

Male (Lu-177) S-value Percent Error ($\frac{\triangle s}{s} * 100$)								
	Spleen	R. Kidney	L. Kidney	Liver	Stomach	Pancreas	L. Lung	R. Lung
m1	0.653	0.0609	0.0609	0.235	0.527	1.02	0.631	0.592
m2	0.623	0.061	0.0608	0.271	0.487	1.01	0.643	0.609
m3	0.488	0.061	0.0608	0.251	0.454	0.863	0.514	0.48
m4	0.612	0.0608	0.0608	0.231	0.406	0.826	0.558	0.501
m5	1.01	0.0308	0	0.208	0.421	0.708	0.586	0.469
m6	0.66	0.0609	0.0609	0.244	0.612	0.791	0.615	0.551
m7	0.449	0.0609	0.0609	0.231	0.473	0.719	0.443	0.512
m8	0.587	0.0609	0.0609	0.231	0.452	0.819	0.561	0.487
m9	0.351	0	0.0308	0.224	0.431	0.98	0.571	0.511
m10	0.543	0.0609	0.0609	0.22	0.402	0.811	0.418	0.447
m11	0.946	0.0508	0.0711	0.2	0.474	0.927	0.643	0.555
m12	0.514	0.0609	0.0609	0.208	0.408	0.676	0.537	0.444
m13	0	0	0	0	0	0	0	0
m14	0.746	0.0607	0.0609	0.219	0.494	1.5	0.592	0.477
m15	0.91	0.061	0.0608	0.225	0.423	1.03	0.588	0.423
m16	0.636	1.11	0.0308	0.266	0.373	1.19	0.515	0.637
m17	0.672	0.0609	0.0511	0.228	0.472	0.998	0.54	0.448
m18	0.696	0.0609	0.0609	0.225	0.483	0.937	0.563	0.515
m19	1.14	0.0608	0.0608	0.253	0.448	0.918	0.575	0.537
m20	0.426	0.061	0.0608	0.162	0.476	0.736	0.681	0.577
m21	0.458	0.0811	0.041	0.226	0.311	0.987	0.636	0.727
m22	0.5	0.061	0.0607	0.207	0.391	0.842	0.526	0.48
m23	0.636	0.0608	0.061	0.208	0.535	0.692	0.524	0.547
m24	0.563	0.0609	0.0609	0.243	0.423	0.833	0.542	0.476
m25	0.528	0.0608	0.0609	0.268	0.614	0.774	0.672	0.546

Table A.7: Female (I-131) S-value Percent Error Simulation

Female (I-131) S-value Percent Error ($\frac{\triangle s}{s} * 100$)								
	Spleen	R. Kidney	L. Kidney	Liver	Stomach	Pancreas	L. Lung	R. Lung
f01	0.282	0.0506	0.0407	0.153	0.436	0.393	0.433	0.428
f02	0.189	0.051	0.0408	0.12	0.224	0.459	0.552	0.462
f03	0.302	0.0497	0.0409	0.154	0.329	0.456	0.462	0.431
f04	0.236	0.0493	0.0408	0.12	0.327	0.418	0.425	0.448
f05	0.535	0.0303	0.0623	0.133	0.332	0.755	0.349	0.298
f06	0.293	0.0403	0.05	0.164	0.38	0.531	0.473	0.427
f07	0.343	0.0406	0.0492	0.111	0.215	0.392	0.378	0.318
f08	0.306	0.0493	0.0495	0.153	0.398	0.44	0.407	0.427
f09	0.341	0.0408	0.0506	0.131	0.376	0.567	0.428	0.427
f10	0.236	0.0498	0.0402	0.122	0.383	0.514	0.408	0.411
f11	0.258	0.0407	0.0507	0.132	0.446	0.495	0.431	0.371
f12	0.259	0.0495	0.0408	0.122	0.248	0.418	0.32	0.31
f13	0.308	0.0406	0.0503	0.132	0.335	0.456	0.342	0.337
f14	0.339	0.051	0.0402	0.142	0.432	0.383	0.425	0.449
f15	0.237	0.04	0.0508	0.133	0.405	0.582	0.399	0.395
f16	0.307	0.0502	0.0405	0.143	0.246	0.451	0.377	0.329
f17	0.316	0.0407	0.0502	0.143	0.333	0.473	0.403	0.383
f18	0.5	0.0407	0.0495	0.153	0.3	0.452	0.401	0.42
f19	0.271	0.0492	0.0402	0.144	0.361	0.455	0.412	0.357
f20	0.599	0.0283	0.0931	0.133	0.415	0.619	0.448	0.365
f21	0.225	0.0499	0.0403	0.122	0.372	0.455	0.409	0.372
f22	0.298	0.0493	0.0493	0.133	0.358	0.454	0.308	0.314
f23	0.263	0.0495	0.0399	0.144	0.413	0.566	0.327	0.345
f24	0.227	0.0494	0.0406	0.132	0.31	0.45	0.447	0.438
f25	0.261	0.0405	0.0493	0.143	0.337	0.419	0.333	0.326
f26	0.203	0.0403	0.0504	0.12	0.369	0.52	0.434	0.378
f27	0.236	0.0494	0.0408	0.12	0.313	0.437	0.43	0.431
f28	0.303	0.0405	0.0502	0.152	0.314	0.467	0.457	0.441
f29	0.281	0.0497	0.0402	0.143	0.271	0.537	0.398	0.373
f30	0.226	0.0509	0.0396	0.156	0.269	0.463	0.341	0.334

Table A.8: Male (I-131) S-value Percent Error Simulation

Male (I-131) S-value Percent Error ($\frac{\triangle s}{s} * 100$)								
	Spleen	R. Kidney	L. Kidney	Liver	Stomach	Pancreas	L. Lung	R. Lung
m1	0.377	0.0505	0.0405	0.141	0.366	0.614	0.42	0.43
m2	0.32	0.0502	0.0406	0.145	0.313	0.52	0.374	0.405
m3	0.277	0.0496	0.0409	0.152	0.312	0.467	0.333	0.355
m4	0.327	0.0499	0.0497	0.132	0.288	0.453	0.33	0.331
m5	0.602	0.0187	0	0.121	0.358	0.549	0.526	0.345
m6	0.369	0.0499	0.0413	0.152	0.444	0.46	0.401	0.394
m7	0.245	0.0503	0.0402	0.132	0.322	0.472	0.326	0.331
m8	0.325	0.0494	0.0493	0.142	0.319	0.461	0.408	0.365
m9	0.191	0	0.0198	0.203	0.327	0.545	0.348	0.454
m10	0.301	0.0502	0.0415	0.122	0.297	0.447	0.357	0.359
m11	0.481	0.0396	0.0612	0.12	0.313	0.508	0.339	0.337
m12	0.271	0.0492	0.0492	0.121	0.305	0.392	0.352	0.326
m13	0	0	0	0	0	0	0	0
m14	0.378	0.0405	0.0501	0.131	0.288	0.752	0.315	0.302
m15	0.485	0.0499	0.0413	0.131	0.262	0.587	0.394	0.368
m16	0.322	0.896	0.0187	0.207	0.23	0.624	0.281	0.425
m17	0.352	0.0499	0.0401	0.132	0.304	0.536	0.283	0.317
m18	0.373	0.0504	0.0404	0.131	0.36	0.512	0.332	0.35
m19	0.603	0.0408	0.0504	0.153	0.292	0.517	0.384	0.327
m20	0.244	0.0497	0.041	0.107	0.333	0.456	0.391	0.394
m21	0.247	0.0631	0.0296	0.141	0.196	0.565	0.452	0.61
m22	0.27	0.0508	0.0405	0.13	0.287	0.503	0.318	0.303
m23	0.349	0.0408	0.0495	0.13	0.4	0.41	0.394	0.379
m24	0.304	0.0411	0.0497	0.143	0.281	0.471	0.362	0.346
m25	0.301	0.0411	0.0508	0.164	0.427	0.482	0.405	0.381

Appendix B

Correlation between Weight and S-values

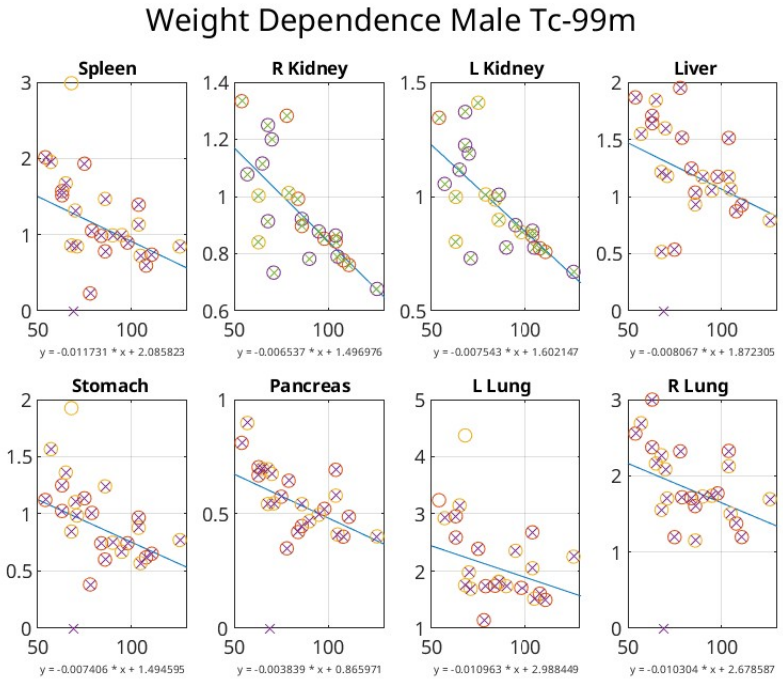

Figure B.1: Male Patient's S-value Dependence (Tc-99m) on Weight

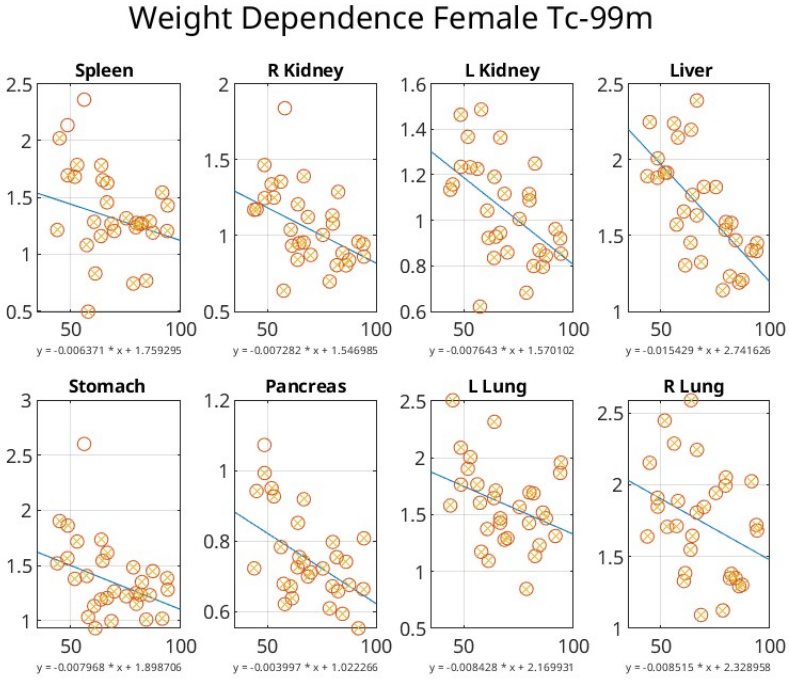

Figure B.2: Female Patient's S-value Dependence (Tc-99m) on Weight

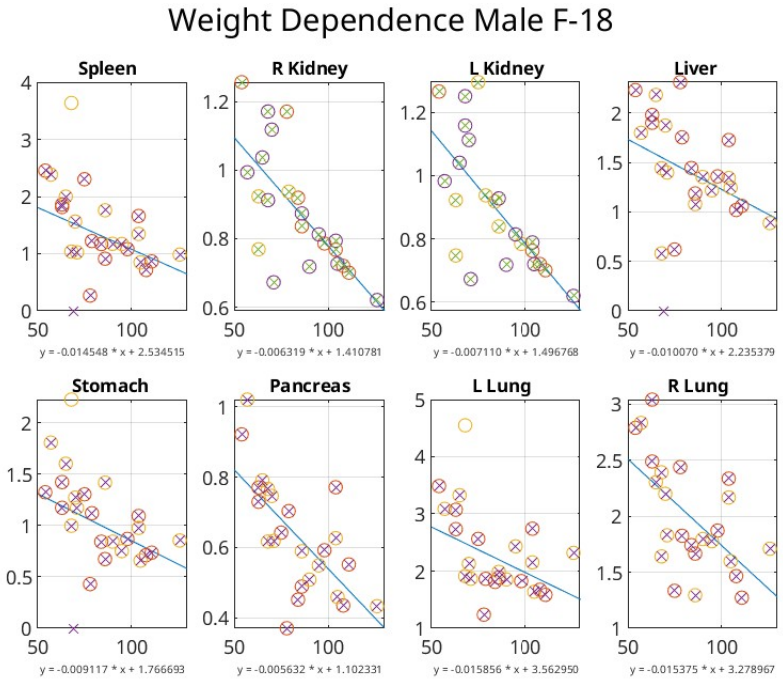

Figure B.3: Male Patient's S-value Dependence (F-18) on Weight

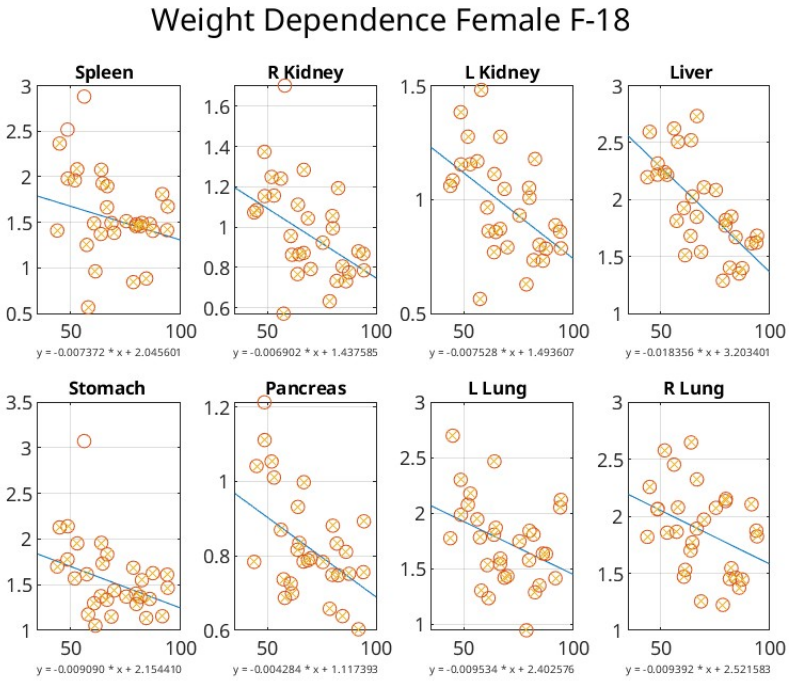

Figure B.4: Female Patient's S-value Dependence (F-18) on Weight

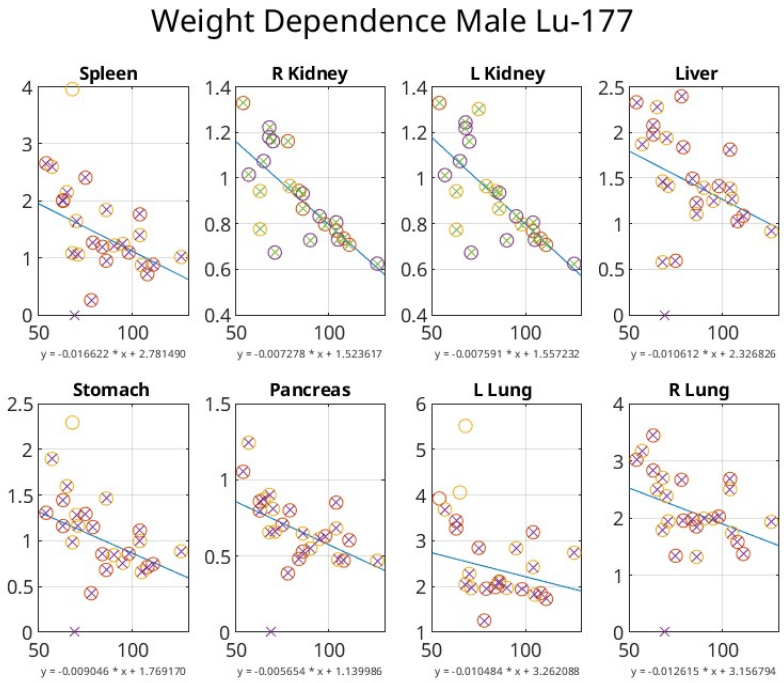

Figure B.5: Male Patient's S-value Dependence (Lu-177) on Weight

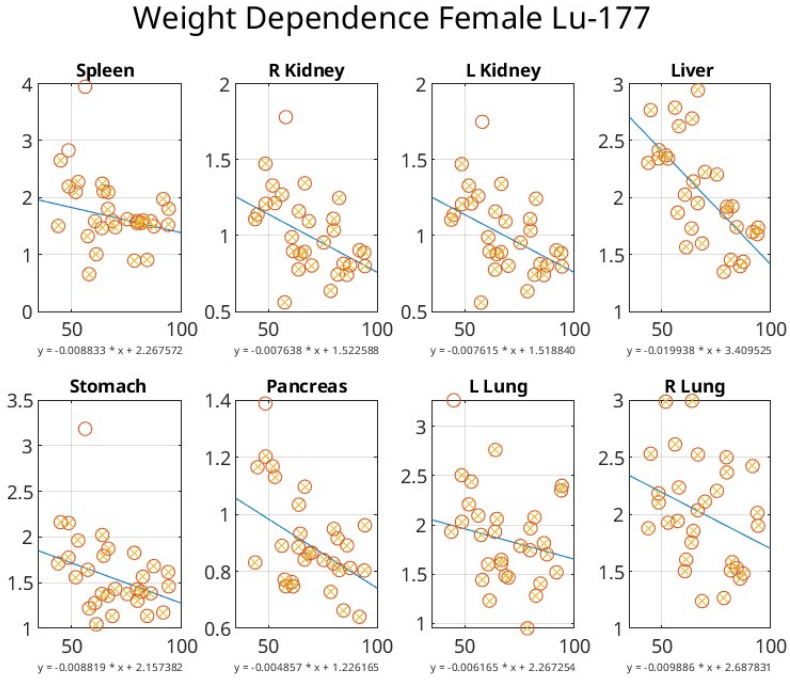

Figure B.6: Female Patient's S-value Dependence (Lu-177) on Weight

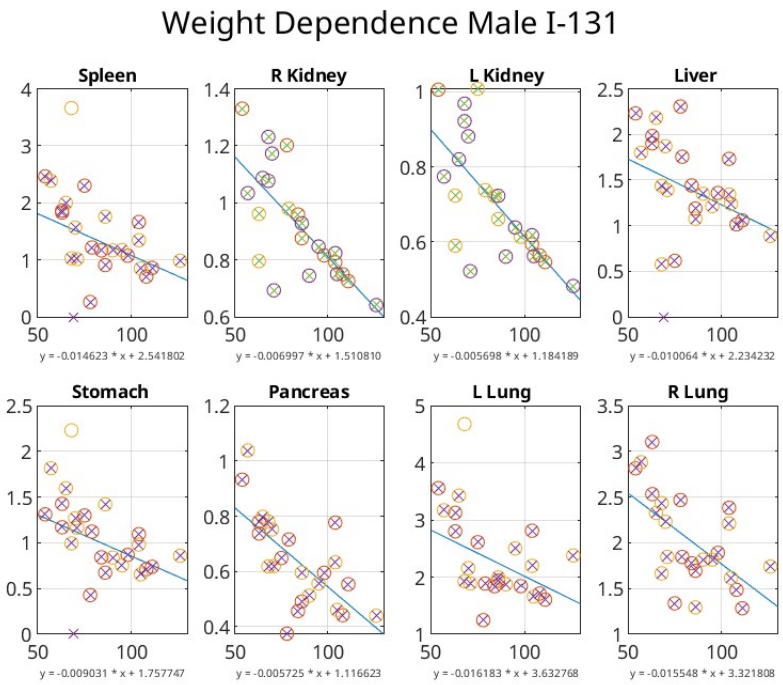

Figure B.7: Male Patient's S-value Dependence (I-131) on Weight

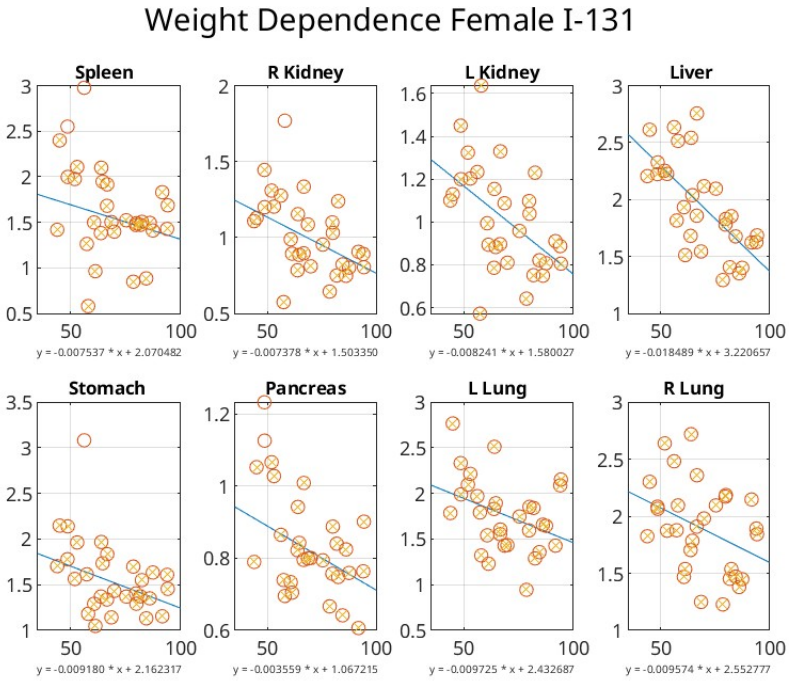

Figure B.8: Female Patient's S-value Dependence (I-131) on Weight

Appendix C

Correlation between Height and S-values

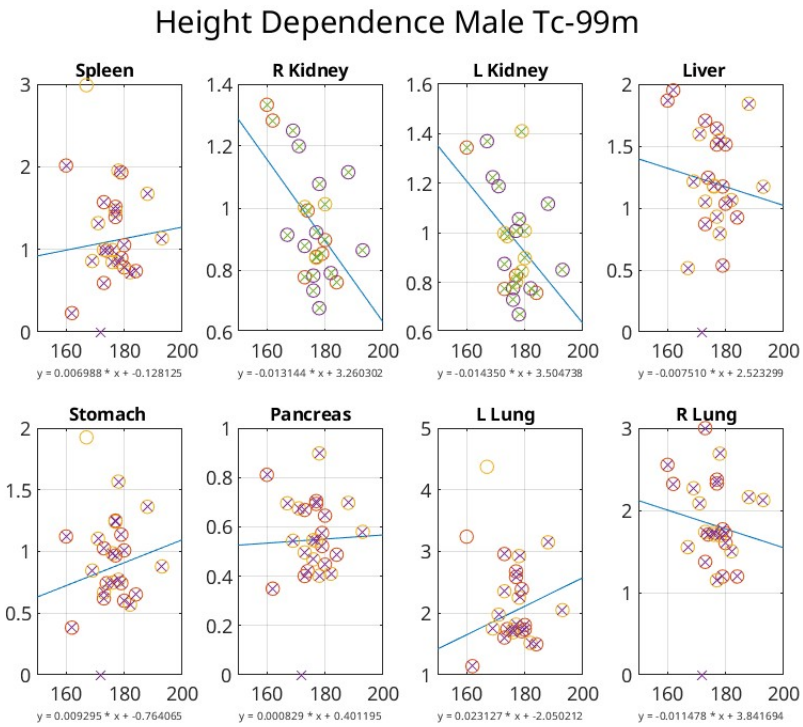

Figure C.1: Male Patient's S-value Dependence (Tc-99m) on Height

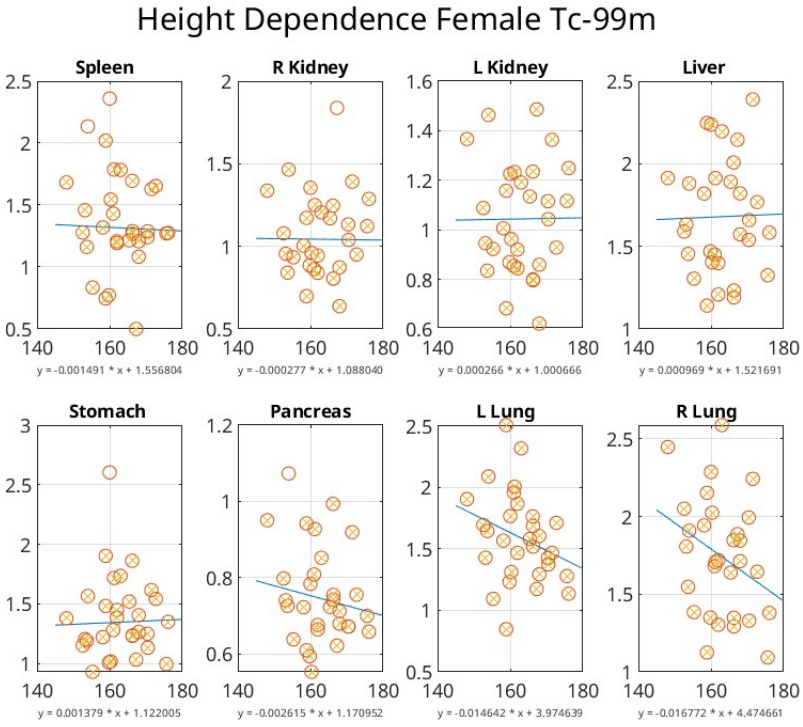

Figure C.2: Female Patient's S-value Dependence (Tc-99m) on Height

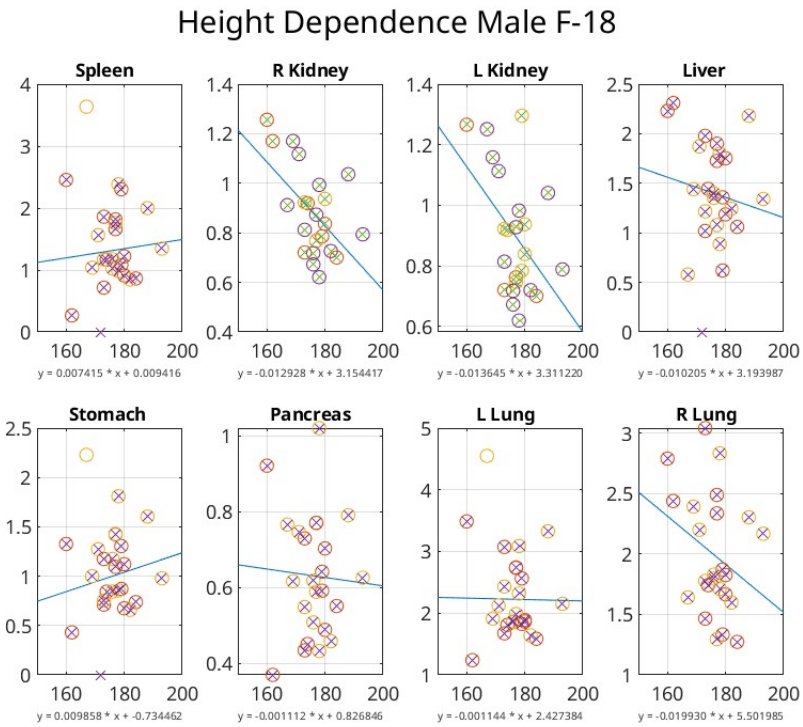

Figure C.3: Male Patient's S-value Dependence (F-18) on Height

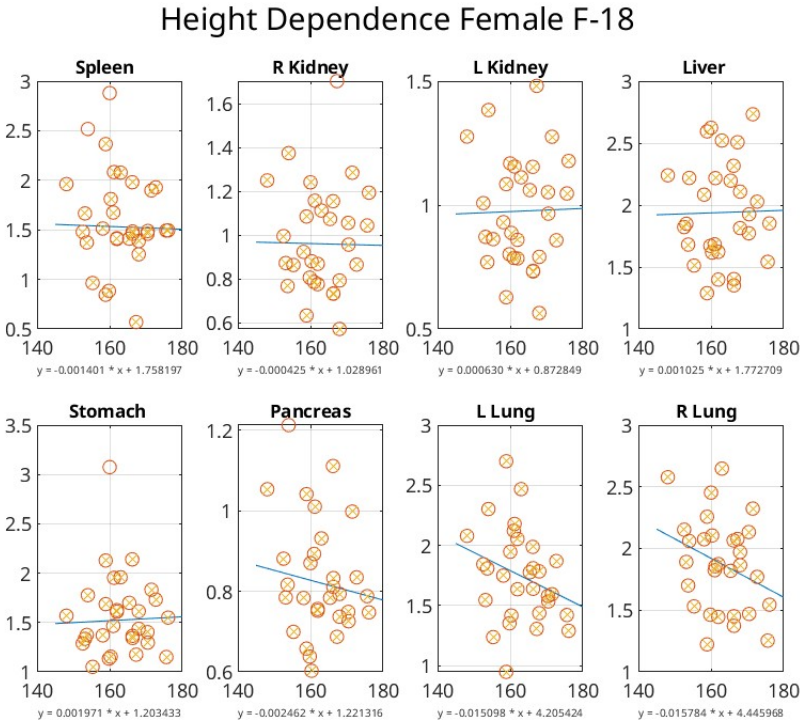

Figure C.4: Female Patient's S-value Dependence (F-18) on Height

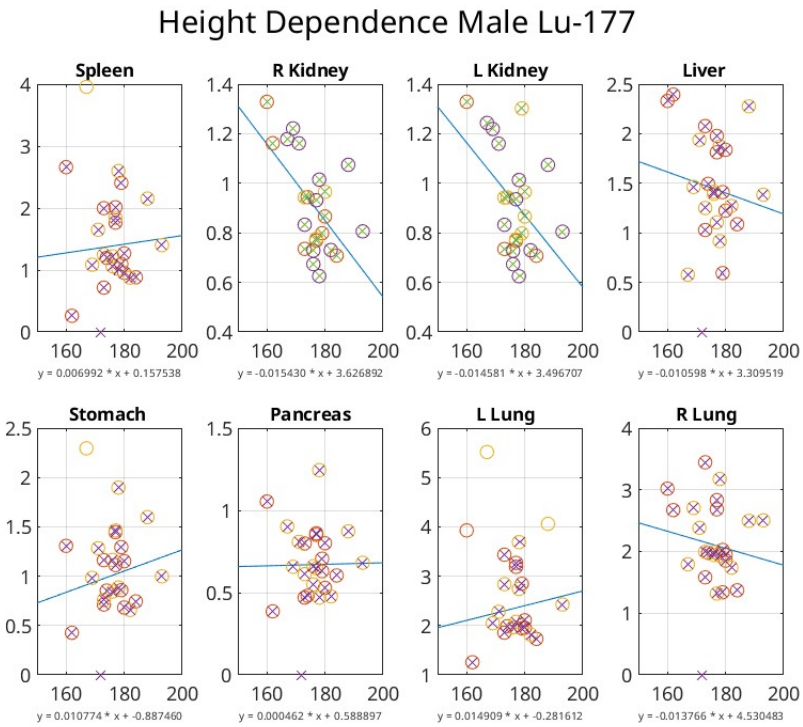

Figure C.5: Male Patient's S-value Dependence (Lu-177) on Height

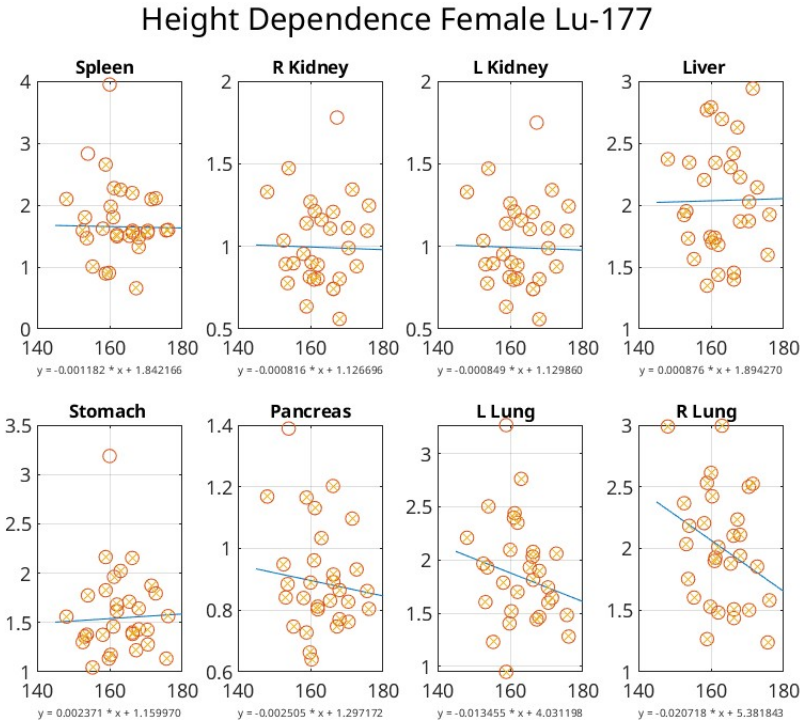

Figure C.6: Female Patient's S-value Dependence (Lu-177) on Height

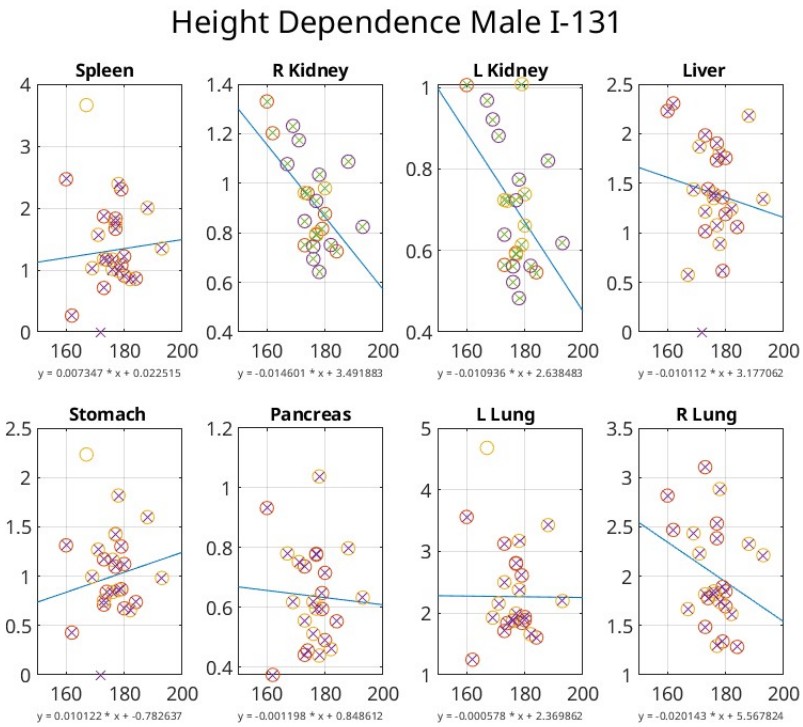

Figure C.7: Male Patient's S-value Dependence (I-131) on Height

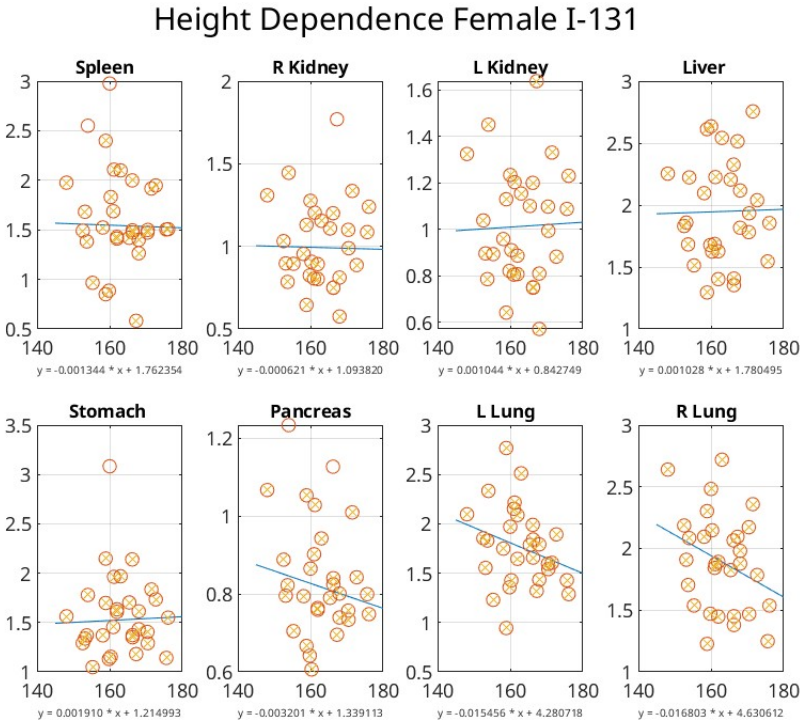

Figure C.8: Female Patient's S-value Dependence (I-131) on Height

Appendix D

Correlation between Age and S-values

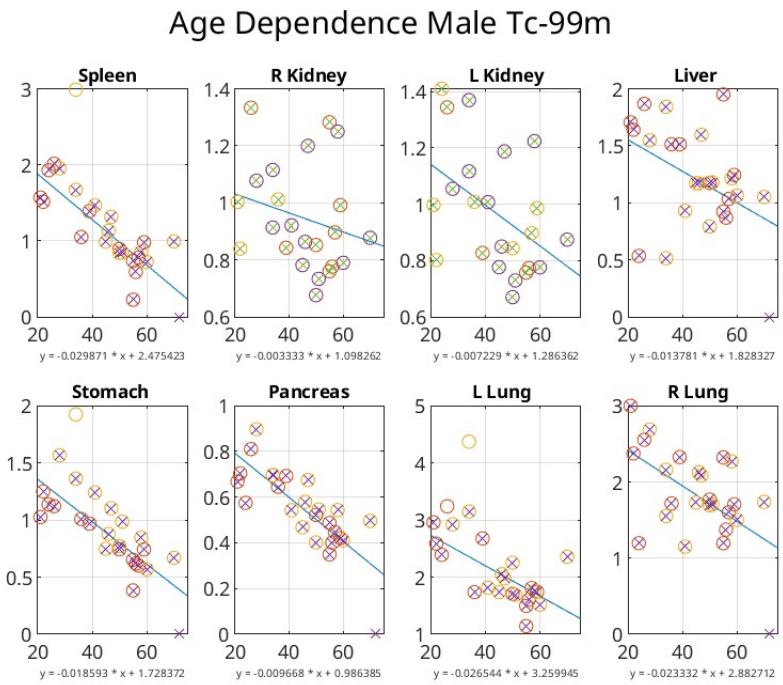

Figure D.1: Male Patient's S-value Dependence (Tc-99m) on Age

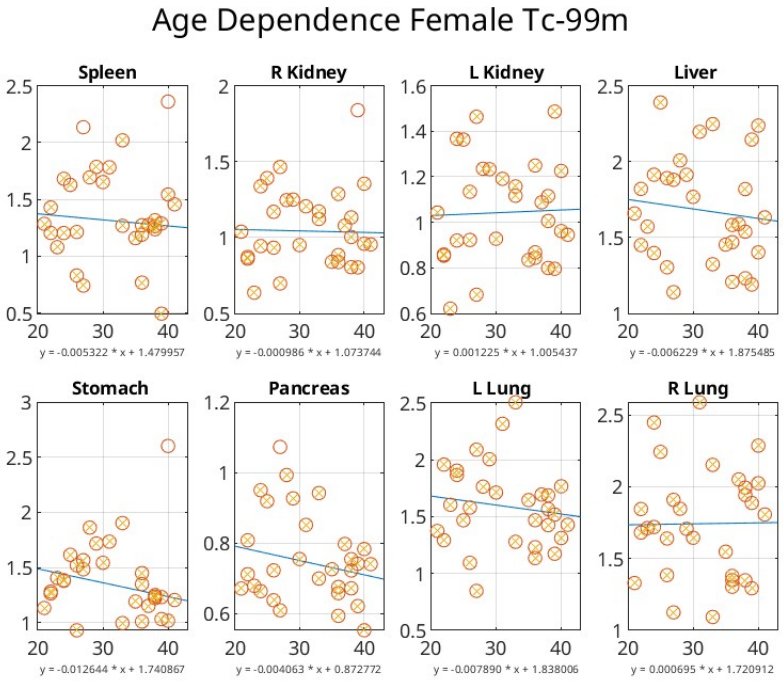

Figure D.2: Female Patient's S-value Dependence (Tc-99m) on Age

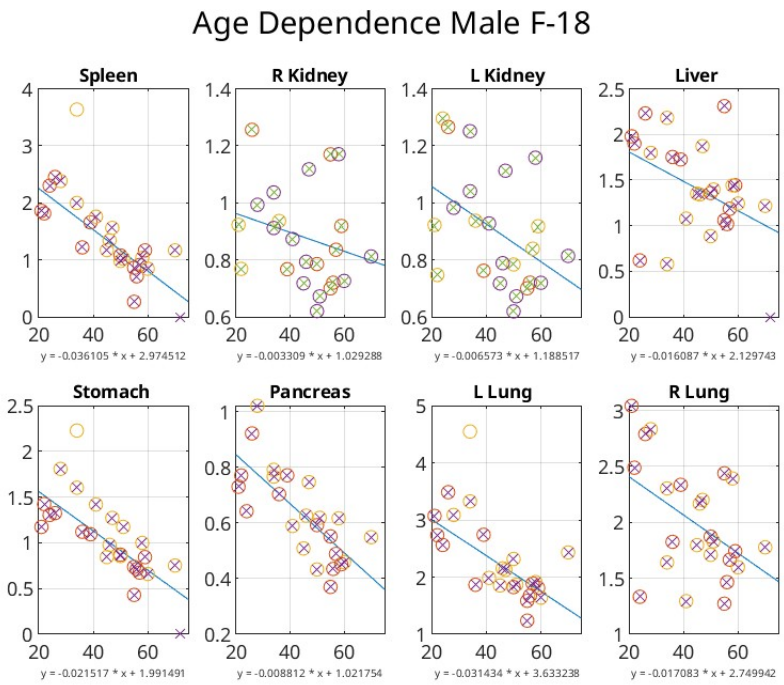

Figure D.3: Male Patient's S-value Dependence (F-18) on Age

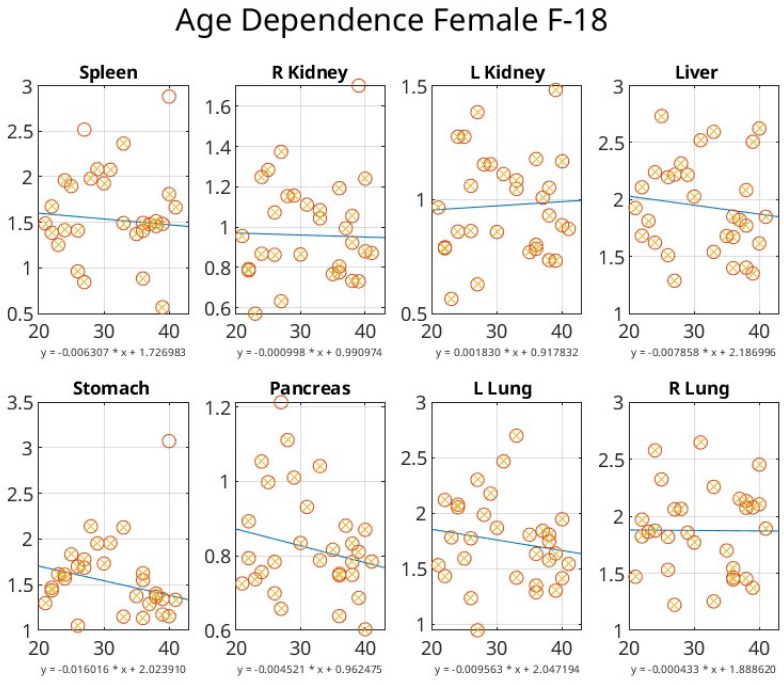

Figure D.4: Female Patient's S-value Dependence (F-18) on Age

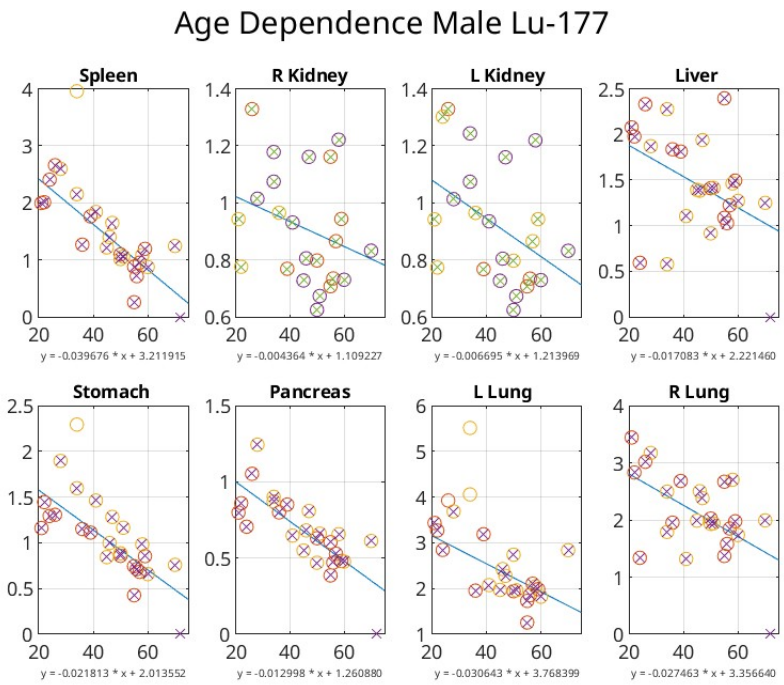

Figure D.5: Male Patient's S-value Dependence (Lu-177) on Age

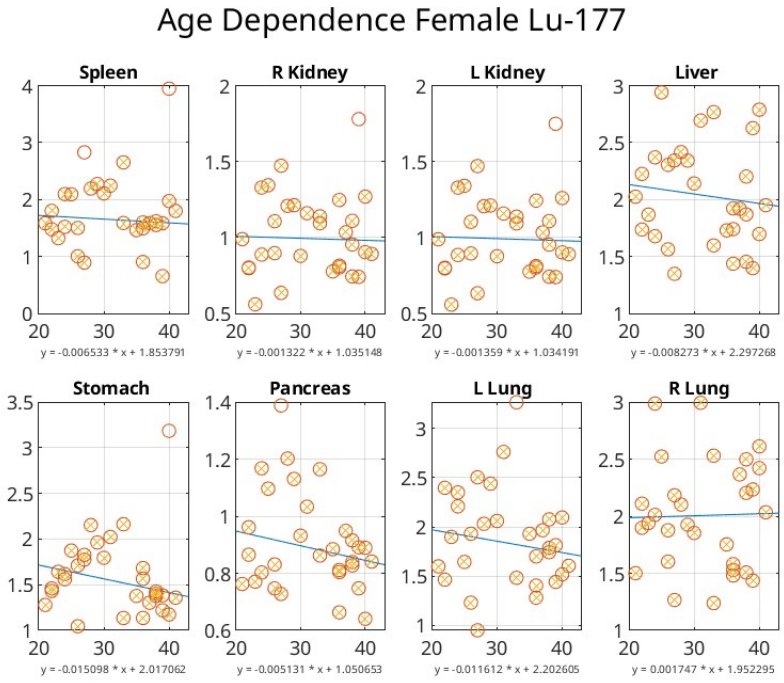

Figure D.6: Female Patient's S-value Dependence (Lu-177) on Age

Figure D.7: Male Patient's S-value Dependence (I-131) on Age

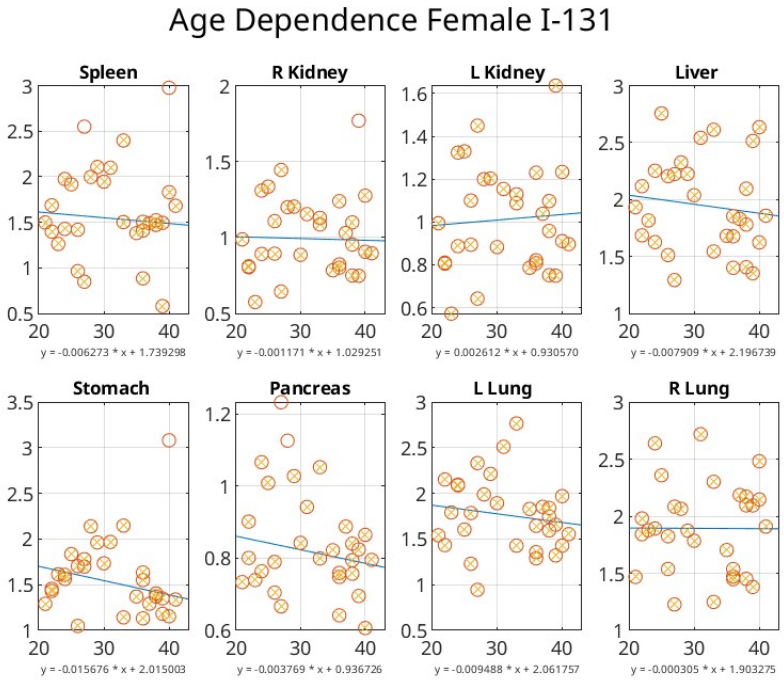

Figure D.8: Female Patient's S-value Dependence (I-131) on Age

Appendix E

Correlation between BMI and S-values

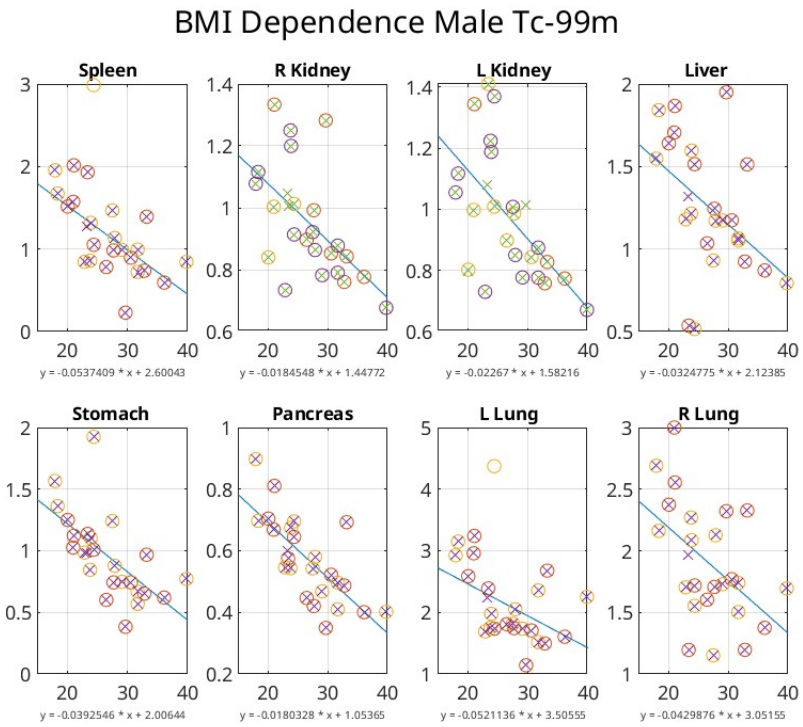

Figure E.1: Male Patient's S-value Dependence (Tc-99m) on BMI

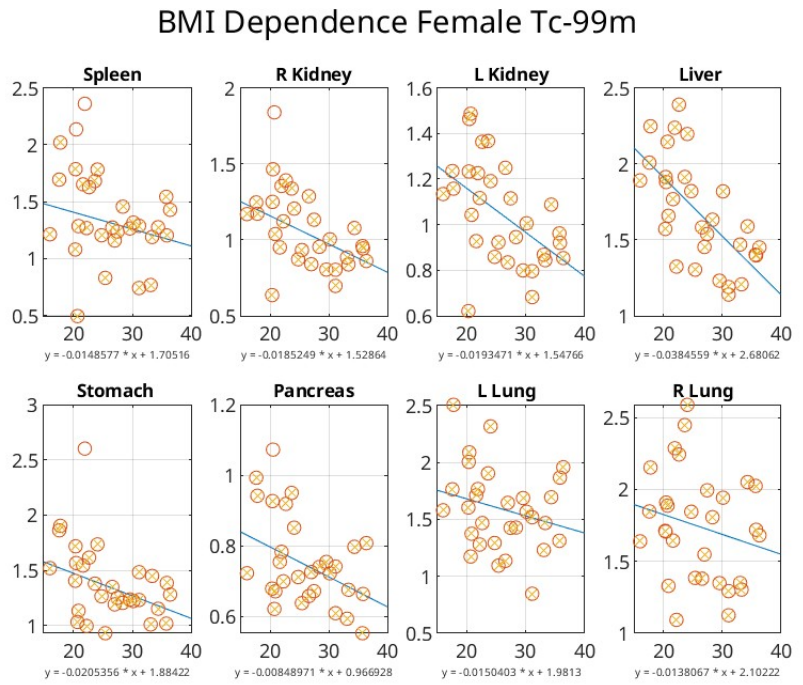

Figure E.2: Female Patient's S-value Dependence (Tc-99m) on BMI

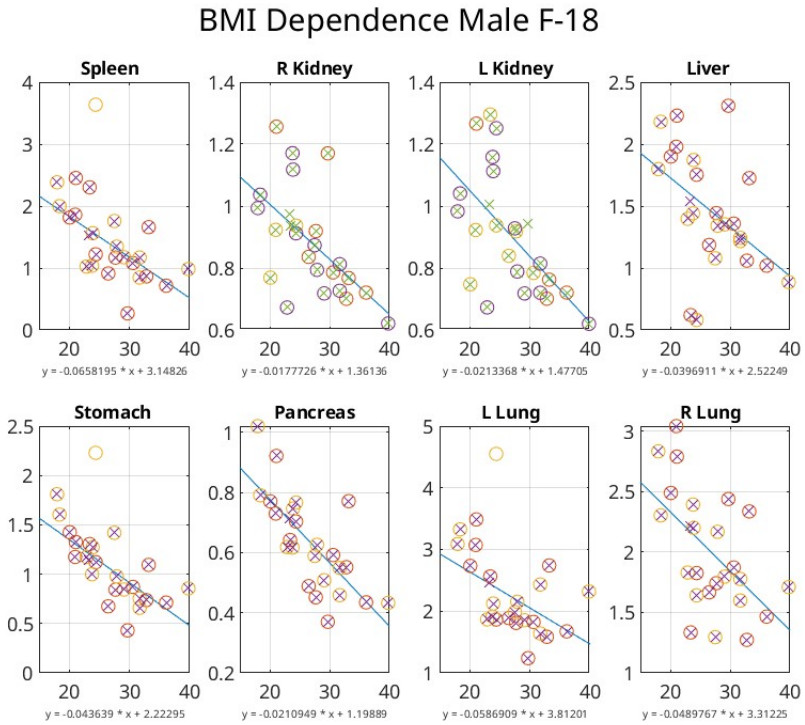

Figure E.3: Male Patient's S-value Dependence (F-18) on BMI

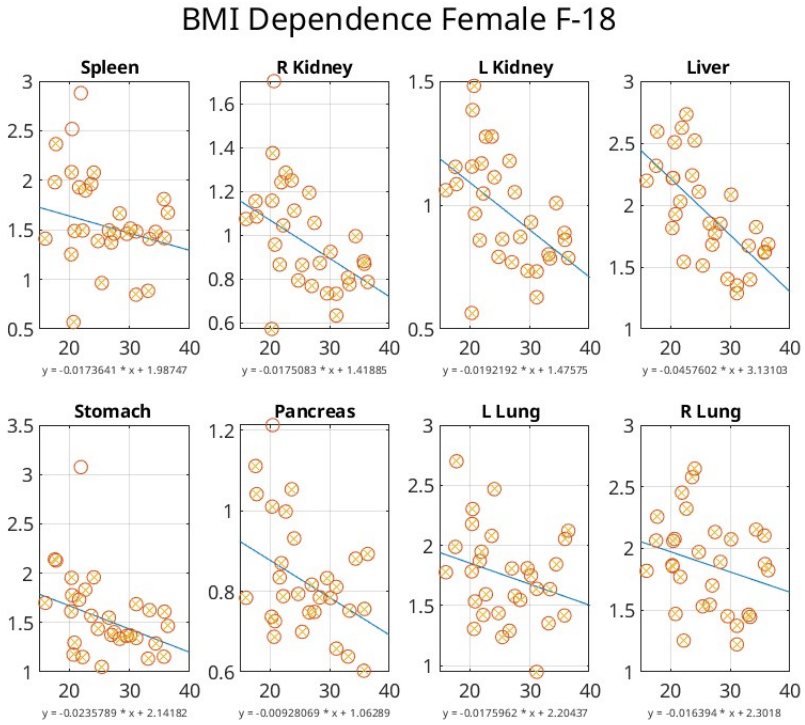

Figure E.4: Female Patient's S-value Dependence (F-18) on BMI

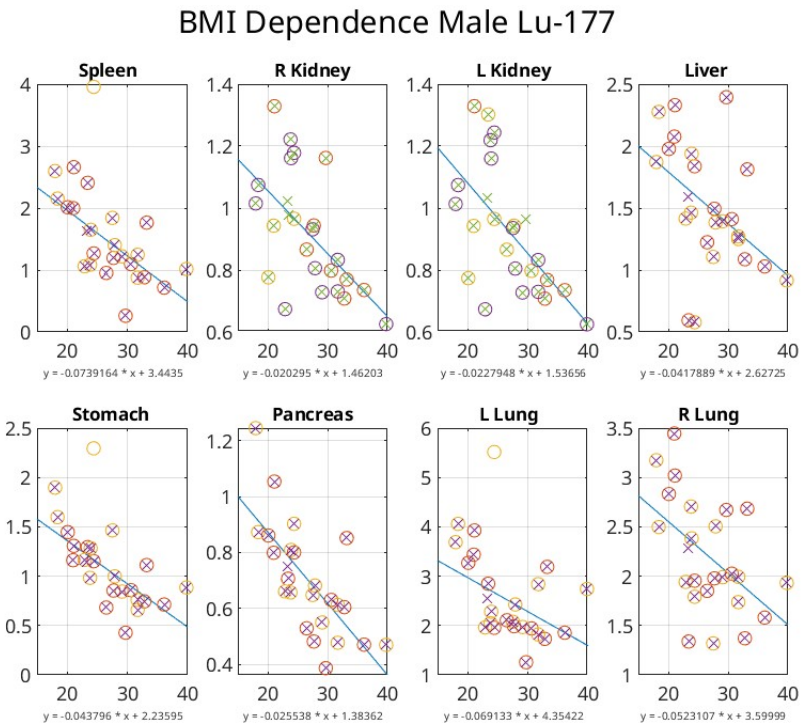

Figure E.5: Male Patient's S-value Dependence (Lu-177) on BMI

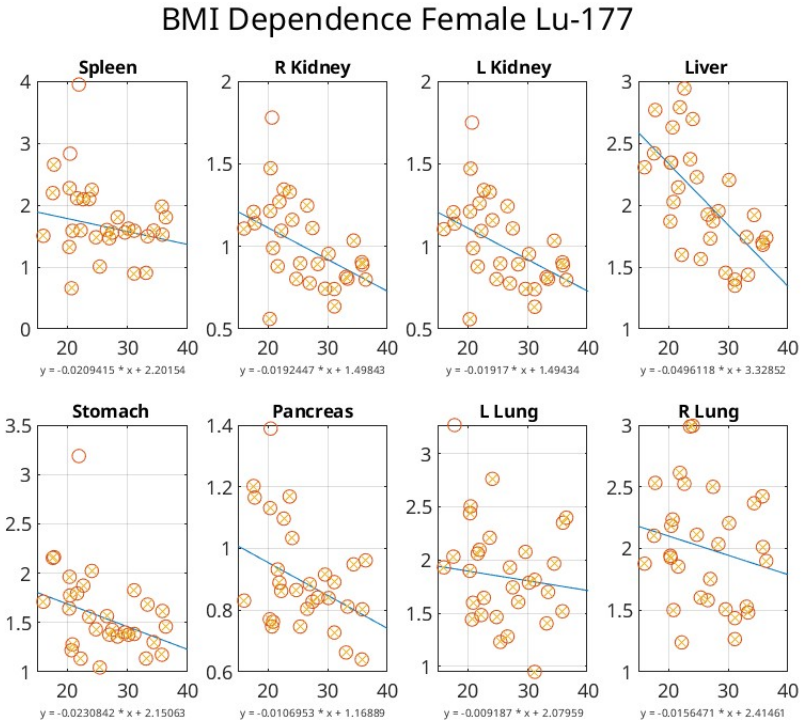

Figure E.6: Female Patient's S-value Dependence (Lu-177) on BMI

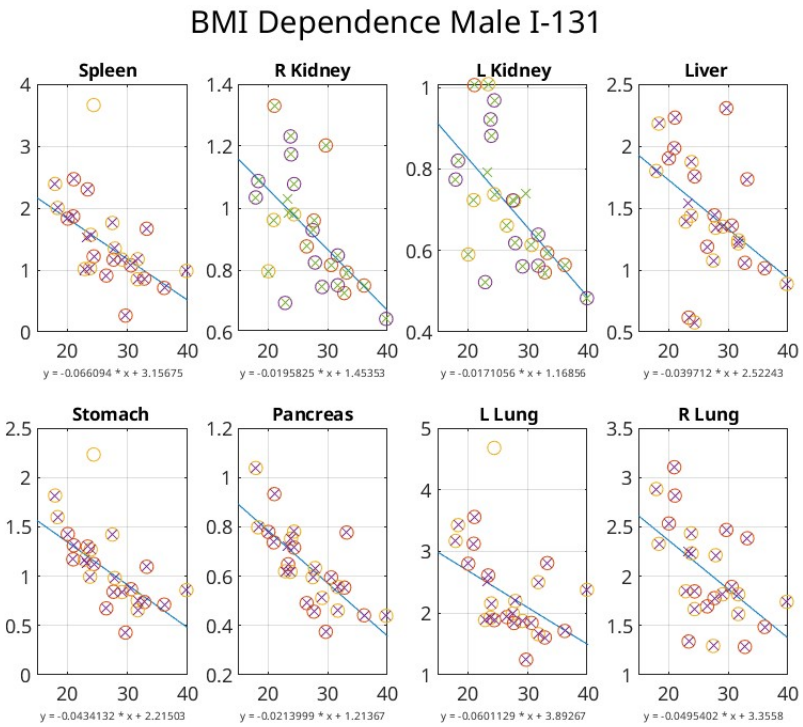

Figure E.7: Male Patient's S-value Dependence (I-131) on BMI

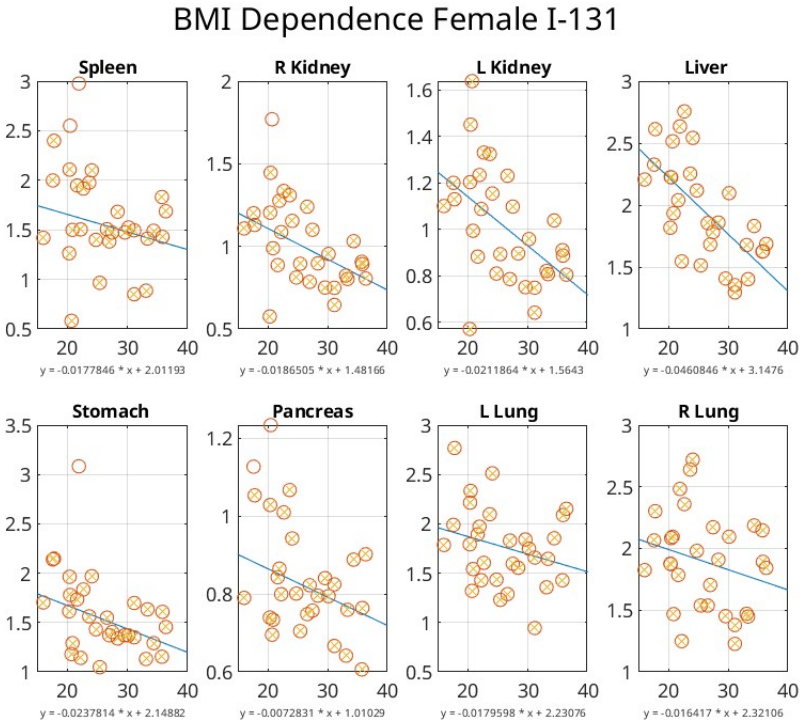

Figure E.8: Female Patient's S-value Dependence (I-131) on BMI